Course Materials for II M. Sc Physics

Subject Name: ***Nano Physics***

Subject Code: ***P16PYE5***

Prepared by

Dr. S. Sathiskumar

Assistant Professor

Post Graduate Department of Physics

Srinivasan College of Arts and Science

Perambalur – 621 212

Unit - I Introduction to Nano and Types of Nano Materials

5. Nano Devices

Introduction – electron density in bulk material – Size dependence of Fermi energy – quantum confinement – quantum structures – Density of states in quantum well, quantum wire and quantum dot structures – Band gap of nanomaterials – Tunneling: single electron phenomena and single electron transistor - Quantum dot laser. Conductivity of metallic nanowires - Ballistic transport - Quantum resistance and conductance - Carbon nanotubes: Properties and applications.

5.1 INTRODUCTION

A **nanometre** (nm) is one billionth $\left(\frac{1}{10^9}\right)$ of a metre. For comparison, thickness of a single human hair is about 80,000 nm (80 μm), a red blood cell is approximately 7,000 nm (7 μm) wide and a water molecule is almost 0.3 nm across.

Scientists and engineers are nowadays interested in nanoscale which is from 1 nm to 100 nm. At nanoscale, the properties of materials are very different from those at larger scale. Therefore, the nano-world is in between quantum world and macro world.

Nanoscience is concerned with the study of phenomena and manipulation of materials at nanometere scales.

Nanotechnology is the design, characterization, production and application of structures, devices and systems by controlling shape and size at the nanometre scale.

Nanotechnology means putting to use the unique physical properties of atoms, molecules and other things measuring roughly 1 to 100 nanometers.

The word "nano" comes from nanos, a Greek word meaning dwarf.

Presently, we are using many devices made of nanoelectronic devices. The microelectronics industry was born out of the invention of the bi-polar transistor in 1947 and by the invention of the integrated circuit (IC) in 1958.

Gordon Moore (co-founder of INTEL Corporation) observed that the number of transistors per square inch on IC chip roughly doubled by every 18 to 24 months. This general rule of thumb is now called as **"Moore's law"**.

By 1960, the minimum feature size of a transistor was approximately 100 μm. At present, manufacturing technology is at transistor size of 22 nm.

Because of the diminishing feature size of transistors and other components, we can say that the electronics industry is already "doing" nanotechnology.

Nanomaterials

Definition

Nanophase materials are newly developed materials with grain size at the nanometre range (10^{-9} m), i.e., in the order of 1 - 100 nm. The particle size in a nano material is 1 nm. They are simply called nanomaterials.

Different forms of Nanomaterials

Nano-structured material

The structures whose characteristic variations in design length is at the nanoscale.

Nano particles

The particle size is in the order of 10^{-9} m.

Nano dots

Nanoparticles which consist of homogeneous material, especially those that are almost spherical or cubical in shape.

Nanorods

Nanostructures which are shaped like long sticks or rods with diameter in nanoscale and a length very much longer.

Nanotubes

The carbon nanotubes are the wires of pure carbon like rolled sheets of graphite or like soda straws.

Nanowires

Nanowires are nanorods which especially conduct electricity.

Fullerenes

A form of carbon having a large molecule consisting of an empty cage of 60 or more carbon atoms.

Nanocomposites

Composite structures whose characteristic dimensions are found at nanoscale.

Cluster

A collection of units (atoms or reactive molecules) upto about 50 units.

Colloids

A stable liquid phase containing particles in the 1-1000 nm range.

Nano electronics

Nanoelectronics refers to the use of nanotechnology in electronic components, especially **transistors.**

It often refers to transistor devices that are so small that inter-atomic interactions and quantum mechanical properties need to be studied extensively.

Besides, being small and allowing more transistors to be packed into a single chip, the uniform and symmetrical structure of nanotubes allows a higher electron mobility, a symmetrical electron/hole characteristic.

Need for Nanotechnology in Electronics

Today microelectronics are used and they solve our most of the problems.

The two exceptional disadvantages of micro electronics are:

- Physical size
- Increasing cost of fabrication of integrated circuits.

To overcome these disadvantages, nanotechnology is used.

Advantages of Using Nanotechnology in Electronics

- Increasing the density of memory chips
- Decreasing the weight and thickness of the screens.
- Nanolithography is used for fabrication of chips.
- Reducing the size of transistors used in integrated circuits.
- Improving display screens on electronics devices.
- Reducing power consumption.

5.2 ELECTRON DENSITY IN BULK MATERIAL

Definition

Electron density is the number of electrons per unit volume in a material. It is determined by using density of states.

In bottom-up approach, low-volume structures are built atom by atom. In the top-down approach, material is removed from one or more of three dimensions (length, width, height) of a larger solid.

In both cases, a structure small enough for quantum behavior to manifest can be produced.

5.5 QUANTUM STRUCTURES

Definition

When a bulk material is reduced in its size, atleast one of its dimension, in the order of few nanometres, then the structure is known as quantum structure.

Explanation

The volume of a box can be reduced by shortening its length, width or, and height. The same is true for the region occupied by the electrons in a solid.

There are three dimensions to confine the bulk material. The quantum confinement needs confining at least one of these dimensions to less than 100 nanometers or even just a few nanometers.

The more the dimensions are confined, the more the density of states function looks like that of an atom. This progressive **discretization** gives new ways to understand real atoms, behavior of electrons and developing quantum confined electronic devices.

When the electrons are confined inside a region of minimal width, ie., confinement in one dimension **"quantum-well"** is created as shown in fig. 5.1(b). The quantum wells is made from alternating layers of different semiconductors or by deposition of very thin metal films.

By further reducing the depth of the electron's domain, **"quantum-wire"** is created (fig. 5.1 (c)). **Example: nanotube.**

A structure in which the motion of the electrons or holes are confined in one or more directions by potential barriers is called quantum confined structure.

The quantum confined structure is classified into three types based on the confinement directions. They are

(i) **quantum well**

(ii) **quantum wire**

(iii) **quantum dot**

(i) Quantum well (2 - dimension)

Definition

When the electrons are confined inside a region of minimal width, ie., confinement in one dimension **"quantum-well"** is created.

In other words, if one dimension is reduced to the nanometre range while the other two dimensions remain large, then we get a structure known as **quantum well**.

Fig. 5.1 shows a quantum well or 2-D structure

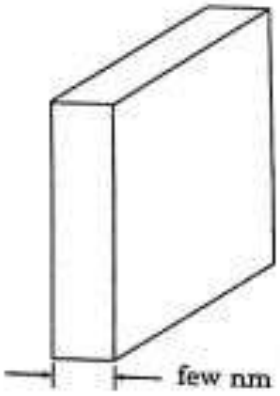

Fig. 5.1 quantum Well (2D)

Construction

Quantum wells are made from alternative layers of different semiconductors or by deposition of very thin metal films.

Explanation

The quantum well is a larger structure in which the carrier particles are free to move in two dimensions. The particles are confined in one dimension hence, they are considered to be **quantum confinement**.

Due to the confinement of carriers, the quantum well structure has important applications in making useful devices.

Use

Quantum wells are now widely used to make semiconductor lasers and other important devices.

(ii) Quantum wire (1 dimension)

Definition

When the electrons are confined in two mutually perpendicular directions, then the structure is known as quantum wire.

In other words, if two dimensions are reduced and one remains large, the resulting structure is quantum wire.

Fig. 5.2 shows a quantum wire or 1-D structure

Fig. 5.2 Quantum wire (1D)

Explanation

The carriers trapped in such structures are considered to be in 1-D quantum confinement. In this case, a carrier is only free to move its trajectory along the wire.

Example

Examples of quantum wire structures are nanowires, nanorod and nanotube.

(iii) Quantum Dots (0 - dimension)

Definition

When all the three dimensions are minimized the resulting structure is known as quantum dot.

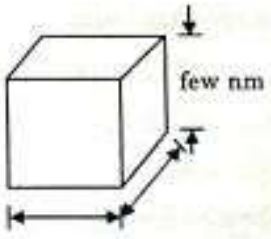

Fig. 5.3 Quantum dot

The dot can be particle located inside a larger structure or on its surface. It can also be a place where electrons have been trapped using electrical fields.

Fig. 5.3 shows a quantum dot or 0-D structure

Explanation

In quantum dot, the carriers has only confined states i.e., there are no freely moving carriers. Though a quantum dot has many thousands of atoms, carriers it is considered more like a single atom due to its peculiar properties.

Use

Quantum dot can be used in a quantum computer and lasers etc.

Fig. 5.4 and Fig. 5.5 explains the processes of diminishing the size in the case of rectilinear geometry and curvilinear geometry, respectively.

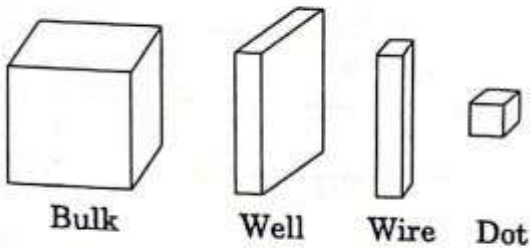

Fig. 5.4 Progressive generation of rectangular nanostructures

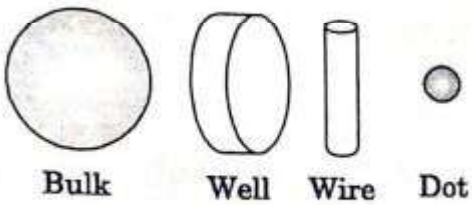

Fig. 5.5 Progressive generation of curvilinear nanostructures

Fig. 5.6 shows a comparison of three quantum confined structures with bulk material.

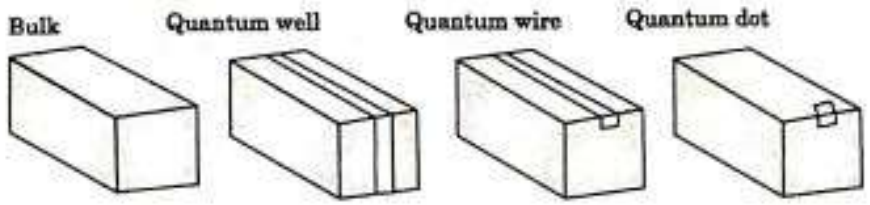

Fig. 5.6 Three quantum structures

As quantum wells and quantum wires each have at least one dimension in which the electrons are free to move and these structures exhibit **"partial confinement"**. However, quantum dots exhibit **"total confinement"**.

The classification of quantum confined structures is shown in **Table 5.1**.

Table 5.1 classification of quantum confined structures

Structure	Quantum confinement directions	Number of unconfined dimensions
Bulk	0	3
Quantum well	1	2
Quantum wire	2	1
Quantum dot	3	0

5.5 DENSITY OF STATES IN QUANTUM WELL, QUANTUM WIRE AND QUANTUM DOT STRUCTURE

Bulk Structure

The density of state of a bulk material is given by

$$Z(E) = \frac{8\pi\sqrt{2}\, m^{*3/2} (E - E_c)^{1/2}}{h^3}$$

Applications

- The main fields of application of the single electron transistor is used in sensor technology and digital electronic circuits.
- A variety of digital logic functions, including AND or NOR gates, is obtained based on SET operating at room temperature.
- It is used for mass data storage.
- It is used in highly sensitive electrometer.
- SET can be used as a temperature probe, particularly in the range of very low temperatures.
- SET is a suitable measurement set-up for single electron spectroscopy.
- It is used for the fabrication of a homo-dyn receiver operating at frequencies between 10 and 300 MHz.

Quantum Dots (QD)

Rapid progress in the fabrication of semiconductor structures has resulted into the reduction of three dimensional systems to two-dimensional, one-dimensional, and finally to zero dimensional systems.

Quantum dots represent the ultimate reduction in the dimensionality of semiconductor devices. These are three dimensional semiconductors structures only nanometers in size confining electrons and holes.

QDs operate at the level of a single electron which is certainly the ultimate limit for an electronic device and they are used as the gain material in lasers.

Definition

Quantum dots are tiny particles or nanocrystals of a semiconducting material with diameters in the range of 2 - 10 nanometers (10 - 50 atoms).

Applications of Quantum dots

- QDs are used in quantum dot lasers, QD memory devices, QD photo-detectors and quantum cryptography.
- The emission wavelength of a quantum dot is a function of its size. Obviously, by making QDs different sizes, we can create light of different colours.
- They have potential uses in LED displays, amplifiers, biological sensors, tumor targeting and diagnostics, molecular electronics, and catalysis.

5.11 QUANTUM DOT LASERS

They are the new generation semiconductor lasers. They consist of several million nano-sized crystals called quantum dots in the active region and they act as light emitters.

Quantum dot laser consists of an active layer (QD) embedded in a waveguide, surrounded by layers of lower refractive index material. This arrangement ensures light confinement.

The active layer consists of quantum wells or quantum dots where the band gap is lower than that of the waveguide material.

The wavelength of the emitted light is determined by the energy levels of the quantum dot.

Therefore, the emission wavelength can be tuned by changing the average size of the dots.

The band-gap of the quantum dot material is lower than the band gap of the surrounding medium. It ensures charge carrier confinement.

The structure of a quantum dot laser based on InAs dots in the InGaAs quantum well layer is shown in fig. 5.6(a).

Unit - II Carbon Nano Materials

Carbon is a unique atom among other elements because of its ability to exist in a wide variety of structures and forms as shown in the fig. 5.9.

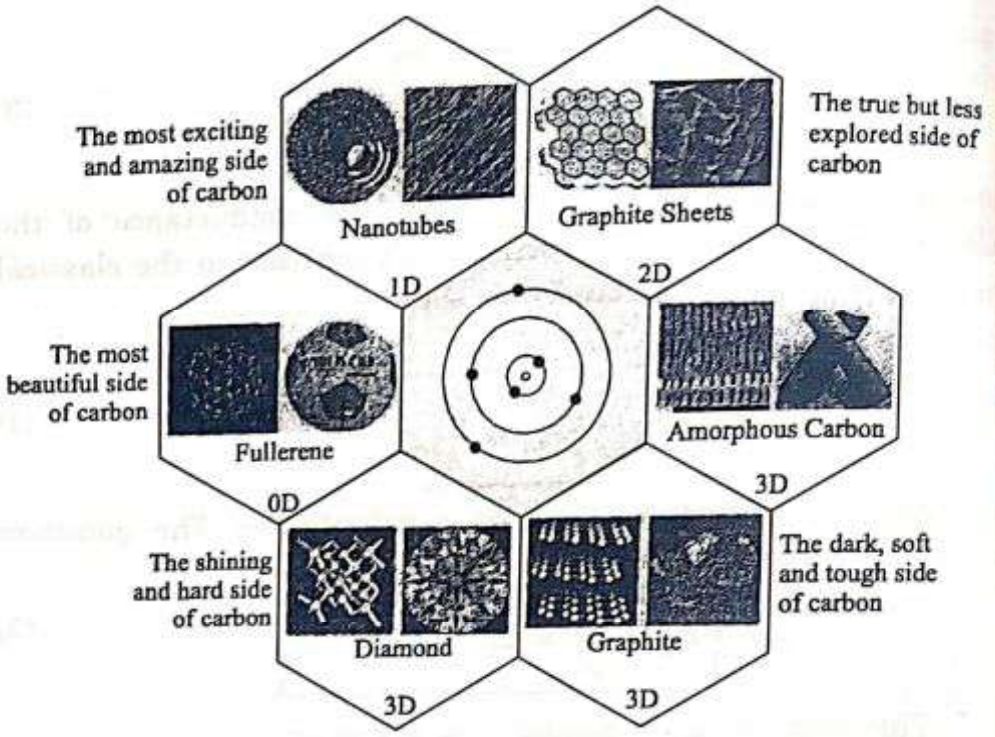

Fig. 5.9 Different forms of carbon molecules

Pure carbon exists in four different crystalline forms namely **Diamond, Graphite, Fullerenes and Nanotubes.**

Carbon atom is the basic building block of these crystalline structure. Among these, **Fullerenes** and **Nanotubes** are found to be useful in nanotechnology for various fabrication of nanostructures.

5.15 CARBON NANOTUBES (CNT)

A group of nanostructures with large potential applications are **carbon nanotubes**. The hexagonal lattice of carbon is simply graphite. A single layer of graphite is called **graphene**. (fig. 5.10)

The carbon nanotube (CNT) consists of a graphene layer which is rolled up into a cylindrical shape as shown in fig.5.10.

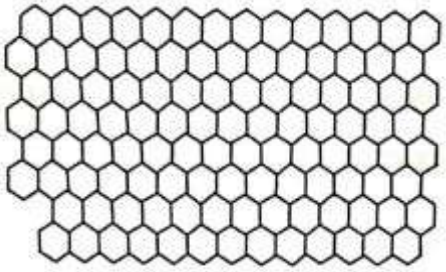

Fig. 5.10 Graphene sheet

When the graphene layer is rolled, the structure is tube like and it is a single molecule. Each single molecule nanotube is made up of a hexagonal network of covalently bonded carbon atoms.

In some cases, the hexagons are arranged in a spiral form. The layer appears like a rolled-up chicken wire (net having a large hexagonal mesh) with carbon atoms at the apexes of the hexagon as shown in fig.5.11.

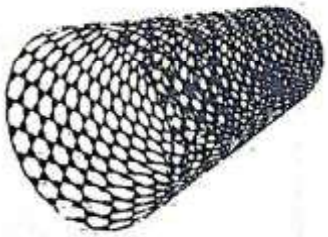

Fig. 5.11 SWCNT formed from graphene sheet

The carbon nanotubes are hollow cylinders of extremely thin diameter, 10,000 times smaller than a human hair.

Structures of CNT

The CNTs have many structures on the basis of their length, type of spiral and number of layers. Their electrical properties depend on their structure and they act as both a metal or a semiconductor.

There are a variety of structures of carbon nanotubes with different properties.

Types CNT structures

Three types of nanotube structures are considered by rolling a graphite sheet with different orientations about the axis.

They are

(i) **Armchair structure** (ii) **Zig-zag structure**

(iii) **Chiral structure**

Armchair structure

When the axis of the tube parallel to C–C bonds of the carbon hexagons, the structure shown in fig. 5.12(a) is obtained. It is referred as **"armchair"** structure.

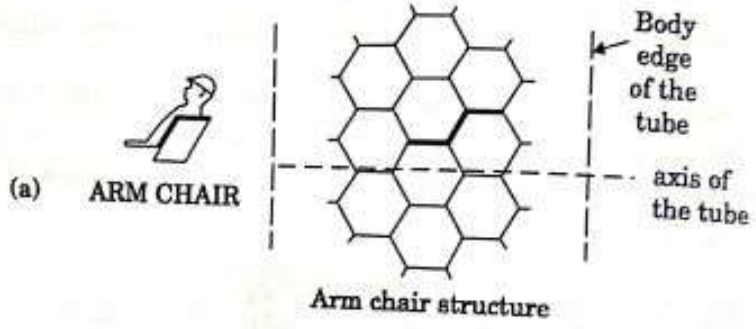

Fig. 5.12 Illustration structures of carbon nanotubes
(a) armchair structure ;
(b) zigzag structure
(c) chiral structure

Zig-zag and Chiral structure

The tubes sketched in figs. 5.12(b) and 5.12(c), referred as **zig-zag** and **chiral structure.** They are formed by rolling graphene sheet such that the axis of the tube is not parallel to *C–C* bonds.

Zig-zag structure consists of tube axis perpendicular to *C–C* bonds.

In chiral structure, *C–C* bond is inclined towards the axis of the tube.

Generally, nanotubes are closed at both ends with half of fullerene structure.

Classification of CNT

Based on the number of layers, the carbon nanotubes are classified as

(i) **Single-walled (SWNTs)**

(ii) **Multi-walled (MWNTs).**

In multi-walled nanotubes, more than one CNTs are coaxially arranged.

5.16 PROPERTIES OF CNTs

(a) Electrical Properties

(i) Carbon nanotubes are metallic or semiconducting depending on the diameter and chirality (ie., how the tubes are rolled).

(ii) The energy gap of semiconducting chiral carbon nanotubes is inversely proportional to the diameter of the tube as shown in fig 5.13.

The energy bandgap decreases with increase of diameter of the CNTs.

(iii) The energy gap also varies along the tube axis and reaches a minimum value at the tube ends. This is due to the presence of localized defects at the ends due to the extra energy states.

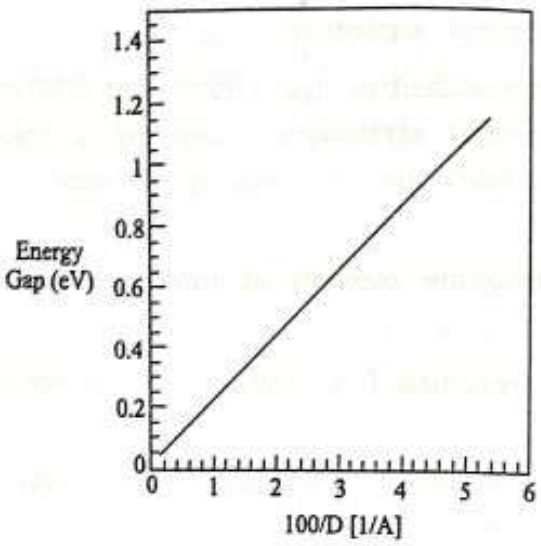

Fig. 5.13 Plot of the magnitude of the energy band gap of a semiconducting, chiral carbon nanotube versus the reciprocal of the diameter of the tube (10 Å = 1 nm).

(iv) In SWNTs, conduction occurs through discrete electronic states that are coherent between the electrical contacts (hundreds of nanometers).

This means that nanotubes can be treated as quantum wires atleast at very low temperatures.

(b) Mechanical Properties

(i) The strength of the carbon-carbon bond is very high therefore any structure based on aligned carbon-carbon bonds will ultimately have high strength.

(ii) Young's modulus of CNT is about 1.8 TPa (10^{12} Pa about 10 times larger than that of steel).

Nanotubes have therefore high ultimate tensile-strength

(iii) One of the important properties of nanotubes is their ability to withstand extreme strain.

(iv) The carbon nano tubes can recover from severe structural distortions. This is due to the ability of carbon atoms to rehybridize.

6.2. Carbon Fullerenes and Nanotubes

Carbon is a unique material, and can be a good metallic conductor in the form of graphite, a wide band gap semiconductor in the form of diamond, or a polymer when reacted with hydrogen. Carbon provides examples of materials showing the entire range of intrinsic nanometer scaled structures from fullerenes, which are zero-dimensional nanoparticles, to carbon nanotubes, one-dimensional nanowires to graphite, a two-dimensional layered anisotropic material, to fullerene solids, a three-dimensional bulk materials with the fullerene molecules as the fundamental building block of the crystalline phase. In this section, we will briefly discuss the synthesis and some properties of fullerenes, fullerene crystals and carbon nanotubes. For more general research information about carbon science or detailed information on carbon fullerenes and carbon nanotubes, the readers are referred to excellent review articles and books, such as that by Dresselhaus[1,2] and references therein.

6.2.1. *Carbon fullerenes*

Carbon fullerene commonly refers to a molecule with 60 carbon atoms, C_{60}, and with an icosahedral symmetry,[3] but also includes larger molecular weight fullerenes $C_n (n > 60)$. Examples of larger molecular weight fullerenes are C_{70}, C_{76}, C_{78}, C_{80}, and higher mass fullerenes, which possess different geometric structure,[4-6] e.g. C_{70} has a rugby ball-shaped symmetry. Figure 6.1 shows the structure and geometry of some fullerene molecules.[7] The name of fullerene was given to this family of carbon molecules because of the resemblance of these molecules to the geodesic dome designed and built by R. Buckminster Fuller,[8] whereas the name of buckminster fullerene or buckyball was specifically given to the C_{60} molecules, which are the most widely studied in the fullerene family and deserve a little more discussion on its structure and properties.

The 60 carbon atoms in C_{60} are located at the vertices of a regular truncated icosahedron and every carbon site on C_{60} is equivalent to every other site. The average nearest neighbor C–C distant in C_{60} (1.44 Å)[9] is almost identical to that in graphite (1.42 Å). Each carbon atom in C_{60} is trigonally bonded to other carbon atoms, the same as that in graphite, and most of the faces on the regular truncated icosahedron are hexagons. There are 20 hexagonal faces and 12 additional pentagonal faces in each C_{60} molecule, which has a molecule diameter of 7.10 Å.[3,10] Although each carbon atom in C_{60} is equivalent to every other carbon atom, the three bonds emanating

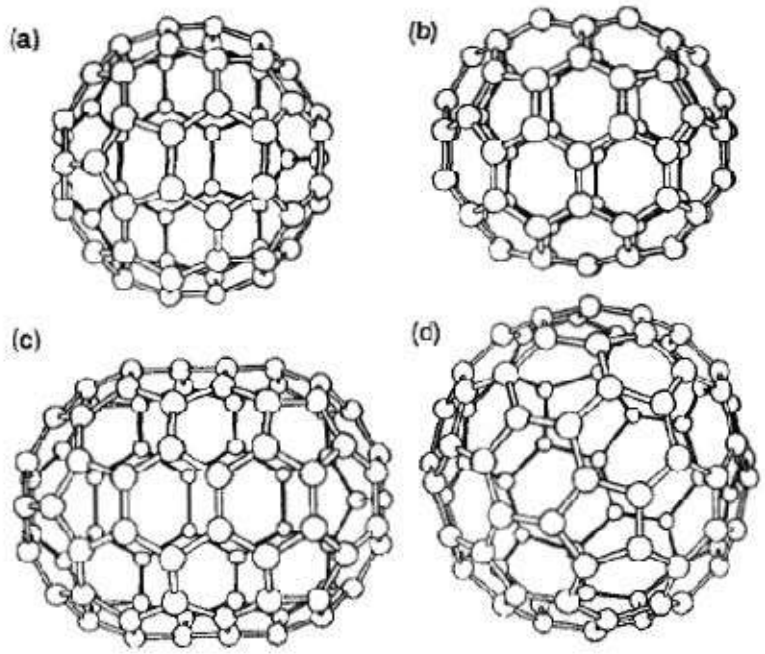

Fig. 6.1. (a) The icosahedral C_{60} molecule. (b) The C_{70} molecule as a rugby ball-shaped molecule. (c) The C_{80} molecule as an extended rugby ball-shaped molecule. (d) The C_{80} molecule as an icosahedron. [M.S. Dresselhaus and G. Gresselhaus, *Ann. Rev. Mater. Sci.* 25, 487 (1995).]

from each atom are not equivalent. Each carbon atom has four valence electrons for the formation of three chemical bonds, and there will be two single bonds and one double bond. The hexagonal faces consist of alternating single and double bonds, whereas the pentagonal faces are defined by single bonds. In addition, the length of single bonds is 1.46 Å, longer than the average bond length, 1.44 Å, while the double bonds are shorter, 1.40 Å.[11,12] The structures of other fullerene molecules can be considered as a modification of C_{60} by varying the number of hexagonal faces as far as the Euler's theorem is not violated, which states that a closed surface consisting of hexagons and pentagons has exactly 12 pentagons and an arbitrary number of hexagons.[13] For example, C_{70} structure can be envisioned by adding a belt of five hexagons around the equatorial plane of the C_{60} molecule normal to one of the five-fold axis.

Fullerenes are usually synthesized by using an arc discharge between graphite electrodes in approximately 200 torr of He gas, first demonstrated in 1990 by Krätschmer and coworkers.[14] The heat generated at the contact point between the electrodes evaporates carbon to form soot and fullerenes, which condense on the water-cooled walls of the reactor. This discharge produces a carbon soot that can contain up to ~15% fullerenes: C_{60} (~13%) and C_{70} (~2%). The fullerenes are next separated from the soot, according to their mass, by use of liquid chromatography and using

a solvent such as a toluene. However, there is no definite understanding of the growth mechanism of the fullerenes. Fullerene chemistry has been a very active research field, because of the uniqueness of the C_{60} molecule and its ability to have a variety of chemical reactions.[15,16]

6.2.2. *Fullerene-derived crystals*

In a solid state, fullerene molecules crystallize into crystal structures through weak intermolecular forces and each fullerene molecule serves as a fundamental building block of the crystalline phase. For example, the C_{60} molecules crystallize into a face-centered cubic (FCC) structure with lattice constant of 14.17 Å and a C_{60} C_{60} distance of 10.02 Å.[17] The molecules are almost freely rotating with three degree of rotation at room temperature, as shown by nuclear magnetic resonance methods. The crystalline forms of fullerenes are often called fullerites.[18] Single crystals can be grown either from solution using solvents such as CS_2 and toluene or by vacuum sublimation, though the sublimation yields better crystals and is generally the method of choice.[19]

6.2.3. *Carbon nanotubes*

There are excellent reviews and books on the synthesis and the physical properties of carbon nanotubes,[20–23] and therefore, in this section, only a brief summary of the fundamentals and general approaches for the synthesis of carbon nanotubes is presented. There are single-wall carbon nanotube or SWCNT, and multi-wall carbon nanotube or MWCNT. The fundamental carbon nanotube is a single-wall structure and can be understood by referring to Fig. 6.2.[1] In this figure we see that points O and A are crystallographically equivalent on the graphene sheet, where X-axis is placed parallel to one side of the honeycomb lattice. The points O and A can be connected by a vector $C_h = na_1 + ma_2$, where a_1 and a_2 are unit vectors for the honeycomb lattice of the graphene sheet. Next we can draw normals to C_h at points O and A to obtain lines OB and AB′. If we now superimpose OB onto AB′, we obtain a cylinder of carbon atoms that constitutes a carbon nanotube when properly capped at both ends with half of a fullerene. Such a single-wall carbon nanotube is uniquely determined by the integers (n,m). However, from an experimental standpoint, it is more convenient to denote each carbon nanotube by its diameter $d_t = C_h/\pi$ and the chiral angle θ. Depending on the chiral angle, a single-wall carbon

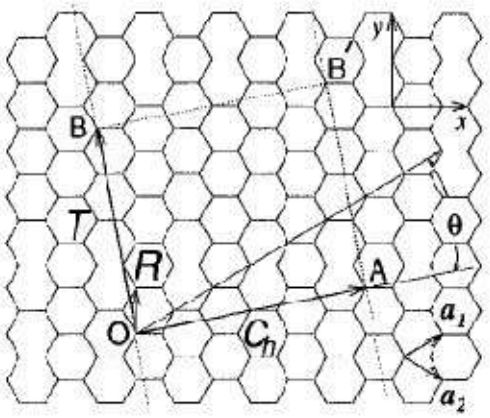

Fig. 6.2. The chiral vector OA or $C_h = na_1 + ma_2$ is defined on the honeycomb lattice of carbon atoms by unit vectors a1 and a2 and the chiral angle θ with respect to the zigzag axis. Along the zigzag axis, θ = 0°. Also shown is the lattice vector OB = *T* of the one-dimensional nanotube unit cell. The rotation angle ψ and the translation τ (not shown) constitute the basic symmetry operation R = (ψ|τ) for the carbon nanotube. The diagram is constructed for (*n,m*) = (4,2). The area defined by the rectangle (OAB'B) is the area of the one-dimensional unit cell of the nanotube. [M.S. Dresselhaus, *Ann. Rev. Mater. Sci.* 27, 1 (1997).]

nanotube can have three basic geometries—armchair with θ = 30°, zigzag with θ = 0°, and chiral with 0<θ<30°, as shown in Fig. 6.3.[24]

Multi-wall carbon nanotube consists of several nested coaxial single-wall tubules. The arrangement of the carbon atoms in the hexagonal network of the multi-wall carbon nanotube is often helicoidal, resulting in the formation of chiral tubes.[31] However, there appears to be no particular ordering between individual cylindrical planes forming the multi-wall carbon nanotube such as can be found in graphite where the planes are stacked relative to each other in an ABAB configuration. In other words, a given multi-wall carbon nanotube will typically be composed of a mixture of cylindrical tubes having different helicity or no hecility, thereby resembling turbostratic graphite. Typical dimensions of multi-wall carbon nanotube are outer diameter: 2–20 nm, inner diameter: 1–3 nm, and length: 1–100 μm. The intertubular distance is 0.340 nm, which is slightly larger than the interplanar distance in graphite.

Carbon nanotubes can be prepared by arc evaporation,[25] laser ablation,[26] pyrolysis,[27] PECVD,[28] and electrochemical methods.[29,30] Carbon nanotubes were first synthesized by Iijima in 1991 in the carbon cathode by arc discharge.[31] However, the experimental discovery of single-wall carbon nanotubes came in 1993,[32,33] whereas the discovery in 1996 of a much more efficient synthesis route, involving laser vaporization of graphite to prepare arrays of ordered single-wall nanotubes,[34] offered major new opportunities for quantitative experimental studies of carbon nanotubes.

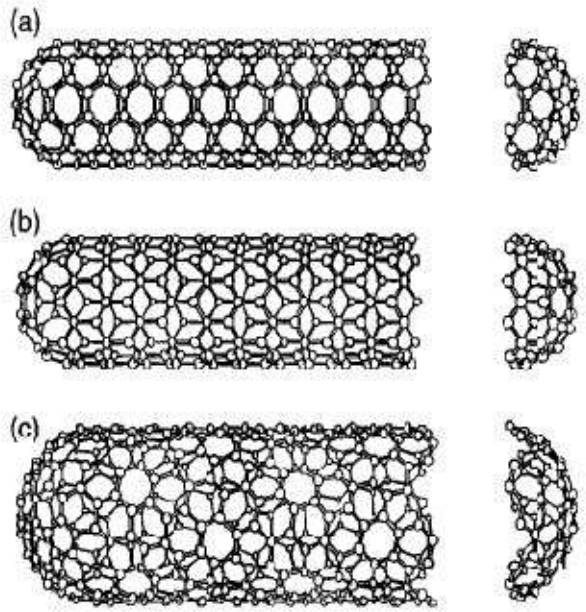

Fig. 6.3. Schematic models for single-wall carbon nanotubes with the nanotube axis normal to (a) the $\theta = 30°$ direction (an armchair (n,n) nanotube); (b) the $\theta = 0°$ direction (a zigzag $(n,0)$ nanotube); and (c) a general direction OB (see Fig. 6.2) with $0° < \theta < 30°$ [a chiral (n,m) nanotube]. The actual nanotubes shown in the figure correspond to (n,m) values of (a) (5,5), (b) (9,0), and (c) (10,5). [M.S. Dresselhaus, G. Dresselhaus, and R. Saito, *Carbon* **33**, 883 (1995).]

The formation of the carbon nanotubes in most cases requires an "open end" where the carbon atoms arriving from the gas phase could coherently land and incorporate into the structure. Growth of nested multi-wall nanotubes can be stabilized by the strained "lip–lip" bonding between the coaxial edges, highly fluctuating and, therefore, accessible for new atoms. In general the open end can be maintained either by a high electric field, by the entropy opposing the orderly cap termination, or by the presence of a metal cluster.

The presence of an electric field in the arc-discharge is believed to promote the growth of carbon nanotubes.[35,37] Nanotubes form only where the current flows, on the larger negative electrodes. Typical rate of the cathode deposition is about a millimeter per minute, with the current and voltage in the range of 100 A and 20 V respectively, which maintains a high temperature of 2000–3000°C. For example, Ebbesen and Ajayan[36] used carbon arc evaporation to produce carbon nanotubes in high yields. In their experiment, an arc plasma is generated between the two carbon electrodes in an inert atmosphere, e.g. He, by applying a DC current density of $\sim$150 A/cm^2 with a voltage of $\sim$20 V. The extremely high growth temperatures required in the arc discharge experiments can cause the grown carbon nanotubes to sinter, and the sintering of carbon nanotubes is believed to be the predominant source of defects.[37]

An addition of a small amount of transition metal powder such as Co, Ni or Fe, favors a growth of single-wall nanotubes.[32,33] Thess *et al.*[34] grew uniform diameter (10,10) nanotubes with high yield, by condensation of laser-vaporized carbon catalyst mixture at a lower temperature of ~1200°C. It is believed that the alloy cluster anneals all unfavorable structures into hexagons, which in turn welcome the newcomers and promote the continuous growth of straight nanotubes. Figure 6.4 illustrates the energetics of growth, the relative binding energies in nanotubes, graphite and the feedstock components.[18]

Growth of aligned carbon nanotubes was first demonstrated by CVD directly on Fe nanoparticles embedded in mesoporous silica.[38] The diameter, growth rate and density of vertically aligned carbon nanotubes are found to be dependent on the size of the catalyst.[39] Plasma induced well-aligned carbon nanotubes can be grown on contoured surfaces and with a growth direction always perpendicular to the local substrate surface as shown in Fig. 6.5.[40] The alignment is primarily induced by the electrical self-bias field imposed on the substrate surface from the plasma environment. It was found that switching the plasma off effectively turns the alignment mechanism off, leading to a smooth transition between the plasma-grown straight nanotubes and the thermally grown "curly" nanotubes as shown in Fig. 6.6.[40] DC-bias has found to enhance the nucleation and growth of aligned carbon nanotubes.[41]

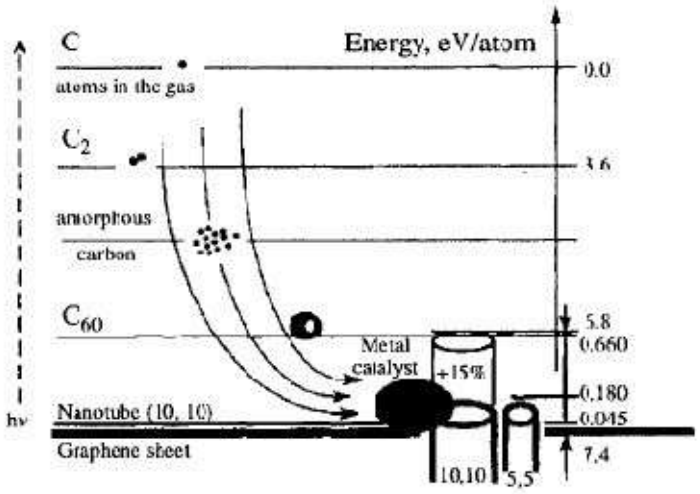

Fig. 6.4. "Food chain" illustrates how the metal (Ni/Co) cluster is able to eat essentially any carbon material it encounters and feed the digested carbon bits to the growing end of the nanotube. The vertical axis shows the cohesive energy per atom for the different forms of carbon consumed in nanotube growth. The energy cost for curving the graphene sheet into the cylinder of the (10,10) tube is only 0.045 eV, or 0.08 eV nm^2/d^2 for a tube of any diameter d. The elastic stretching of a tube by 15% adds approximately 0.66 eV per atom above the graphene. [R.E. Smalley and B.I. Yakobson, *Solid State Commun.* **107**, 597 (1998).]

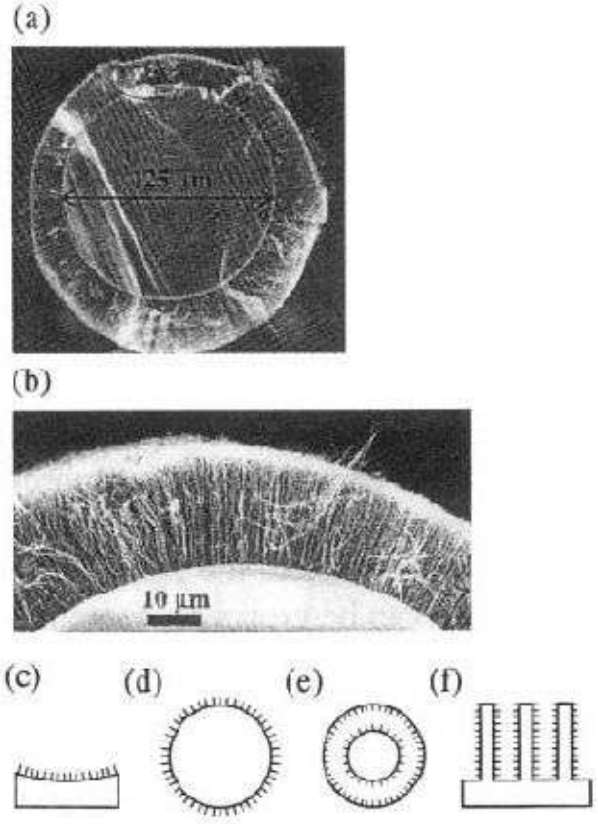

Fig. 6.5. (a) An SEM micrograph showing the radially grown nanotubes on the surface of a 125 μm-diameter optical fiber. (b) A close-up micrograph showing the conformally perpendicular nature of the nanotube grown on the fiber. (c)–(f) are examples of nonplanar, complex surfaces where nanotubes can be conformally grown perpendicular to the local surface. [C. Bower, W. Zhu, S. Jin, and O. Zhou, *Appl. Phys. Lett.* 77, 830 (2000).]

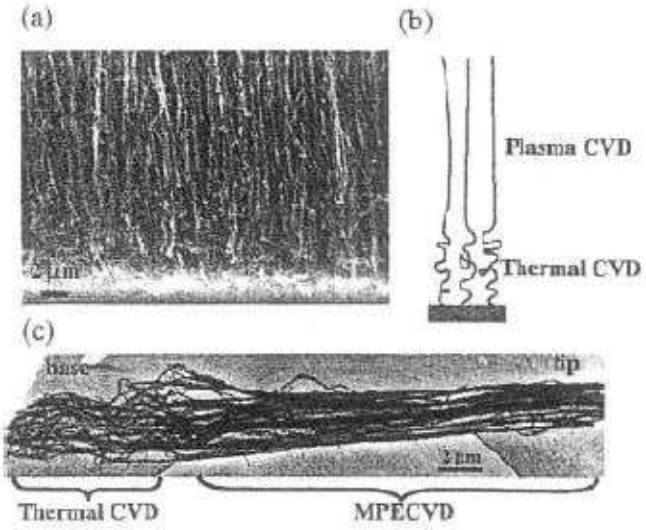

Fig. 6.6. (a) An SEM micrograph and (b) a schematic showing the straight/curled nanotube structure produced by an alternating plasma and thermal process (a 2 min plasma process followed by a 70 min thermal process), indicating both the field induced alignment effect and the base growth mechanism. (c) TEM micrograph showing a bundle of nanotubes with the upper portion straight and the lower portion curled. [C. Bower, W. Zhu, S. Jin, and O. Zhou, *Appl. Phys. Lett.* 77, 830 (2000).]

It should be noted that the catalyst growth mechanism of carbon nanotubes is similar to that of VLS growth of nanowires or nanorods discussed in Chapter 4. Baker and Harris proposed this model for the catalytic carbon filament growth.[42] Atomic carbon dissolves into the metal droplets, then diffuses to and deposits at the growth surface, resulting in the growth of carbon nanotubes. The catalyst growth offers an additional advantage; it is relatively easy to prepare patterned carbon nanotube films by standard lithographic techniques[43,44] and to grow aligned carbon nanotubes with or without the substrate.[45,46] Methods of CVD growth of carbon nanotubes, assisted by the transition metal catalysts, are also considered as the method for the mass production.[47] CVD methods also allow the growth of carbon nanotubes at much lower growth temperatures such as 700 or 800°C.[48,49] The as-grown nanotubes generally show poor crystallinity, but can be much improved by a heat treatment at 2500–3000°C in argon.[50]

For the catalytic growth, two models have been proposed to explain the experimental observations: the base growth and tip growth, which were originally developed for the catalytic growth of carbon filaments.[51] Both models are used to explain the growth of carbon nanotubes. In the case of PECVD and pyrolysis growth, the catalytic particles are usually found at the tip and explained by the tip growth model.[52–55] The base model has been used to explain the vertically aligned carbon nanotube growth by thermal CVD using iron as catalyst.[56–59] However, experiments showed that the vertical growth of aligned carbon nanotubes does not necessarily follow the base-growth model.[60] The growth of aligned carbon nanotubes is possible through both tip-growth and base-growth models, depending on the catalyst and substrate used in the deposition method. Furthermore, the diffusion of precursor molecules to the catalyst at the bottom of the growing nanotubes would be difficult, particularly considering the high density and large length (up to 100 μm) of the grown carbon nanotubes. However, no research has been done to address this issue yet.

Another proposed mechanism for the carbon nanotube growth assumes that the nanotubes are always capped.[61] The growth is nucleated at active sites of a vapor-grown carbon fiber and the growth involves C_2 dimer absorption near a pentagon at the cap of the nanotube. Subsequent restructuring would result in the formation of an additional carbon hexagon, which is added into the nanotube and leads to the growth of the tube.

In almost all the synthesis methods, carbon nanotubes are found along with other carbon materials, such as amorphous carbon and carbon nanoparticles. Purification is generally required and refers to the isolation

of carbon nanotubes from other entities. Three basic methods have been used for purification: gas phase, liquid phase and intercalation methods.[52] The gas phase purification method removes nanoparticles and amorphous carbon in the presence of nanotubes by an oxidation process.[63,64] The gas phase purification process also tends to burn off many of the nanotubes, particularly the smaller diameter nanotubes. Liquid phase removal of nanoparticles and other unwanted carbons is achieved using a potassium permanganate, $KMnO_4$ treatment.[65] This method retains most of carbon nanotubes, a higher yield than gas phase purification, but with shorter length. Carbon nanoparticles and other carbon species can be intercalated by reacting with $CuCl_2$–KCl, whereas the nanotubes would not intercalate since they have closed cage structures. Subsequent chemical reactions can remove the intercalated species.[66]

Properties of carbon nanotubes have been extensively studied. Langer *et al.*[67] were the first to study the transport properties of carbon nanotubes, and further measurements were done by many research groups.[68–70] Carbon nanotubes are excellent candidates for stiff and robust structures, since the carbon–carbon bond in graphite is one of the strongest in nature. TEM observation revealed that carbon nanotubes are flexible and do not break upon bending.[71] Thermal conductivity of carbon nanotubes could be extremely high, considering the fact that thermal conductivity of diamond and graphite (in-plane) are extremely high,[72] and thermal conductivity of individual carbon nanotubes was found much higher than that of graphite and bulk nanotubes.[73] Carbon nanotubes have a wide spectrum of potential applications. Examples include use in catalysis,[74] storage of hydrogen and other gases,[75] biological cell electrodes,[76] quantum resistors,[77] nanoscale electronic and mechanical devices,[78] electron field emission tips,[79] scanning probe tip,[80] flow sensors[81] and nanocomposites.[82]

6.3. Micro and Mesoporous Materials

According to the classification made by IUPAC,[83] porous solids can be grouped into three categories, depending on their pore diameter: microporous ($d < 2\,\text{nm}$), mesoporous ($2\,\text{nm} < d < 50\,\text{nm}$), and macroporous ($d > 50\,\text{nm}$) materials. Almost all of zeolites and their derivatives are microporous, whereas surfactant templated mesoporous materials and most xerogels and aerogels are mesoporous materials. In this section, we will briefly introduce these meso and microporous materials and their respective synthesis techniques. This field has been extensively covered with excellent review articles.[84,85]

Unit - III Fabrication of Nano Materials

also play an important role. In addition to the interchain van der Waals and electrostatic interactions, alkyl chains may provide space for better arrangement of head groups resulting in the formation of closely packed SA monolayers or restrict packing and ordering in the self-assembly, depending on the molecular structures of alkyl chains.[108,110]

SA monolayers have been exploited for applications of surface chemistry modification, introduction of functional groups on the surface, construction of multilayer structures. SA monolayers have also been used to enhance the adhesion at the interfaces.[90] Various functional groups can also be incorporated into or partially substitute alkyl chains in surfactant molecules. SA monolayers have also be used in the synthesis and fabrication of core-shell nanostructures with silane groups linking to oxides and amines linking to metals.[109]

Self-assembly is a wet chemical route to the synthesis of thin films, mostly organic or inorganic–organic hybrid films. This method is often used for the surface modification by formation of a single layer of molecules, which is commonly referred to as self-assembled monolayer (SAM). This method has also been explored to assemble nanostructured materials, such as nanoparticles into an ordered macroscale structures, such as arrays or photonic bandgap crystals. Self-assembly of nanoparticles and nanowires is one of the topics to be discussed in Chapter 7. Arguably, all spontaneous growth processes of formation of materials such as single crystal growth or thin film deposition can be considered as self-assembly process. In these processes, growth species self-assemble at low energy sites. Growth species here for self-assembly are commonly atoms. For more conventional definition of self-assembly, the growth species are commonly molecules. However, nanoparticles or even micron-sized particles are also used as growth species for self-assembly.

5.9. Langmuir–Blodgett Films

Langmuir–Blodgett films (LB films) are monolayers and multilayers of amphiphilic molecules transferred from the liquid–gas interface (commonly water–air interface) onto a solid substrate and the process is generally referred to as Langmuir–Blodgett technique (LB technique).[110] Langmuir carried out the first systematic study on monolayers of amphiphilic molecules at the water–air interface and the first study on a deposition of multilayers of long-chain carboxylic acid onto a solid substrate was carried out.[111]

Before discussing in more detail about the LB films, let us briefly review what is the amphiphile. The amphiphile is a molecule that is insoluble in

water, with one end that is hydrophilic, and therefore is preferentially immersed in the water and the other that is hydrophobic and preferentially resides in the air or in the nonpolar solvent. A classical example of an amphiphile is stearic acid, $C_{17}H_{35}CO_2H$. In this molecule, the long hydrocarbon tail, $C_{17}H_{35}$ — is hydrophobic, and the carboxylic acid head group, $-CO_2H$ is hydrophilic. Since the amphiphiles have one end that is hydrophilic and the other that is hydrophobic, they like to locate in interfaces such as between air and water, or between oil and water. This is the reason they are also called surfactants. However, it should be noted that the solubility of an amphiphilic molecule in water depends on the balance between the alkyl chain length and the strength of its hydrophilic head. Certain strength of the hydrophilic head is required to form LB films. If the hydrophilicity is too weak, no LB film can be formed. However, if the strength of the hydrophilic head is too strong, the amphiphilic molecule is too soluble in water to allow the formation of a monolayer. Table 5.6 summarizes the properties of different head groups.[112] The soluble amphiphile molecules may form micelles in water when their concentration exceeds their critical micellar concentration, which will be discussed further in the synthesis of ordered mesoporous materials in the next chapter.

The LB technique is unique, since monolayers can be transferred to many different substrates. Most LB depositions have involved hydrophilic substrates where the monolayers are transferred in the retraction mode.[113] Glass, quartz and other metal substrates with an oxidized surface are used as substrate, but silicon wafer with a surface of silicon dioxide is the most commonly used substrate. Gold is an oxide-free substrate and also commonly used to deposit LB films. However, gold has a high surface energy ($\sim 1000\,mJ/m^2$) and is easily contaminated, which results in an uneven

Table 5.6. The effect of different functional groups on LB film formation of C_{16}-compounds.[112]

Very weak (no film)	*Weak (unstable film)*	*Strong (stable LB film)*	*Very strong (soluble)*
Hydrocarbon	$-CH_2OCH_3$	$-CH_2OH$	$-SO_3^-$
$-CH_2I$	$-C_6H_4OCH_3$	$-COOH$	$-OSO_3^-$
$-CH_2Br$	$-COOCH_3$	$-CN$	$-C_6H_4SO_4^-$
$-CH_2Cl$		$-CONH_2$	$-NR_4^+$
$-NO_2$		$-CH{=}NOH$	
		$-C_6H_4OH$	
		$-CH_2COCH_3$	
		$-NHCONH_2$	
		$-NHCOCH_3$	

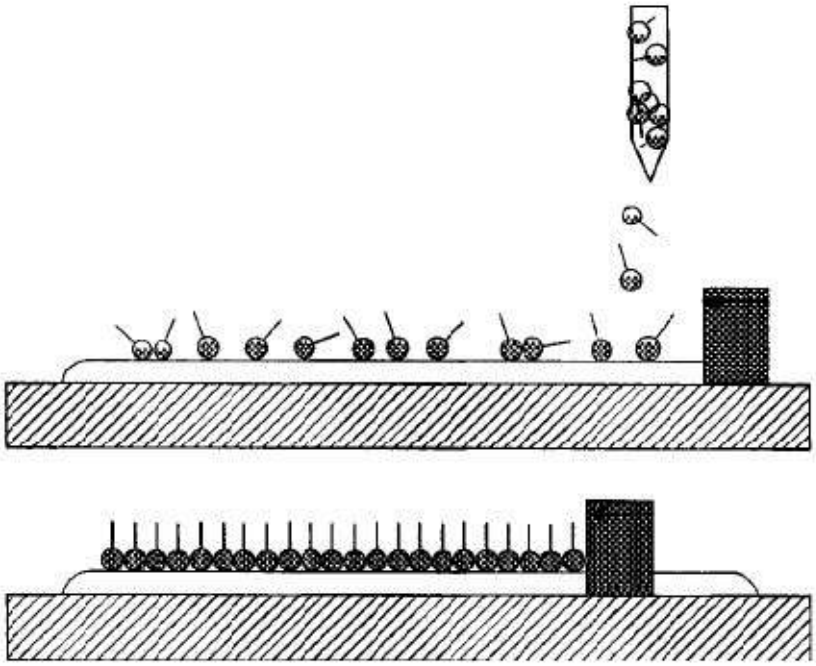

Fig. 5.23. Schematic showing the formation of Langmuir films, which denote the molecular films at the water–air interface, a drop of a dilute solution of an amphiphilic molecule in a volatile solvent, such as $CHCl_3$, is spread on the water–air interface of a trough.

quality of LB films. Cleanliness of the substrate surface is crucial to high quality LB films. In addition, the purity of the organic amphiphiles under study is of great importance, since any contamination in the amphiphile will be incorporated into the monolayer.

Figure 5.23 schematically shows the formation of Langmuir films, which denote the molecular films at the water–air interface, a drop of a dilute solution of an amphiphilic molecule in a volatile solvent, such as $CHCl_3$, is spread on the water–air interface of a trough. As the solvent evaporates, the amphiphilic molecules are dispersed on the interface. The barrier moves and compresses the molecules on the water–air interface; the intermolecular distance decreases and the surface pressure increases. A phase transition may occur, which is assigned to a transition from the "gas" to the "liquid" state. In the liquid state, the monolayer is coherent, except the molecules occupy a larger area than in the condensed phase. When the barrier compresses the film further, a second phase transition can be observed from the "liquid" to the "solid" state. In this condensed phase, the molecules are closely packed and uniformly oriented.

Two methods are commonly used to transfer monolayers from the water–air interface onto a solid substrate. The more conventional method is the vertical deposition as sketched in Fig. 5.24. When a substrate is moved through the monolayer at the water–air interface, the monolayer can be transferred during emersion (retraction or upstroke) or immersion

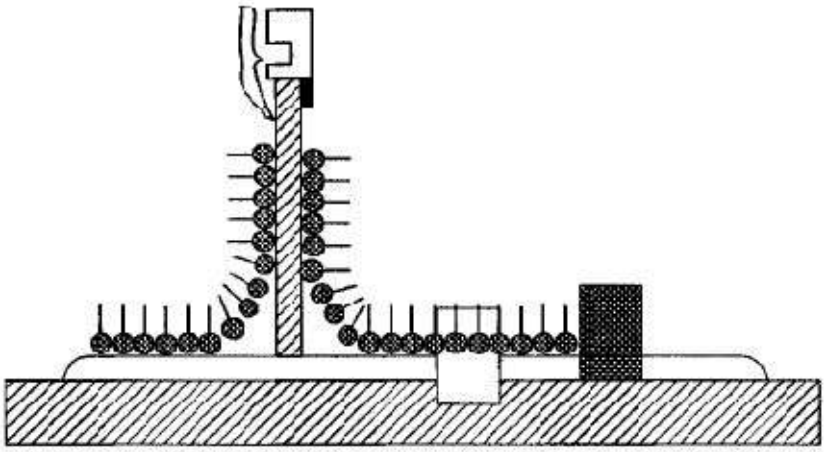

Fig. 5.24. The more conventional vertical deposition method for the formation of LB films on substrates.

(dipping or down stroke). A monolayer usually will be transferred during retraction when the substrate surface is hydrophilic, and the hydrophilic head groups interact with the surface. However, if the substrate surface is hydrophobic, the monolayer will be transferred in the immersion, and the hydrophobic alkyl chains interact with the surface. If the deposition process starts with a hydrophilic substrate, it becomes hydrophobic after the first monolayer transfer, and thus the second monolayer will be transferred in the immersion. Multiple layer films can be synthesized just by repeating the process. Figure 5.25 shows the film thickness proportionally increased with the number of layers.[114]

Another method to build LB multilayer structure is the horizontal lifting, also referred to as Schaefer's method. Schaefer's method is useful for the deposition of very rigid films. In this method as sketched in Fig. 5.26, a compressed monolayer is first formed at the water and air interface, a flat substrate is placed horizontally on the monolayer film. When the substrate is lifted and separated from the water surface, the monolayer is transferred onto the substrate.

Thermal stability and order–disorder transition are two important issues for any practical applications of LB films. Although a lot of research has been done in the past two decades, many issues remain unsolved and our understanding on the structures and stability of LB films is still very limited.

Self-assembly and LB technique offer the possibility of design and the construction of stable organic superlattices. For example, SA can be applied to assemble electron donor and electron acceptor groups, separated by well-defined distances — that can exchange electrons following optical excitation. This may allow the construction, for example, of an

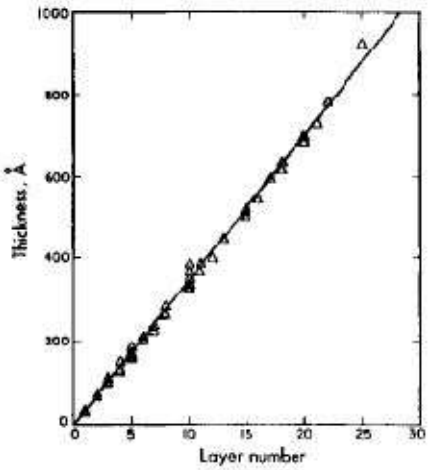

Fig. 5.25. Film thickness proportionally increased with the number of layers. [N. Tillman, A. Ulman, and T.L. Penner, *Langmuir* **5**, 101 (1989).]

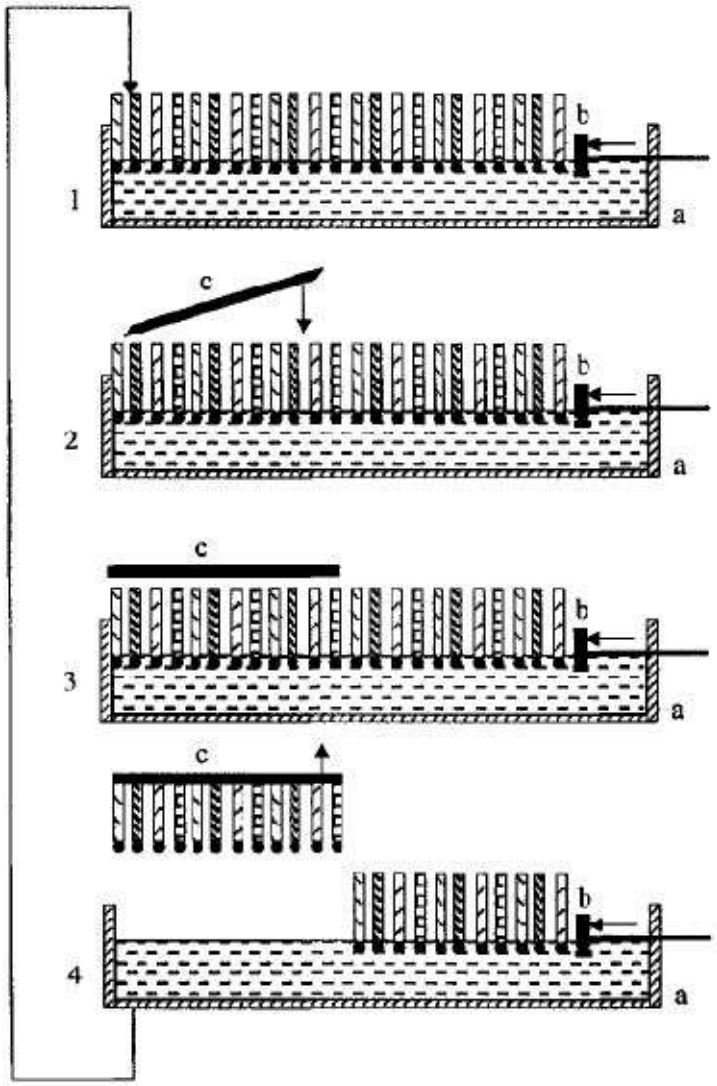

Fig. 5.26. Schaefer's method useful for the deposition of very rigid films, in which, a compressed monolayer is first formed at the water and air interface, a flat substrate is placed horizontally on the monolayer film.

electronic shift register memory based on molecular electron transfer reactions.[115]

5.10. Electrochemical Deposition

Electrochemical deposition or electrodeposition is a very well established thin film growth method. In the previous chapter, we discussed the growth of nanowires using this method, and some fundamentals of the process have been introduced already. In this section, our focus will be on the deposition of films. The key parameters in the electrodeposition of elemental films can be conveniently grouped into thermodynamic and kinetic considerations.

As discussed in the previous chapter, the electrochemical potential of a metal electrode, E, is given by the Nernst equation:

$$E = E_0 + \frac{R_g T}{n_i F} \ln a_i \tag{5.38}$$

where E_0 is the standard electrode potential, or the potential difference between the electrode and the solution, when the activity, a_i, of the ions is unity, F, the Faraday's constant, R_g, the gas constant and T, temperature. The Nernst equation represents an equilibrium state. When the electrochemical potential is deviated from its equilibrium value by, for example, applying an external electric field, either reduction (leading to deposition of solid) or oxidation (dissolution of solid) reaction will take place on the surface or metal electrode till a new equilibrium state is reached. The difference in potential is referred to as the over-potential or over-voltage. A careful control of over-potential is very important to avoid electrolysis of solvent or deposition of impurity phase. In addition, the interactions of the solute ion M^{m+} with the solvent, or with complex-forming ligands should be considered. These interactions and other factors such as the ionic strength of the solution must be carefully controlled. Besides thermodynamics, there are many kinetic factors that influence the deposition of elemental films. The rate of the electron transfer reaction, i.e. the oxidation–reduction kinetics, influences the nature and morphology of the deposit. The nucleation rate of crystals is a function of the over potential,[116] and also influences the nature of the deposit. In the case of a diffusion-limited deposition, the rate of mass transport of solute species to the electrode surface has great effect on the rate of deposition that can be achieved. Electrolyte agitation can lessen the diffusion layer thickness and favor rapid deposition, but maximum stable growth is generally produced in solutions of relatively high solute activity, high diffusion coefficient (low solution viscosity), and low growth velocity.[117] Dissociation kinetics of solvated or complex ions influences the metal ion

activity at the electrode surface and may limit the deposition rate that can be achieved for desired deposition morphology.

Electrodeposition of alloys and compounds is far more complex.[118–120] In alloy and compound electrodeposition, the equilibrium potentials of the alloy or compound components, the activities of the ions in solution, and the stability of the resultant deposit all are important thermodynamic considerations. For a compound M_nN_m, the conditions necessary to obtain the simultaneous deposition of two different kinds of ions at the cathode is:

$$E_M + \eta^m = E_N + \eta^n \tag{5.39}$$

where E_M and E_N are the respective equilibrium potentials of M and N, η^m and η^n are the over potentials required for electrodepositing M and N, respectively. Considering the fact that the activities of the metals M and N in the compound or alloy are determined by their concentrations in the solution and by the thermodynamic stability of the deposit, and often vary during deposition, it is very difficult to control deposit stoichiometry. In addition, control of ionic strength and solute concentration are important for uniform deposition.

For the growth of films by electrodeposition, a few practical concerns deserve a brief discussion here:

(1) Though aqueous solutions are often used, nonaqueous solvent or molten salts are also used. Electrolysis of water is one of the main reasons that nonaqueous solvent or molten salts are used.
(2) The electrical conductivity of the deposit must be high enough to permit the deposition of successive layers. The electrodeposition is therefore applied only for the growth of metal, semiconductors and conductive polymer films.
(3) Deposition can be accomplished at constant current or constant potential, or by other means, such as involving pulsed current or voltage.
(4) Post treatment may be employed to improve the characteristics of the deposits.

5.11. Sol-Gel Films

Sol-gel processing is widely used in the synthesis of inorganic and organic–inorganic hybrid materials and capable of producing nanoparticles, nanorods, thin films and monolith. In the previous chapters, we discussed the fabrication of nanoparticles and nanorods using sol-gel processing. A general introduction to sol-gel processing was presented in Chapter 3. For more detailed information, the readers are recommended to excellent books by Brinker and Scherer,[121] Pierre,[112] and Wright and

Sommerdijk.[123] Sol-gel methods for oxide coatings were reviewed by Francis.[124] Here we will focus our discussion only on the fundamentals and methods of the formation of sol-gel thin films. Prior to sol-gel transition or gelation, sol is a highly diluted suspension of nanoclusters in a solvent, and typically sol-gel films are made by coating sols onto substrates. Although some two-dozen methods are available for applying liquid coatings to substrates, the best choice depends on several factors including solution viscosity, desired coating thickness and coating speed.[125] Most commonly used methods for sol-gel film deposition are spin- and dip-coatings,[126,127] though spray and ultrasonically pulverized spray were also used.[128,129]

In dip-coating, a substrate is immersed in a solution and withdrawn at a constant speed. As the substrate is withdrawn upward, a layer of solution is entrained, and a combination of viscous drag and gravitational forces determines the film thickness, H[130]:

$$H = c_1\left(\frac{\eta U_0}{\rho g}\right)^{\frac{1}{2}} \tag{5.40}$$

where η is the viscosity, U_0 the withdrawal speed, ρ the density of the coating sol, and c_1 is a constant. Figure 5.27 illustrates various stages of the dip-coating process.[131] It should be noted that the equation does not account for the evaporation of solvent and continuous condensation between nanoclusters dispersed in the sol as illustrated in Fig. 5.28.[132] However, the relationship between the thickness and the coating variables is the same and supported by

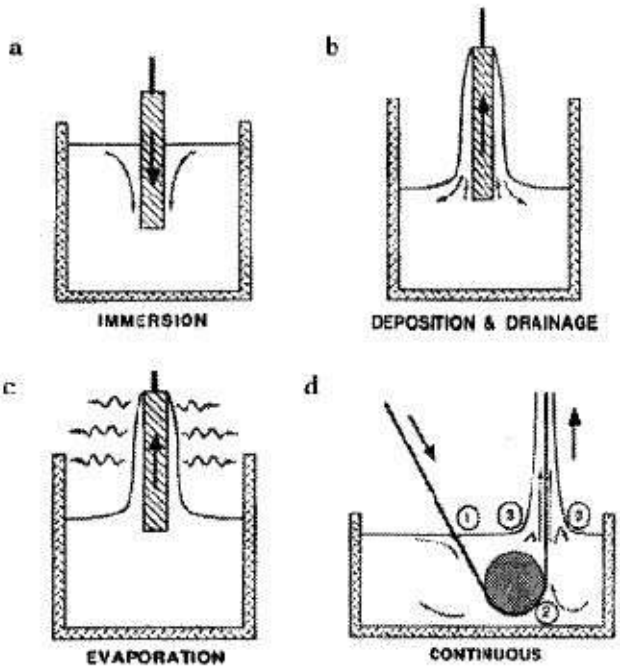

Fig. 5.27. Stages of the dip-coating process: (a–e) batch and (f) continuous. [L.E. Scriven, in *Better Ceramics Through Chemistry III*, eds. C.J. Brinker, D.E. Clark, and D.R. Ulrich, The Materials Research Society, Pittsburgh, PA, p. 717, 1988.]

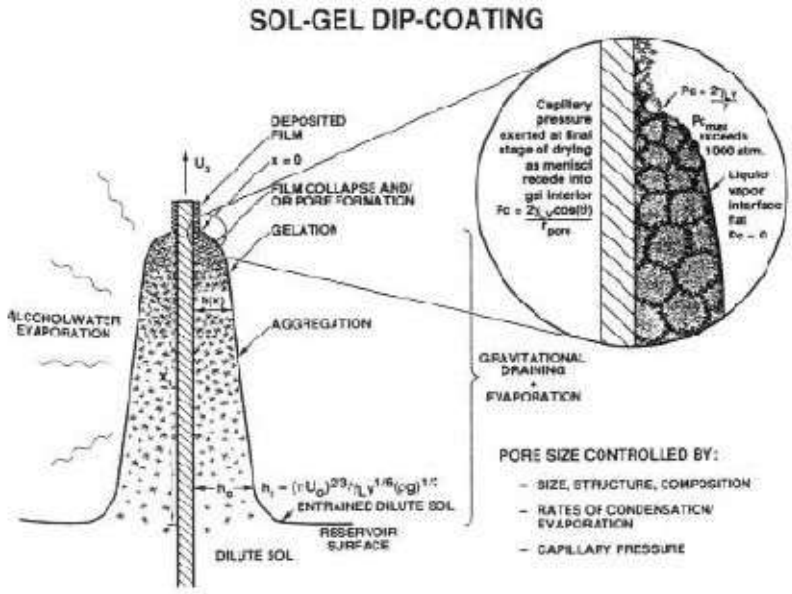

Fig. 5.28. Schematic showing the competing processes of evaporation of solvent and continuous condensation between nanoclusters dispersed in the sol during dip-coating. [C.J. Brinker and A.J. Hurd, *J. Phys. III* (Fr.) **4**, 1231 (1994).]

the experimental results,[133] but the proportionality constant is different. The thickness of a dip-coated film is commonly in the range of 50–500 nm,[134] though a thinner film of ~8 nm per coating was also reported.[135]

Spin-coating is used routinely in microelectronics to deposit photoresists and specialty polymers and has been well studied.[136,137] A typical spin coating consists of four stages: delivery of solution or sol onto the substrate center, spin-up, spin-off and evaporation (overlaps with all stages). After delivering the liquid to the substrate, centrifugal forces drive the liquid across the substrate (spin-up). The excess liquid leaves the substrate during spin off. When flow in the thin coating is no longer possible, evaporation takes over to further reduce the film thickness. A uniform film can be obtained when the viscosity of the liquid is not dependent on shear rate (i.e. Newtonian) and the evaporation rate is independent of position. The thickness of a spin-coated film, H, is given by[138]

$$H = \left(1 - \frac{\rho_A^\circ}{\rho_A}\right)\left(\frac{3\eta e}{2\rho_A^\circ \omega^2}\right) \tag{5.41}$$

where ρ_A is the mass of volatile solvent per unit volume, ρ_A° its initial volume, ω the angular velocity, η the liquid viscosity, and e the evaporation rate, which is related to the mass transfer coefficient. It is clear from the equation that the film thickness can be controlled by adjusting the solution properties and the deposition conditions.

In the process of creating a sol-gel coating, the removal of solvent or drying of the coating proceeds simultaneously with continuous condensation

and solidification of the gel network. The competing processes lead to capillary pressure and stresses induced by constrained shrinkage, which result in the collapse of the porous gel structure, and may also lead to the formation of cracks in the resultant films. The drying rate plays a very important role in the development of stress and formation of cracks particularly in the later stages and depends on the rate at which solvent or volatile components diffuse to the free surface of the coating and the rate at which the vapor is transported away in the gas.

Stress develops during drying of a solidified coating due to constrained shrinkage. Solvent loss after solidification is a common source of stress in solvent-cast polymer coatings and Croll defines such a stress as[139,140]:

$$\sigma = \frac{E(\sigma)\,(\phi_s - \phi_r)}{(1-\nu)3(1-\phi_r)} \tag{5.35}$$

where $E(\sigma)$ is a nonlinear elastic modulus and ν the Poisson's ratio of the coating, ϕ_s and ϕ_r are the volume fractions of solvent at solidification and residual after drying, respectively. The relationship shows that solvent content at solidification should be minimized to lower the stress in the coating. In the formation of sol-gel coating, it is very important to limit the condensation reaction rate during the removal of solvent upon drying, so that the volume fraction of solvent at solidification is kept small. To relieve stresses, the material can relax internally by molecular motion or it can deform. Internal relaxation slows as the material approaches an elastic solid and deformation is restricted by adherence to the substrate. Since the stress-free state shrinks during solidification and adherence to the substrate confines shrinkage in the coating to the thickness direction, in-plane tensile stresses result. Cracking is another form of stress relief. For sol-gel coatings, the formation of cracks limits the coating thickness commonly less than 1 micron. A critical coating thickness, T_c, has been defined.[141,142]

$$T_c = \frac{EG_c}{A\sigma^2} \tag{5.36}$$

where E is the Young's modulus of the film, A is a dimenionless proportionality constant, and G_c the energy required to form two new crack surfaces. The concept of critical thickness is supported by experimental reports. For example, a critical thickness of 600 nm was reported in Ceria sol-gel films, and cracks formed above this thickness.[143]

It should also been noted that sol-gel coatings are commonly porous and amorphous. For many applications, subsequent heat treatment is required to achieve full densification and convert amorphous to crystalline. Mismatch of thermal expansion coefficients of sol-gel coatings and substrates is another important source of stress, and a residual stress in sol-gel coatings can be as high as 350 MPa.[144]

Organic–inorganic hybrids are a new type of materials, which are not present in nature, and sol-gel is the obliged route to synthesize them.[122,145] The organic and inorganic components can interpenetrate each other on a nanometer scale. Depending on the interaction between organic and inorganic components, hybrids are divided into two classes: (i) hybrids consisting of organic molecules, oligomers or low molecular weight polymers embedded in an inorganic matrix to which they are held by weak hydrogen bond or van der Waals force and (ii) in those, the organic and inorganic components are bonded to each other by strong covalent or partially covalent chemical bonds. The organic component can significantly modify the mechanical properties of the inorganic component.[146] The porosity can also be controlled as well as the hydrophilic and hydrophobic balance.[147] Hybrids with new optical[148,149] or electrical[150] properties can be tailored. Some hybrids can display new electrochemical reactions as well as special chemical or biochemical reactivity.[151,152]

Porosity is another important property of sol-gel film. Although for many applications, heat-treatment at elevated temperatures is employed to remove the porosity, the inherited porosity enables sol-gel film for many applications such as matrix of catalyst, host of sensing organic or biocomponents, electrode in solar cells. Porosity itself also renders other unique physical properties such as low dielectric constant, low thermal conductivity, etc. Organic molecules such as surfactants and diblock polymers have been used to form templates in the synthesis of ordered mesoporous materials, which will be another subject of discussion in the next chapter.

There are many other chemical solution deposition (CSD) methods. Fundamentals discussed above are generally applicable to other CSD methods. For example, the competing processes during drying, the development of stresses and the formation of cracks are similar to that in sol-gel films.

5.12. Summary

A variety of methods for thin film deposition has been summarized and briefly discussed. Although all the methods can make films with thickness less than 100 nm, they do offer varied degree of control of thickness and surface smoothness. Both MBE and ALD offer the most precise control of deposition at the single atomic level, and the best quality of the grown film. However, they suffer from the complicated deposition instrumentation and slow growth rate. Self-assembly is another method offering a single atomic level control; however, it is in general limited to the fabrication of organic or inorganic–organic hybrid thin films.

capillary force, which is the fundamental concept of using supercritical drying and is discussed above. Another is to manipulate the inbalance between the huge capillary force and the small mechanical strength of the gel network, so that the gel network is strong enough to resist the capillary force during the removal of solvent. Organic components is incorporated into inorganic gel network to change the surface chemistry of the silica gel network and, thus, to minimize the capillary force and prevent the collapse of gel network. Organic components can be introduced through either copolymerization with organic components introduced in the form of organic precursor,[137,138] or self-assembly with solvent exchange.[139] The incorporation of organic components into silica gel network resulted in the formation of highly porous silica under ambient conditions, with a porosity of 75% or higher and a specific surface area of 1000 m^2/g. Organic aerogels can be made by polymerizing organic precursors and subsequent supercritical drying of aged wet gels. The most extensively studied organic aerogels are the resorcinol-formaldehyde (RF) and formaldehyde (MF) aerogels.[140,141] Carbon aerogels are formed by pyrolysis of organic aerogels, typically at temperatures above 500°C. Carbon aerogels retain the high surface area and pore volume of their parent organic aerogels.[142]

6.3.3. *Crystalline microporous materials: zeolites*

Zeolites are crystalline aluminosilicates and were first discovered in 1756.[143,144] There are 34 naturally occurring zeolites and nearly 100 synthetic type zeolites. A zeolite has a three-dimensional framework structure with uniformly sized pores of molecular dimensions, typically ranging from ~0.3 to 1 nm in diameter, and pore volumes vary from about 0.1 to 0.35 cc/g. Zeolites have a broad diverse spectrum of applications, and examples include catalysts, adsorbents and molecular sieves. Many review articles and books have been published.[145–147] Details of the structures and specific names of various zeolites have been summarized in literature.[148–150] Only a brief description is given below.

Zeolites are tectoaluminosilicates with a formal composition $M_{2/n}O{\cdot}Al_2O_3{\cdot}xSiO_2{\cdot}yH_2O$ (n = valence state of the mobile cation, M^+ and $x \geq 2$), in that they are composed of TO_4 tetrahedra (T = tetrahedral atom, i.e. Si, Al), each oxygen atom is shared between adjacent tetrahedral, which leads to the framework ratio of O/T being equal to 2 for all zeolites.[151] A dimensional framework is formed by 4-corner connecting TO_4 tetrahedra. When a zeolite is made of pure silica without any defects, each

oxygen atom at the corner is shared by two SiO_4 tetrahedra and the charge is balanced. When silicon is replaced by aluminum, alkali metal ions, such as K^+, Na^+, alkaline earth ions, such as Ba^{2+}, Ca^{2+}, and protons, H^+ are typically introduced to balance the charges. Such a framework formed is relatively open and characterized by the presence of channels and cavities. The size of the pores and the dimensionality of the channel system are determined by arrangement of TO_4 tetrahedra. More specifically, the pore sizes are determined by the size of the rings that are formed by connecting various numbers of TO_4 tetrahedra or *T* atoms. An 8-ring is designated to a ring comprised of 8 TO_4 tetrahedra and is considered to be a small pore opening (0.41 nm in diameter), a 10-ring medium one (0.55 nm), and a 12-ring large one (0.74 nm), when rings are free of distortion. Depending on the arrangement or the connection of various rings, different structures or pore openings, such as cages, channels, chains and sheets, can be formed. Figure 6.12 shows some of these subunits, in which each cross point is designated to a TO_4 tetrahedron for clarity.[150] In this figure, the designations in terms of the *n*-rings defining the faces of these subunits are also included. For example, a cancrinite cage subunit is defined by six 4-rings

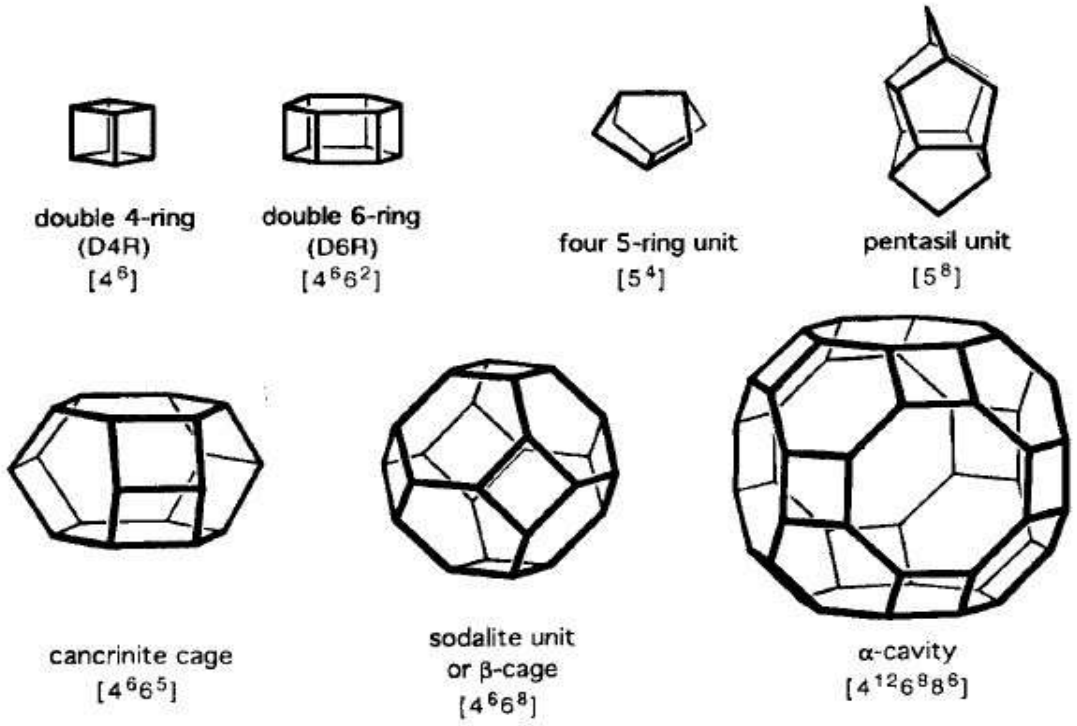

Fig. 6.12. Some subunits and cages that recur in several framework types of zeolites; each cross point is designated to a TO_4 tetrahedron where *T* is a metal such as silicon or aluminum. [L.B. McCusker and C. Baerlocher, in *Introduction to Zeolite Science and Practice*, 2nd edition, eds., H. van Bekkum, E.M. Flanigen, P.A. Jacobs, and J.C. Jansen, Elsevier, Amsterdam, p. 37, 2001.]

and five 6-rings, and is thus designated a $[4^6 6^5]$ cage. A nomenclature similar to that used for cages has also been developed to describe channels, chains and sheets. Different frameworks are formed by stacking various subunits and/or with different stacking sequences. There are 133 confirmed zeolite framework types. Figure 6.13 shows two schematics of zeolite frameworks: SOD and LTA framework types.[150]

Zeolites are normally prepared by hydrothermal synthesis techniques.[152,153] A typical synthesis procedure involves the use of water, a silica source, an alumina source, a mineralizing agent and a structure-directing agent. The sources of silica are numerous and include colloidal silica, fumed silica, precipitated silica and silicon alkoxides. Typical alumina sources include sodium aluminate, boehmite, aluminum hydroxide, aluminum nitrate and alumina. The typical mineralizing agent is hydroxyl ion, OH^- and fluorine ion, F^-. The structure-directing agent is a soluble organic species, such as quaternary ammonium ion, which assists in the formation of the silica framework and ultimately resides within the intracrystalline voids. Alkali metal ions can also play a structure-directing role in the crystallization process. Table 6.4 lists the reactants, synthesis temperatures, and the physical and chemical properties of zeolites Na-A and TPA-ZSM-5.[153] Figure 6.14 gives SEM images of a few zeolites.[153]

The syntheses can be sensitive to the reagent type, the order of addition, the degree of mixing, the crystallization temperature and time and the composition. There are numerous complex chemical reactions and organic–inorganic interactions occurring during the synthesis process.

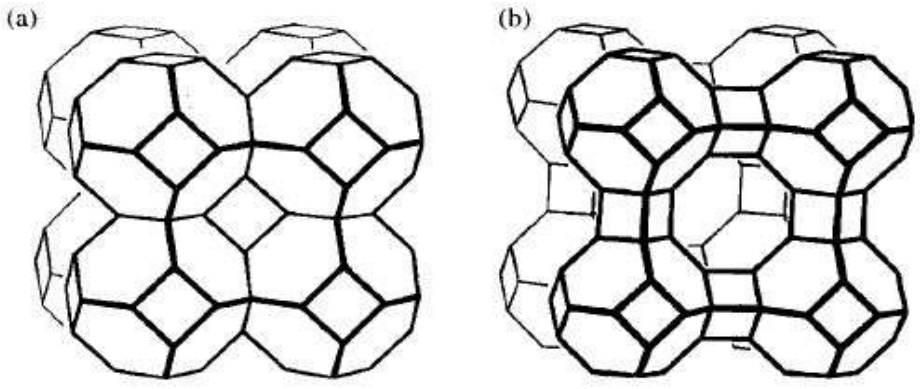

Fig. 6.13. (a) The SOD framework type, having a body centered cubic arrangement of β or sodalite cages (see Fig. 6.12). (b) The LTA framework type with a primitive cubic arrangement of α-cages joined through single 8-rings (producing a sodalite cage in the center). [L.B. McCusker and C. Baerlocher, in *Introduction to Zeolite Science and Practice*, 2nd edition, eds. H. van Bekkum, E.M. Flanigen, P.A. Jacobs, and J.C. Jansen, Elsevier, Amsterdam, p. 37, 2001.]

Table 6.4. Synthesis mixtures (in molar ratio), physical and chemical properties of zeolites Na-A and TPA-ZSM-5.[153]

Materials & properties	*Na-A*	*TPA-SZM-5*
SiO_2	1	1
Al_2O_3	0.5	<0.14
Na_2O	1	0.16
TPA_2O	–	0.3
H_2O	17	49
T (°C)	<100	<150
Pore structure	3D, cages linked via windows	2D, intersecting channels
Density (g/cm^3)	1.28	1.77
Pore volume (cm^3/g)	0.37	0.18
Lattice stabilization	Na^+, H_2O	TPA^-
Si/Al ratio	1	0.12
Bronsted activity	Low	High
Affinity	Hydrophilic	Hydrophobic

Depending on the mixture composition, the extent of reactions and the synthesis temperature, at least four types of liquids can be yielded[153]:

(i) Clear solution that consists of molecular, monomeric and ionic species only,
(ii) Sol or colloidal consisting of amorphous clusters with open structure (also called dispersed low density gel),
(iii) Sol or colloidal with dispersed amorphous clusters with dense structure (also referred to as separated high density gel), and
(iv) Sol or colloidal with metastable crystalline solid nanoparticles (also called solid phase).

Zeolites are subsequently formed through nucleation and crystallization from these systems. Various studies have been carried out to establish an understanding on the crystal growth mechanisms at the molecular level and the crystal-building units.[152,153] At least three types of crystal building units have been suggested for the growth of zeolites: (i) tetrahedral monomeric species are considered as the primary building units, (ii) secondary building units are the crystal building units, and (iii) clathrates are the building units in the nucleation and crystallization of zeolites. Two recent synthesis models are outlined below. Figure 6.15 illustrates the mechanism of structure direction and crystal growth in the synthesis of TPA-Si-ZSM-5 proposed by Burkett and Davis.[154] During the synthesis, the inorganic–organic composite clusters are first formed by overlapping the hydrophobic hydration spheres of the inorganic and organic components and subsequent releasing of ordered water to establish favorable

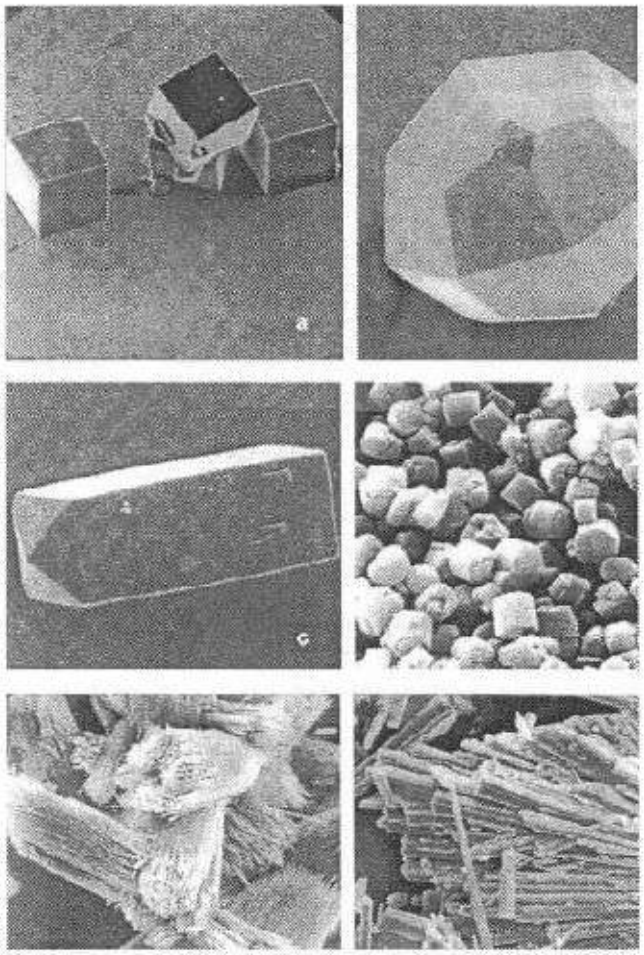

Fig. 6.14. SEM images showing the crystalline nature of zeolites. Single crystals of (a) zeolite A, (b) analcime, and (c) natrolite. (d) A batch of zeolite L and (e) typical needle aggregates of zeolite mordenite. [J.C. Jansen, in *Introduction to Zeolite Science and Practice*, 2nd edition, eds. H. van Bekkum, E.M. Flanigen, P.A. Jacobs, and J.C. Jansen, Elsevier, Amsterdam, p. 175, 2001.]

van der Waals interactions. Such inorganic–organic composite clusters serve as growth species for both initial nucleation and subsequent growth of zeolite crystals. The nucleation occurs through epitaxial aggregation of these composite clusters, whereas the crystal growth proceeds through diffusion of the same species to the growing surface to give a layer-by-layer growth mechanism. Another mechanism, called "nanoslab" hypothesis,[155] builds on the mechanism discussed above. The difference is that the inorganic–organic composite clusters form "nanoslabs" through epitaxial aggregation first. Such formed "nanoslabs" aggregates with other "nanoslabs" to form bigger slabs as shown in Fig. 6.16.[155]

Effects of structure-directing agent. When different organic molecules as structure-directing agents are included in an otherwise identical synthesis mixture, zeolites with completely different crystal structures can

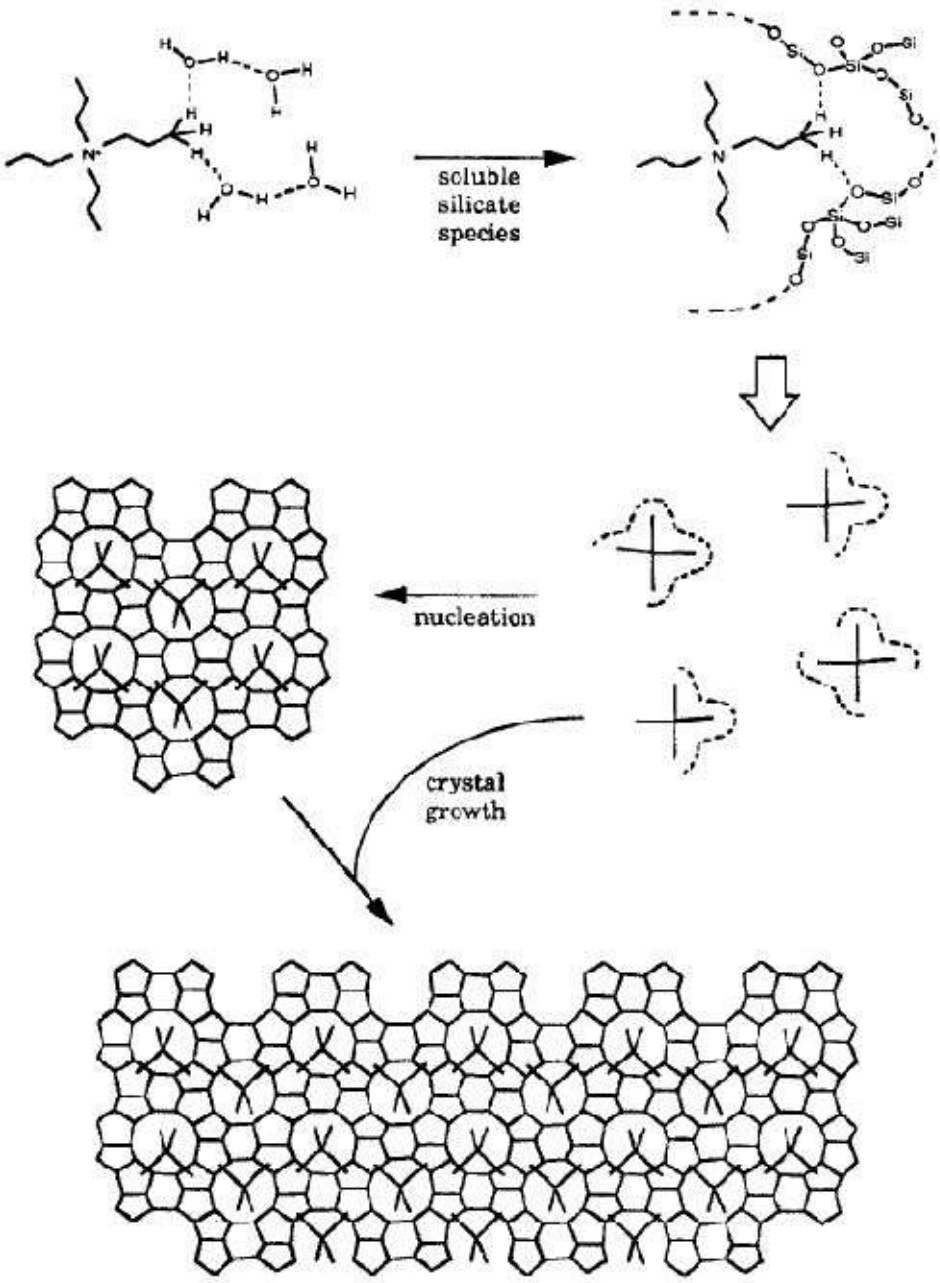

Fig. 6.15. Mechanism of structure-direction crystal growth involving organic–inorganic composites in the synthesis of pure-silica ZSM-5 zeolite using TPA$^+$ as structure-directing agent. [S.L. Burkett and M.E. Davis, *J. Phys. Chem.* **98**, 4647 (1994).]

be formed. For example, when N,N,N-trimethyl 1-adamantammonium hydroxide is used as a structure-directing agent, zeolite SSZ-24 was formed, while ZSM-5 was produced by using tetrapropylammonium hydroxide as structure-directing agent. In addition, the choice of a structure-directing agent can affect the synthesis rate.[156]

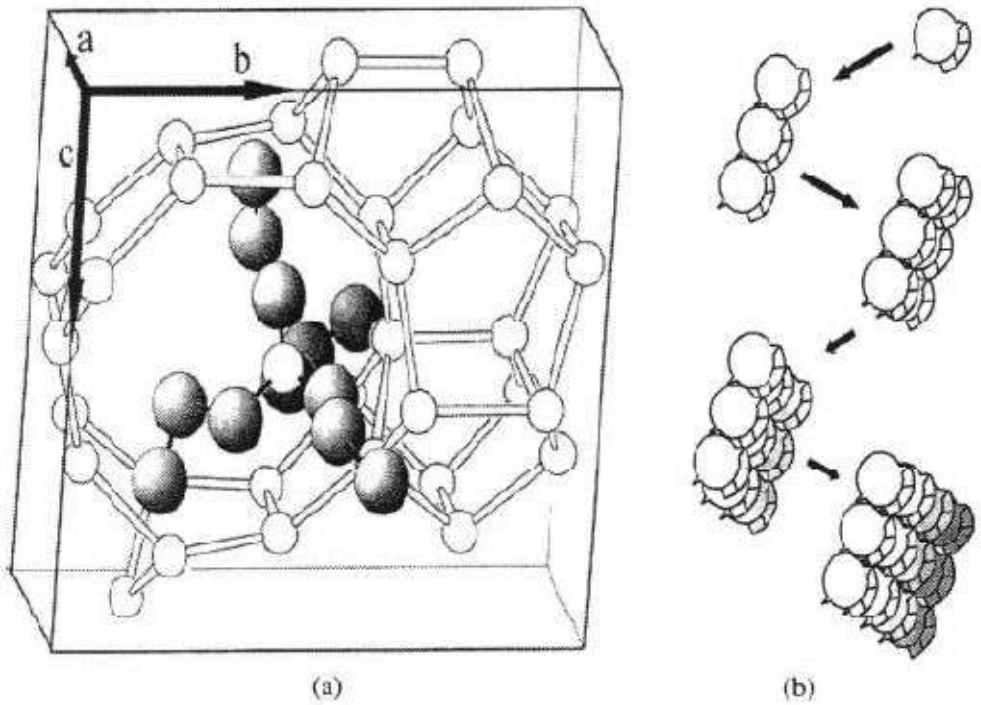

Fig. 6.16. The "nanoslab" hypothesis: (a) the precursor unit containing one TPA cation and (b) schematic representation of nanoslab formation by aggregation of precursor units. [C.E.A. Kirschhock, R. Ravishankar, L. Van Looveren, P.A. Jacobs, and J.A. Martens, *J. Phys. Chem.* **B103**, 4972 (1999).]

The geometry of the structure-directing agent has a direct impact on the geometry of the zeolite synthesized. For example, SSZ-26 is a zeolite with intersecting 10- and 12-ring pores,[157] and was synthesized with *a priori* design using a propellane-based structure-directing agent.[158] It has been demonstrated experimentally and through molecular force field calculations that the geometry of the pore sections of SSZ-26 matches very well with that of the organic structure-directing molecules and one structure-directing molecule is present at each channel intersection.[159] ZSM-18 is an aluminosilicate zeolite containing 3-member rings[160] and was synthesized using structure-directing agent what was designed using molecular modeling.[161] An excellent fit exists between the zeolite cage and the organic structure-directing agent.

Effects of heteroatoms. The addition of small quantities of tetrahedral cations, such as Al, Zn, B etc., to the synthesis mixtures has dramatic effects and results in significantly different zeolite structures when using identical structure-directing agents.[162] Table 6.5 compares some systems.[144] For example, when other synthesis parameters are kept the same with tetraethylammonium cation, TEA^+, as a structure-directing agent, ZSM-12 is formed when the ratio of SiO_2 to Al_2O_3 is greater than 50. When a small amount of alumina is added, zeolite beta is formed. Further

Table 6.5. Effect of aluminum, boron and zinc on the structure of zeolites or other compounds obtained using organic structural-directing agents.[144]

Organic agent	SiO_2	SiO_2/Al_2O_3 <50	SiO_2/B_2O_3 <30	SiO_2/ZnO <100
$C_8H_{20}N$	ZSM-12	Zeolite Beta	Zeolite Beta	VPI-8
$C_{16}H_{32}N_4$	ZSM-12	Zeolite Beta	Zeolite Beta	VPI-8
$C_{13}H_{24}N^*$	ZSM-12	Mordenite	Zeolite Beta	Layered Mater.
$C_{13}H_{24}N^*$	SSZ-24	SSZ-25	SSZ-33	–
$C_{13}H_{24}N^*$	SSZ-31	Mordenite	SSZ-33	VPI-8
$C_{12}H_{20}N$	SSZ-31	SSZ-37	SSZ-33	–

* with different molecular structures

addition of alumina to reach a ratio of 15 of SiO_2/Al_2O_3, ZSM-20 is then synthesized. The substitution of divalent and trivalent tetrahedral cations for Si^{4+} in the synthesis mixtures results in a negatively charged zeolite framework, which will coordinate more strongly with both the organic structure-directing cations and the inorganic cations, such as alkali metal cations. In addition, the change of both the cation-oxygen bond lengths and the cation-oxygen-cation bond angles would have appreciable influences on the formation of building units.[163]

Effects of alkali metal cations. The presence of alkali metal cations is required for the vast majority of zeolite syntheses at basic conditions.[164] A small concentration of alkali metal cations in aqueous solutions significantly increases the dissolution rate of quartz, up to 15 times as much as the rate in deionized water.[165,166] It is generally accepted that the presence of alkali metal cations can accelerate the rate of nucleation and crystal growth of high-silica zeolites.[164,167] However, it was also found that too much alkali metal cations may result in competition with the organic structure-directing agent for interactions with silica to result in layer-structured products.[168]

Organic–inorganic hybrid zeolites. Recently Yamamoto *et al.*[169] succeeded in synthesis of organic–inorganic hybrid zeolites that contain an organic framework by partially superseding a lattice oxygen atom by a methylene group. Such hybrid zeolites are significantly different from the zeolites containing pendant organic groups.[170] The use of methylene-bridged organosilane as a silicon source gives zeolite materials containing an organic group as lattice, with several zeolitic phases such as the MFI and the LTA structures. In such hybrid zeolites, some of siloxane bonds, Si–O–Si, are replaced by methylene frameworks, $Si–CH_2–Si$.

6.4. Core-Shell Structures

In Chapter 3, we have discussed the synthesis of heteroepitaxial semiconductor core-shell structure. Although the chemical compositions of the core and shell are different, they possess similar crystal structure and lattice constants. Therefore, the formation of the shell material on the surface of grown nanometer sized particle (the core) is an extension of particle growth with different chemical composition. The core-shell structures to be discussed in this section are significantly different. First, the core and shell often have totally different crystal structures. For example, one can be single crystal and another amorphous. Secondly, the physical properties of core and shell often differ significantly from one another; one may be metallic and another dielectric. Furthermore, the synthesis processes of cores and shells in each core-shell structure are significantly different Although a variety of core-shell structures can be fabricated by various techniques, such as coating, self-assembly, and vapor phase deposition, the discussion in this section will be focused mainly on the core-shell structures of novel metal-oxide, novel metal-polymer, and oxide-polymer systems mostly by solution methods. Further, a monolayer of molecules assembled on the surface of nanoparticles will not be included in the following discussion. Polymer monolayers are often used to induce the diffusion-controlled growth and stabilize the nanoparticles, which has been already discussed in Chapter 3. Self-assembly of molecular monolayers has been one of the topics discussed in the previous chapter.

6.4.1. *Metal-oxide structures*

We shall take gold–silica core-shell structure as an example to illustrate the typical experimental approaches.[171,172] Gold surface has very little electrostatic affinity for silica, since gold does not form a passivation oxide layer in solution, and thus no silica layer will form directly on the particle surface. Furthermore, there are usually adsorbed organic monolayers on the surface to stabilize the particles against coagulation. These stabilizers also render the gold surface vitreophobic. A variety of thioalkane and aminoalkane derivatives may be used to stabilize gold nanoparticles.[173] However, for the formation of core-shell structures, the stabilizers are not only needed to stabilize the gold nanoparticle by forming a monolayer on the surface, but also required to interact with silica shell. One approach is to use organic stabilizers with two functionalities at two ends. One would link to gold particle surface and the other to silica

shell. The simplest way to link to silica is to use silane coupling agents.[174] (3-aminopropyl)trimethoxysilane (APS) has been the most widely used complexing agent to link gold core with silica shell.

Figure 6.17 sketched the principal procedures of fabricating gold–silica core-shell structures. There are typically three steps. The first step is to form the gold cores with desired particle size and size distribution. The second step is to modify the surface of gold particle from vitreophobic to vitreophilic through introducing an organic monolayer. The third step involves the deposition of oxide shell. In the first developed fabrication process,[171,172] gold colloidal dispersion is first prepared using the sodium citrate reduction method,[175] resulting in the formation of a stable colloidal solution with gold nanoparticles of ~15 nm and 10% dispersity.

In the second step, a freshly prepared aqueous solution of APS (2.5 mL, 1 mM) is added to 500 mL of gold colloidal solution under vigorous stirring for 15 min. A complete coverage of one monolayer of APS is formed on the gold particle surface. During this process, the previously adsorbed, negatively charged citrate groups are displaced by APS molecules, with the silanol groups pointing into solution. The process is driven by the large complexation constant for gold amines. The silane groups in APS molecules in aqueous solution undergo rapid hydrolysis and convert to silanol groups, which may react with one another through condensation reactions to form three-dimensional network. However, the rate of condensation reaction is rather slow at low concentration.[174] It should also be noted that during the self-assembly of APS on the surface of gold particles, the pH needs to be maintained above the isoelectric point of silica, which is 2–3,[176] so that the silanol groups is negatively charged. In addition, the pH is required to ensure the adequate negative surface charge on the gold

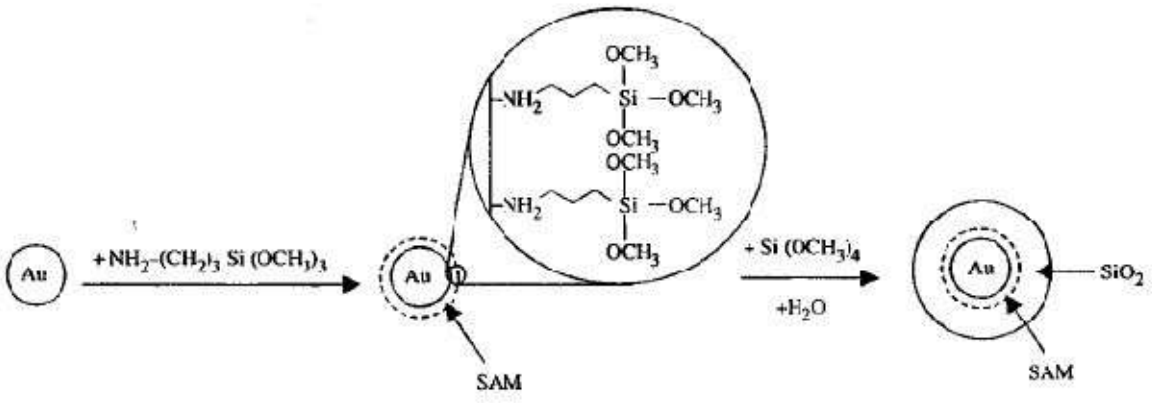

Fig. 6.17. Principal procedures for the formation of gold–silica core-shell structures. (a) Formation of monosized gold particles, (b) modifying the surface of gold nanoparticles by introducing a monolayer of organic molecules through self-assembly, and (c) deposition of silica shell. [L.M. Liz-Marzán, M. Giersig, and P. Mulvaney, *Langmuir* **12**, 4329 (1996).]

nanoparticles, so that the positively charged amino groups are attracted to the gold surface.

In the third step, a silica sol prepared by slowly reducing the pH of a 0.54 wt% sodium silicate solution to 10–11 is added to the gold colloidal solution (with a resulting pH of ~8.5) under vigorous stirring for at least 24 hours. A layer of silica of 2–4 nm thick is formed on the modified surface of the gold nanoparticles. In this step, slow condensation or polymerization reaction is promoted by controlling the pH, so that the formation of a thin, dense and relatively homogeneous silica layer around the gold particle can be produced.[176,177] Further growth of the silica layer was achieved by transferring the core-shell nanostructures to ethanol solution and by controlling the growth condition such that further growth of silica layer would be diffusion predominant, which is often referred to as Stöber method.[178] Figure 6.18 shows TEM images of gold–silica core-shell nanostructure.[172]

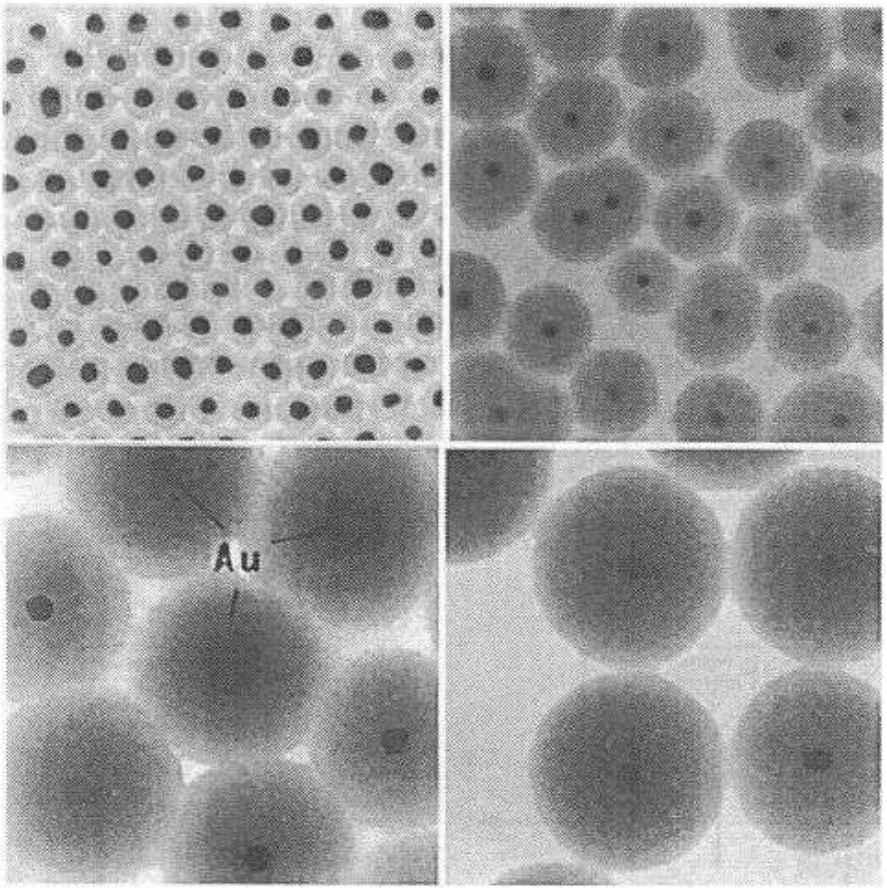

Fig. 6.18. TEM Images of silica-coated gold particles produced during the extensive growth of the silica shell around 15 nm Au particles with TES in 4 : 1 ethanol/water mixtures. The shell thicknesses are (a, top left) 10 nm, (b, top right) 23 nm, (c, bottom left) 58 nm, and (d, bottom right) 83 nm. [L.M. Liz-Marzán, M. Giersig, and P. Mulvaney, *Langmuir* **12**, 4329 (1996).]

6.4.2. *Metal–polymer structures*

Emulsion polymerization is one of the widely used strategies for the creation of metal–polymer core-shell structures.[179] For example, silver-polystyrene/methacrylate core-shell structures were prepared by emulsion polymerization of styrene and/or methacrylic acid in oleic acid. In this system, silver particles are coated with a uniform and well-defined layer with thickness ranging 2–10 nm.[180] The thickness of the layer can be readily controlled by changing the concentrations of monomers. Further etching tests in concentrated chloride solutions revealed that the polymer coatings have a strong protection effect.

Another example of the formation of metal–polymer core-shell structures is membrane-based synthesis.[181–183] In this method, the metal particles are first trapped and aligned inside the pores of membranes by vacuum filtration and then the polymerization of conducting polymers inside the pores are followed as schematically illustrated in Fig. 6.19.[183] A porous alumina membrane with a pore size of 200 nm was used to trap gold nanoparticles, $Fe(ClO_4)_3$ was used as polymerization initiator and poured on top of the membrane. Several drops of pyrrole or N-methylpyrrole were placed underneath the membrane. Upon diffusion of the monomer molecules as a vapor inside the pores, it contacted with the initiators and formed polymer. The deposition of polymer was found to preferentially occur on the surface of the gold nanoparticles. The thickness of polymer shell can be controlled by the polymerization time and can be easily varied from 5 nm to 100 nm. However, further polymerization time resulted in the formation of aggregated core-shell structures. Figure 6.20 shows the

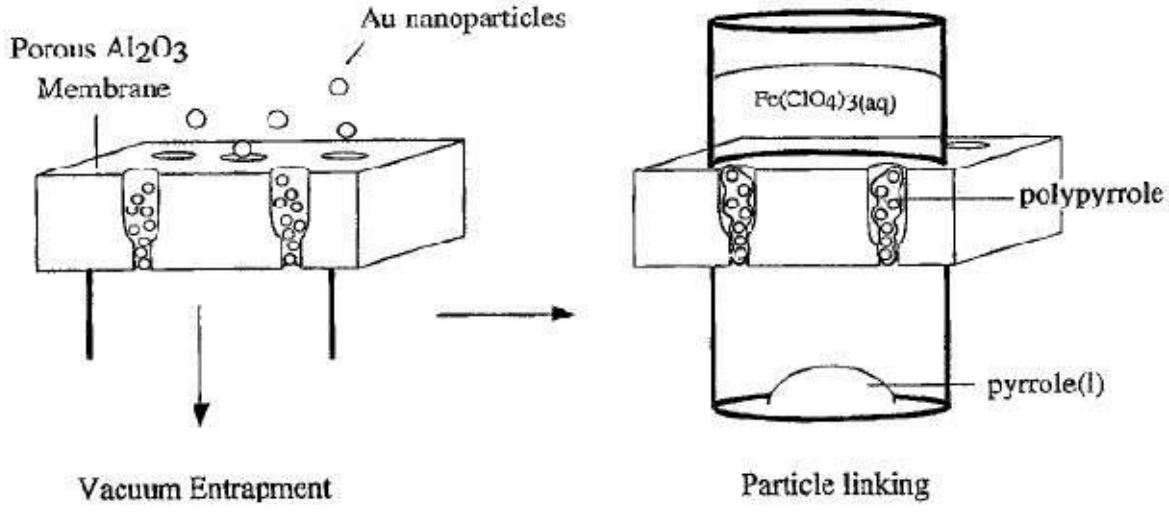

Fig. 6.19. Schematic representing the fabrication procedures of metal-polymer core-shell structures. [S.M. Marinakos, D.A. Shultz, and D.L. Feldheim, *Adv. Mater.* **11**, 34 (1999).]

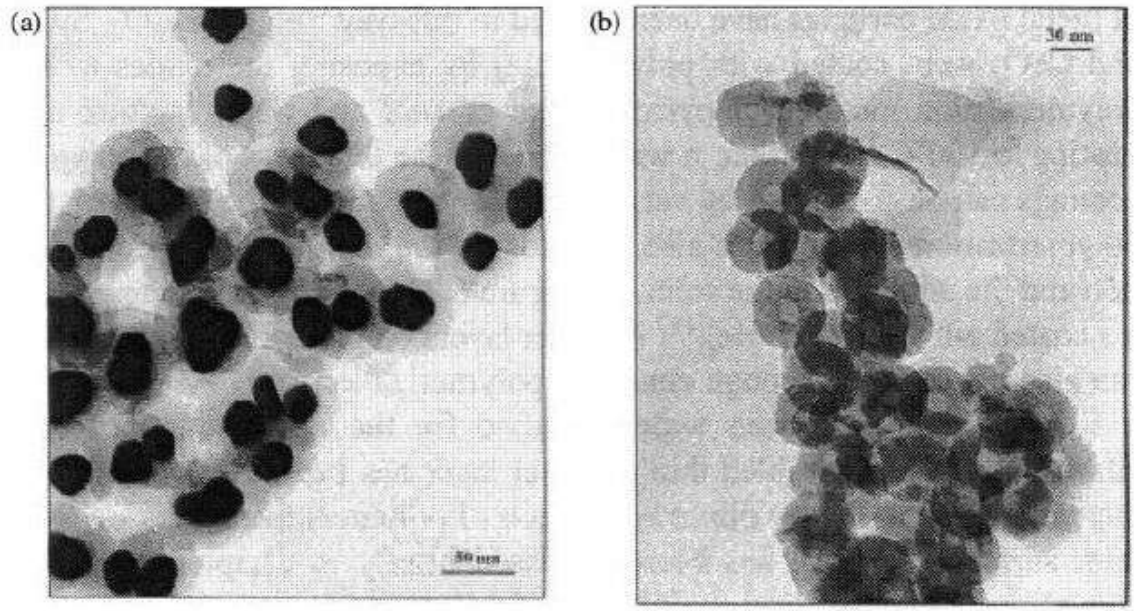

Fig. 6.20. TEM images of the gold-poly(pyrrole) and composite poly(N-methylpyrrole)/poly(pyrrole) core-shell structures: (a) ~30 nm diameter gold particles coated with Ppy and (b) polymer shell after the removal of Au with a mixture of 0.002 M $K_4[Fe(CN)_6]$ and 0.1 M KCN. [S.M. Marinakos, D.A.Shultz, and D.L. Feldheim, *Adv. Mater.* **11**, 34 (1999).]

TEM images of the gold-poly(pyrrole) and composite poly(N-methylpyrrole)/poly(pyrrole) core-shell structures.[183]

6.4.3. *Oxide–polymer structures*

The synthetic routes to produce polymer-coated oxide particles can be grouped into two main classes: polymerization at the particle surface or adsorption onto the particles.[184,185] Polymerization-based methods include monomer adsorption onto particles followed by subsequent polymerization[181,182,186] and emulsion polymerization.[179,180] In the adsorption and polymerization of monomer approach, the polymerization can be activated by either the addition of an initiator or the oxide itself. For example, the coating of aluminum hydrous oxide modified silica particles with poly(divinylbenzene) (PDVB) layers was prepared by pre-treatment of the silica particles with coupling agents such as 4-vinylpyridine or 1-vinyl-2-pyrrolidone, followed by subsequent admixing of divinylbenzene and a radical polymerization initiator.[187] The similar approach can be used to synthesize polymer layers of poly(vinylbenzene chloride) (PVBC), copolymers of PDVB–PVBC, and double shells of PDVB and PVBC.[188] Polymerization of adsorbed monomers can also be initiated by the surface sites of oxide nanoparticles. For example, poly(pyrrole) coatings on a range

of metal oxide particles have been formed in this way.[186,189] α-Fe_2O_3, SiO_2, and CeO_2 were coated with poly(pyrrole) by exposing the oxides to the polymerization medium of pyrrole in an ethanol and water mixture and heating to 100°C.[189] Further, it was found that the thickness of the polymer coatings can be controlled by varying the contact time of the core with the polymerization solution and also depends on the inorganic core composition and the additives in the solution. Figure 6.21 is the TEM images of silica coated with poly(pyrrole).[189] Polymer layers on inorganic nanoparticles can also be obtained through emulsion polymerization.

Self-assembly has been widely studied for the construction of thin films.[190,191] Self-assembled thin polymer layer has been used to stabilize the colloidal particles by direct adsorption of polymers from solution onto their surface,[192] which has been discussed briefly in Chapters 2 and 3. It is also possible to form multilayers of polyelectrolytes by electrostatic self-assembly.

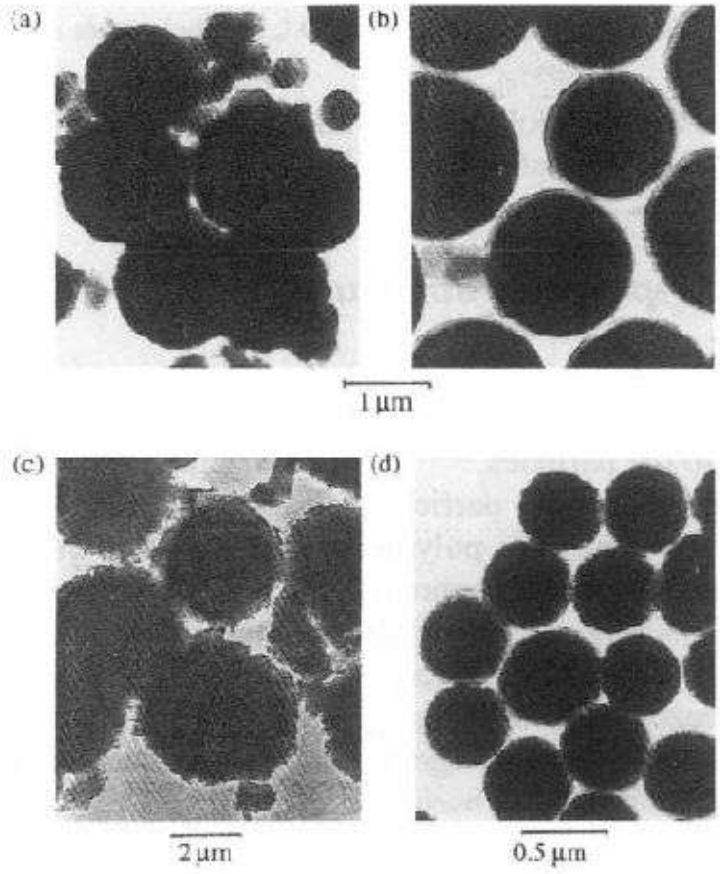

Fig. 6.21. TEM (a,b) CuO, (c) NiO, and (d) SiO2 particles coated with polypyrrole prepared with the same mass of metal oxides (1.0 mg cm^{-3}), pyrrole (0.039 g cm^{-3}), and ethanol (5%), using 0.0016 g cm^{-3} PVA in (b) and no PVA in other cases. [C.L. Huang and E. Metijevic, *J. Mater. Res.* **10**, 1327 (1995).]

6.5. Organic–Inorganic Hybrids

Organic–inorganic hybrids are materials in which organic and inorganic components interpenetrate each other in nanometer scale and both form percolated three-dimensional networks commonly by sol-gel processing. Such organic–inorganic hybrids have also been termed Ormosils (organically modified silicates) or Ormocers (organically modified ceramics) in literature. Hybrids are generally divided into two classes: (i) hybrids that consist of organic molecules, oligomers or low molecular weight polymers embedded in an inorganic matrix to which they are held by weak hydrogen bonds or van der Waals forces, and (ii) hybrids in that the organic and inorganic components are linked to each other through covalent bonds. Class I hybrids can be considered as molecular scale nanocomposites where organic components are physically trapped in an inorganic matrix; whereas class II hybrids can be considered as a huge molecule that links organic and inorganic components through true chemical bonds.

6.5.1. *Class I hybrids*

There are a few routes developed for the synthesis of class I hybrids, including hydrolysis and condensation of alkoxides inside soluble organic polymers, mixing alkoxides and organic compounds in a common solvent, and impregnating a porous oxide gel with organic compounds. All three techniques have been widely explored for the formation of various organic–inorganic hybrids. For example, hybrids comprising organic dyes embedded in inorganic matrix, such as silica, aluminosilicate and transition metal oxides,[193,194] composed of polymers in inorganic matrix, such as poly(N-vinyl pyrrolidone)-silica[195] and poly (methylmethacrylate)-silica[196] are made by hydrolysis-condensation of alkoxides together with soluble organic polymers. Simultaneous gelation of the organic and inorganic components by mixing alkoxides and organic components in a common solvent is a method to ensure the formation of interpenetrated three-dimensional networks of both organic and inorganic components. However, the challenge is to prevent phase segregation and precipitation of organic components during hydrolysis and condensation processing, some precursor modification is desired.[197] Various silica-based hybrids with organics including polyparaphenylene and polyaniline were synthesized using this approach.[198] Infiltration of organic components into highly porous inorganic gel networks is yet another method to make class I hybrids such as PMMA-silica.[199]

Ordered hybrids can also be made by intercalation of organic compounds in ordered inorganic hosts, which include clay silicates, metal phosphates, layered metal oxides, halides or chalcogenides.[200] For example, alkyl amines can be intercalated in between vanadium oxide layers that was made by hydrolyzing and condensing $VO(OPr^n)_3$ in n-propanol.[201] Intercalating materials will be discussed further later in Sect. 6.6.

6.5.2. *Class II hybrids*

Class II hybrids comprise organic and inorganic components chemically bonded with each other and truly differ from organic–inorganic nanocomposites. In general, such hybrids are synthesized by hydrolyzing and polymerizing organic and inorganic precursors simultaneously. Inorganic precursors are referred to inorganic salts, such as $SiCl_4$ and $ErCl_3$, organic salts, such as $Cd(acac)_2$, and alkoxides, such as $Al(OR)_3$ and $Ti(OR)_4$ where R is alkyl group. All the coordination groups associated with the metal cations in inorganic precursors are hydrolysable, i.e. readily replaceable by hydroxyl and/or oxo groups during hydrolysis and condensation process. Organic precursors consist of at least one unhydrolyzable coordination group and examples are $Si(OR)_3R'$ and $Si(OR)_2R'_2$, which are also known as organoalkoxysilanes where R' is also an alkyl group linked to Si through Si-C bond. Such unhydrolyzable organic groups are referred to as pendant organic groups. For organoalkoxysilanes, no three-dimensional network would be formed if there are more than one pendant organic group attached to each silicon atom. There are other forms of organic precursors in which unhydrolyzable organic groups bridge two silicon atoms. Such organic groups are referred to as bridge groups. Examples of such organoalkoxysilanes are given in Fig. 6.22.[202,203] Since metal-carbon bonds are very stable during sol-gel processing and unhydrolyzable, the organic group R' associated with the precursors will be incorporated into inorganic sol-gel network directly together with the metal cations. Typical hydrolysis and condensation reactions in the formation of such hybrids can be described as follows, taking silica-based hybrids as an example:

$$Si(OR)_4 + 4H_2O \Leftrightarrow Si(OH)_4 + 4\,HOR \quad (6.2)$$

$$Si(OR)_3R' + 3H_2O \Leftrightarrow Si(OH)_3R' + 3HOR \quad (6.3)$$

$$Si(OH)_4 + Si(OH)_3R' \Leftrightarrow (HO)_3Si-O-Si(OH)_2R' \quad (6.4)$$

$$Si(OH)_3R' + Si(OH)_3R' \Leftrightarrow R'(HO)_2Si-O-Si(OH)_2R' \quad (6.5)$$

It should be noted that although organoalkoxysilanes are the most useful and widely used family of organometallics for the synthesis of hybrid oxide-organic materials, other organometallics are also synthesized and used for

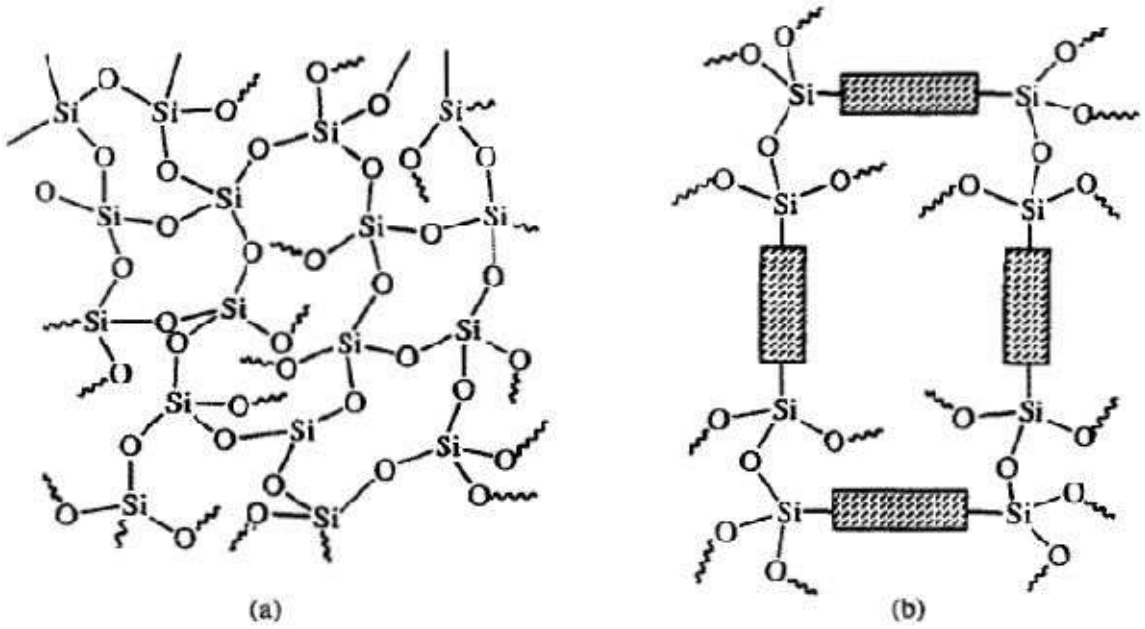

Fig. 6.22. Comparison of inorganic and hybrid structures: (a) silica network with some hydrolysable organic ligands and (b) an example of organoalkoxysilane with organic groups bridging two silicon atoms. In this structure, organic and inorganic components are chemically linked to form a single phase material. [K. Shea, D.A. Loy, and O. Webster, *J. Am. Chem. Soc.* **114**, 6700 (1992).]

the synthesis of organic–inorganic hybrids by co-condensation.[204] For example, butenyl chains were linked to Sn atom directly with C–Sn bonds.

The incorporation of organic components into inorganic matrix through either physical trapping or chemical bonding not only introduces and modifies various physical properties. The presence of organic components would also exert appreciable influences on the sol-gel processing and the resultant microstructures. Organic groups may have catalytic effects to promote hydrolysis and condensation reactions. Long-chained organic ligands may also introduce steric diffusion barrier or increase the viscosity of the sol, resulting in a diffusion-limited condensation or polymerization process. Depending on the nature and amount of organic components introduced into the systems, highly porous[205] or relatively dense hybrids[206,207] can be prepared without subjecting to heat-treatment at elevated temperatures. Some unique hierarchical microstructures can also be obtained by combining both highly porous and relatively dense structures with appropriately designed processing.[208] Although almost all the organic–inorganic hybrids are made through hydrolysis-condensation process, it has been demonstrated that non-hydrolytic sol-gel process is also capable of synthesizing hybrids.[209] Organic–inorganic hybrids with ordered nanostructures can be easily achieved by evaporation-induced self-assembly as demonstrated by Brinker and his coworkers.[210–213]

unsaturated hydrocarbon molecule (e.g. C_2H_2, reaction 5.34). A high concentration of atomic hydrogen has proven a key factor in the successful growth of diamond films, and atomic hydrogen is believed to constantly remove the graphite deposits on the diamond growth surface, so as to ensure continued deposition of diamond.[47] Oxygen species have also proven to be important in the deposition of diamond films by atmospheric combustion flames using oxygen and acetylene.[49,50] Other hydrocarbon fuels including ethylene, propylene and methyl acetylene can all be used as precursors for the growth of diamond films.[51–54]

5.6. Atomic Layer Deposition (ALD)

Atomic layer deposition (ALD) is a unique thin film growth method and differs significantly from other thin film deposition methods. The most distinctive feature of ALD has a self-limiting growth nature, each time only one atomic or molecular layer can grow. Therefore, ALD offers the best possibility of controlling the film thickness and surface smoothness in truly nanometer or sub-nanometer range. Excellent reviews on ALD have been published by Ritala and Leskelä.[55,56] In the literature, ALD is also called atomic layer epitaxy (ALE), atomic layer growth (ALG), atomic layer CVD (ALCVD), and molecular layer epitaxy (MLE). In comparison with other thin film deposition techniques, ALD is a relatively new method and was first employed to grow ZnS film.[57] More publications appeared in open literature in early 1980s.[58–60] ALD can be considered as a special modification of the chemical vapor deposition, or a combination of vapor-phase self-assembly and surface reaction. In a typical ALD process, the surface is first activated by chemical reaction. When precursor molecules are introduced into the deposition chamber, they react with the active surface species and form chemical bonds with the substrate. Since the precursor molecules do not react with each other, no more than one molecular layer could be deposited at this stage. Next, the monolayer of precursor molecules that chemically bonded to the substrate is activated again through surface reaction. Either the same or different precursor molecules are subsequently introduced to the deposition chamber and react with the activated monolayer previously deposited. As the steps repeat, more molecular or atomic layers are deposited one layer at a time.

Figure 5.15 schematically illustrates the process of titania film growth by ALD. The substrate is hydroxylated first, prior to the introduction of precursor, titanium tetrachloride. Titanium tetrachloride will

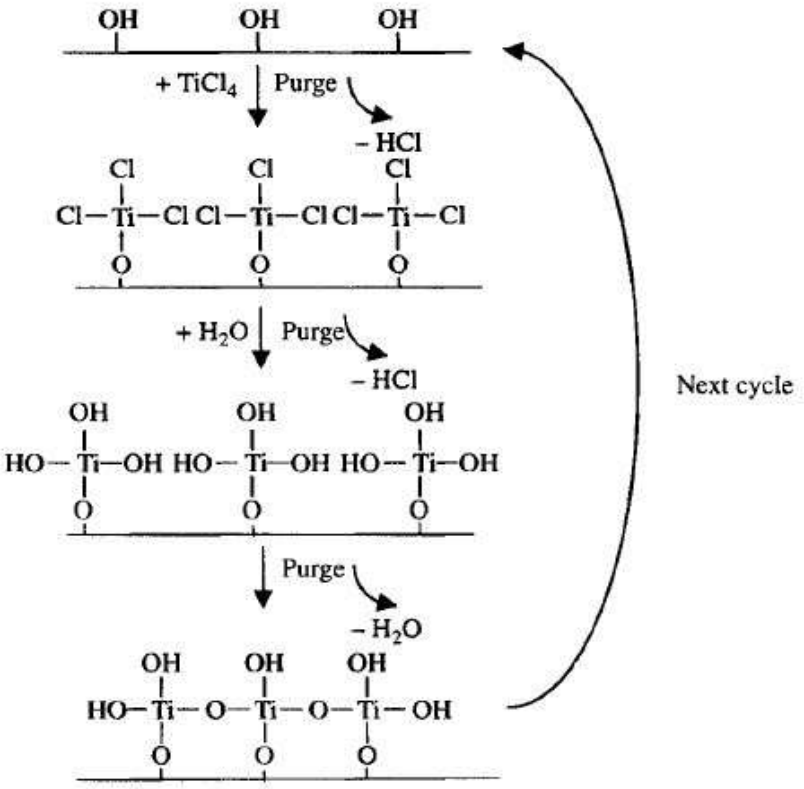

Fig. 5.15. Schematic illustrating the principal reactions and processing steps for the formation of titania film by ALD.

react with the surface hydroxyl groups through a surface condensation reaction:

$$TiCl_4 + HOMe \rightarrow Cl_3Ti\text{–}O\text{–}Me + HCl \qquad (5.35)$$

where Me represents metal or metal oxide substrates. The reaction will stop when all the surface hydroxyl groups reacted with titanium tetrachloride. Then the gaseous by-product, HCl, and excess precursor molecules are purged, and water vapor is subsequently introduced to the system. Titanium trichloride chemically bonded onto the substrate surface undergo hydrolysis reaction:

$$Cl_3Ti\text{–}O\text{–}Me + H_2O \rightarrow (HO)_3Ti\text{–}O\text{–}Me + HCl \qquad (5.36)$$

Neighboring hydrolyzed Ti precursors subsequently condensate to form Ti–O–Ti linkage:

$$(HO)_3Ti\text{–}O\text{–}Me + (HO)_3Ti\text{–}O\text{–}Me \rightarrow Me\text{–}O\text{–}Ti(OH)_2\text{–}O\text{–}Ti\ (HO)_2\text{–}O\text{–}Me + H_2O \qquad (5.37)$$

The by-product HCl and excess H_2O will be removed from the reaction chamber. One layer of TiO_2 has been grown by the completion of one

cycle of chemical reactions. The surface hydroxyl groups are ready to react with titanium precursor molecules again in the next cycle. By repeating the above steps, second and many more TiO_2 layers can be deposited in a very precisely controlled way.

The growth of ZnS film is another often used classical example for the illustration of the principles of ALD process. $ZnCl_2$ and H_2S are used as precursors. First, $ZnCl_2$ is chemisorbed on the substrate, and then H_2S is introduced to react with $ZnCl_2$ to deposit a monolayer of ZnS on the substrate and HCl is released as a by-product. A wide spectrum of precursor materials and chemical reactions has been studied for the deposition of thin films by ALD. Thin films of various materials including various oxides, nitrides, florides, elements, II–VI, II–VI and III–V compounds, in epitaxial, polycrystalline or amorphous form deposited by ALD are summarized in Table 5.2.[55,56]

The choice of proper precursors is the key issue in a successful design of an ALD process. Table 5.3 summarizes the requirements for ALD precursors.[55,56] A variety of precursors have been used in ALD. For example, elemental zinc and sulfur were used in the first ALD experiments for the growth of ZnS.[57] Metal chlorides were studied soon after the first demonstrations of ALD.[61] Metallorganic compounds including both organometallic compounds and metal alkoxides are widely used. For non-metals, the simple hydrides have mostly been used: H_2O, H_2O_2, H_2S, H_2Se, H_2Te, NH_3, N_2H_4, PH_3, AsH_3, SbH_3 and HF.

In comparison to other vapor phase deposition methods, ALD offer advantages particularly in the following aspects: (i) precise control of film

Table 5.2. Thin film materials deposited by ALD.[55,56]

II–VI compounds	ZnS, ZnSe, ZnTe, $ZnS_{1-x}Se_x$, CaS, SrS, BaS, $SrS_{1-x}Se_xCdS$, CdTe, MnTe, HgTe, $Hg_{1-x}Cd_xTe$, $Cd_{1-x}Mn_xTe$
II–VI based phosphors	ZnS:M (M = Mn, Tb, Tm), CaS:M (M = Eu, Ce, Tb, Pb), SrS:M (M = Ce, Tb, Pb, Mn, Cu)
III–V compounds	GaAs, AlAs, AlP, InP, GaP, InAs, $Al_xGa_{1-x}As$, $Ga_xIn_{1-x}As$, $Ga_xIn_{1-x}P$
Nitrides	AlN, GaN, InN, SiN_x, TiN, TaN, Ta_3N_5, NbN, MoN, W_2N, Ti–Si–N
Oxides	Al_2O_3, TiO_2, ZrO_2, HfO_2, Ta_2O_5, Nb_2O_5, Y_2O_3, MgO, CeO_2, SiO_2, La_2O_3, $SrTiO_3$, $BaTiO_3$, $Bi_xTi_yO_z$, In_2O_3, In_2O_3:Sn, In_2O_3:F, In_2O_3:Zr, SnO_2, SnO_2:Sb, ZnO, ZnO:Al, Ga_2O_3, NiO, CoO_x, $YBa_2Cu_3O_{7-x}$, $LaCoO_3$, $LaNiO_3$
Fluorides	CaF_2, SrF_2, ZnF_2
Elements	Si, Ge, Cu, Mo, Ta, W
Others	La_2S_3, PbS, In_2S_3, $CuGaS_2$, SiC

Table 5.3. Requirements for ALD precursors.[55]

Requirement	*Comments*
Volatility	For efficient transportation, a rough limit of 0.1 torr at the applicable maximum source temperature
	Preferably liquids or gases
No self-decomposition	Would destroy the self-limiting film growth mechanism
Aggressive and complete reactions	Ensure fast completion of the surface reactions and thereby short cycle times
	Lead to high film purity
	No problems of gas phase reactions
No etching of the film or substrate material	No competing reaction pathways
	Would prevent the film growth
No dissolution to the film	Would destroy the self-limiting film growth mechanism
Un-reactive byproduct	To avoid corrosion
	Byproduct re-adsorption may decrease the growth rate
Sufficient purity	To meet the requirements specific to each process
Inexpensive	
Easy to synthesize & handle	
Nontoxic and environmentally friendly	

thickness and (ii) conformal coverage. Precise control of film thickness is due to the nature of self-limiting process, and the thickness of a film can be set digitally by counting the number of reaction cycles. Conformal coverage is due to the fact that the film deposition is immune to variations caused by non-uniform distribution of vapor or temperature in the reaction zone. Figure 5.16 shows the X-ray diffraction spectra and the cross-sectional SEM image of 160 nm Ta(Al)N(C) film on patterned silicon wafer.[62] The film is polycrystalline and shows perfect conformality. The deposition temperature was 350°C and precursors used were $TaCl_5$, trimethylaluminum (TMA) and NH_3. However, it should be noted that excellent conformal coverage can only be achieved when the precursor doses and pulse time are sufficient for reaching the saturated state at each step at all surfaces and no extensive precursor decomposition takes place. ALD has demonstrated its capability of depositing multilayer structures or nanolaminates and Fig. 5.17, as an example, shows such a schematic representation of nanolaminates prepared onto glass substrates by ALD.[63]

ALD is an established technique for the production of large area electroluminescent displays,[64] and is a likely future method for the production

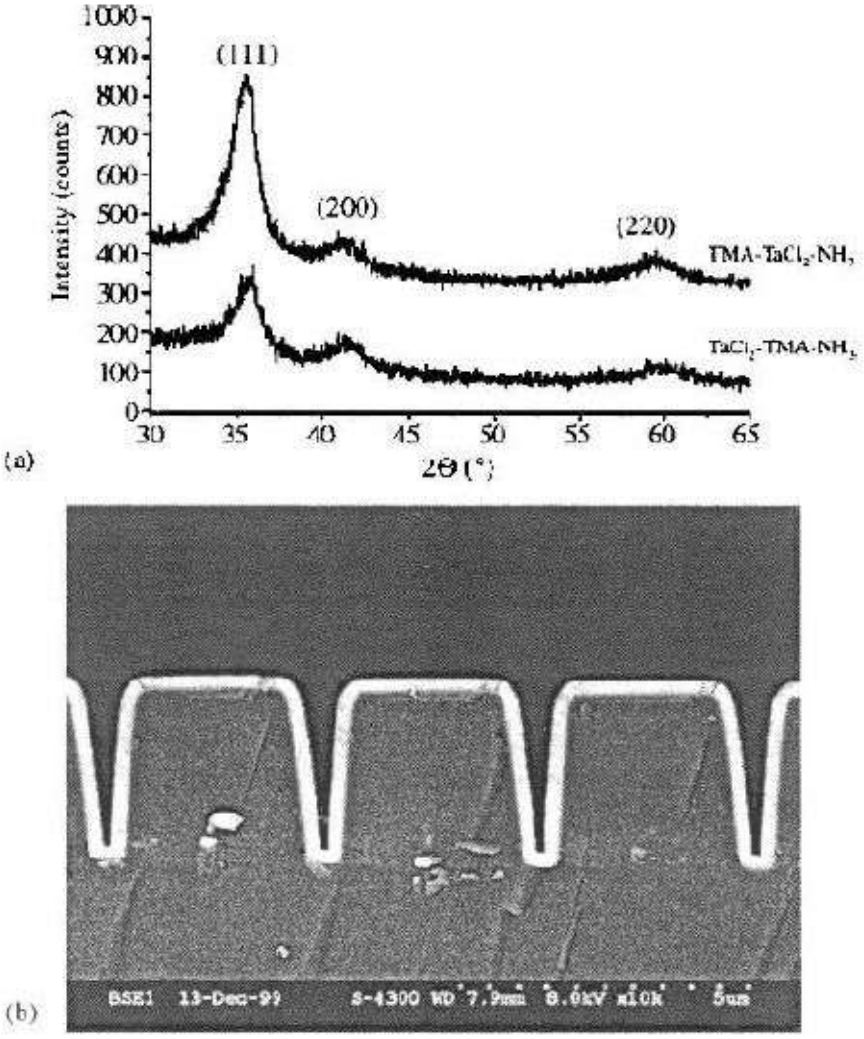

Fig. 5.16. (a) X-ray diffraction spectra and (b) cross-sectional SEM image of 160 nm Ta(Al)N(C) film on patterned silicon wafer. [P. Allén, M. Juppo, M. Ritala, T. Sajavaara, J. Keinonen, and M. Leskelä, *J. Electrochem. Soc.* **148**, G566 (2001).]

of very thin films needed in microelectronics.[65] However, many other potential applications of ALD are discouraged by its low deposition rate, typically <0.2 nm (less than half a monolayer) per cycle. For silica deposition, completing a cycle of reactions typically requires more than 1 min.[66,67] Some recent efforts have been directed towards the development of rapid ALD deposition method. For example, highly conformal layers of amorphous silicon dioxide and aluminum oxide nanolaminates were deposited at rates of 12 nm or <32 monolayers per cycle, and the method has been referred to as "alternating layer deposition".[68] The exact mechanism for such a multilayer deposition in each cycle is unknown, but obviously different from the self-limiting growth discussed above. The precursor employed in this experiment, tris(tert-butoxy)silanol, can react with each other, and thus the growth is not self-limiting.

Unit - IV Characterization of Nano Materials

section. SPM differs from other imaging techniques such as scanning electron microscopy (SEM) and transmission electron microscopy (TEM) and offers the possibility to manipulate molecules and nanostructures on a surface. SPM consists of two major members: scanning tunneling microscopy (STM) for electrically conductive materials and atomic force microscopy (AFM) for dielectrics. In this section, near-field scanning optical microscopy and near-field photolithography are also included, since they share a lot of similarities with SPM.

7.3.1. *Scanning tunneling microscopy (STM)*

STM relies on electron tunneling, which is a phenomenon based on quantum mechanics, and can be briefly explained as follows.[58] For more detailed discussion on the fundamentals, the readers are referred to excellent books.[59,60] Let us first consider a situation where two flat surfaces of a metal or semiconductor are separated by an insulator or a vacuum as schematically illustrated in Fig. 7.9.[61] Electrons in the material cannot transfer from one surface to another through the insulator, since there is an energy barrier. However, when a voltage is imposed between the two, the shape of the energy barrier is changed and there is a driving force for electrons to move across the barrier by tunneling, resulting in a small

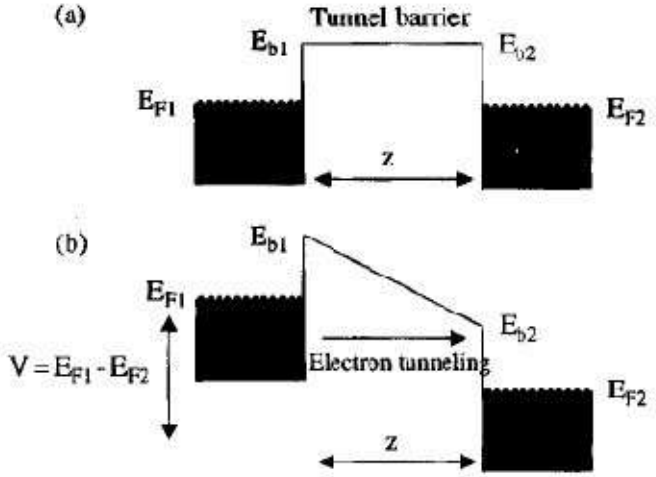

Fig. 7.9. The energy levels in two solids (metals or semiconductors) separated by an insulating or vacuum barrier (a) with no electric field applied between the solids and (b) with an applied electric field. Energies of the electrons in the solids are indicated by the shaded areas up to E_{F1} and E_{F2}, which are the Fermi levels of the respective solids. The applied bias V is $E_{F1} - E_{F2}$, and z is the distance between the two solids. [D.A. Bonnell and B.D. Huey, in *Scanning Probe Microscopy and Spectroscopy*, ed., D. Bonnell, Wiley-VCH, New York, p. 7, 2001.]

current when the distance is sufficiently small so that the electron wave functions extended from the two surfaces overlap. The tunneling current, I, is given by:

$$I \propto e^{-2kz} \tag{7.5}$$

where z is the distance between the two metals or the thickness of the insulator and k is given by:

$$k = \frac{\sqrt{2m(V-E)}}{h} \tag{7.6}$$

where m is the mass of an electron, h is Planck's constant, E is the energy of electron, and V is the potential in the insulator. Similar discussion is applicable to a tip-planar surface geometry, the configuration of a STM. However, the tunneling current is then given by:

$$I = C\rho_t\rho_s e^{-zk^{\frac{1}{2}}} \tag{7.7}$$

where z is the distance between the tip and the planar surface or sample, ρ_t is the tip electronic structure, ρ_s is the sample electronic structure, and C is a constant dependent on the voltage applied between the tip and the sample surface. The tunneling current decays exponentially with the tip-sample distance. For example, a 0.1 nm decrease in the distance will increase the tunneling current by one order of magnitude. Such a quantum mechanical property has been utilized in the STM.

In a typical STM, a conductive tip is positioned above the surface of a sample. When the tip moves back and forth across the sample surface at very small intervals, the height of the tip is continually adjusted to keep the tunneling current constant. The tip positions are used to construct a topographic map of the surface. Figure 7.10 schematically depicts a STM structure. An extremely sharp tip usually made of metals or metal alloys, such as tungsten or PtIr alloy is mounted on to a three-dimensional positioning stage made of an array of piezoelectrics. Such a tip would move above the sample surface in three dimensions accurately controlled by the piezoelectric arrays. Typically the distance between the tip and the sample surface falls between 0.2 and 0.6 nm, thus a tunneling current in the scale of 0.1–10 nA is commonly generated. The scanning resolution is about 0.01 nm in XY direction and 0.002 nm in Z direction, offering true atomic resolution three-dimensional image.

STM can be operated in two modes. In constant current imaging, a feedback mechanism is enabled that a constant current is maintained while a constant bias is applied between the sample and tip. As the tip scans over the sample, the vertical position of the tip is altered to maintain the constant separation. An alternating imaging mode is the constant height operation in

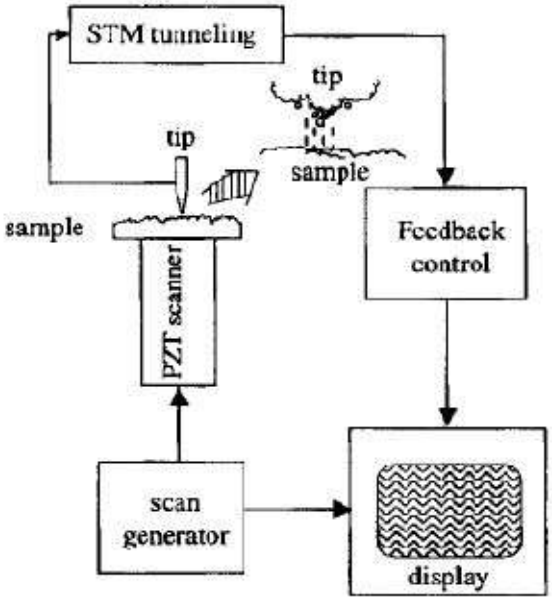

Fig. 7.10. Schematic of scanning tunneling microscope. Two operation modes are commonly used. (i) Constant current mode, in which the distance between the tip and sample surface is kept constant. (ii) Constant voltage mode, in which the tip position is held unchanged during scanning the sample surface.

which constant height and bias are simultaneously maintained. A variation in current results as the tip scans the sample surface because a topographic structure varies the tip-sample separation. The constant current mode produces a contrast directly related to electron charge density profiles, whereas the constant height mode permits faster scan rates. STM was first developed by Binnig and Rohrer in 1982,[62] and STM was first to demonstrate its atomic scale resolution in an image of silicon 7×7 restructured (111) surface.[63]

7.3.2. *Atomic force microscopy (AFM)*

In spite of atomic resolution and other advantages, STM is limited to an electrically conductive surface since it is dependent on monitoring the tunneling current between the sample surface and the tip. AFM was developed as a modification of STM for dielectric materials.[64] A variety of tip–sample interactions may be measured by an AFM, depending on the separation. At short distances, the van der Waals interactions are predominant. Van der Waals force consists of interactions of three components: permanent dipoles, induced dipoles and electronic polarization. A more detailed discussion on van der Waals force was presented in Chapter 2. Long-range forces act in addition to short-range forces between the tip

fields from biological structures to porosity in coals to dispersoids in structural engineering materials. It should also be noted that the theory of visible light scattering[22] is almost identical to that of SAXS described above if the following condition is met:

$$\frac{8\pi R(n_1 - n_2)}{n_2\lambda} \ll 1 \tag{8.6}$$

where n_1 and n_2 are the refractive indices of a particle and its environment, respectively. However, visible light scattering is limited to systems only when R is larger than approximately 80 nm.

8.2.3. *Scanning electron microscopy (SEM)*

SEM is one of the most widely used techniques used in characterization of nanomaterials and nanostructures. The resolution of the SEM approaches a few nanometers, and the instruments can operate at magnifications that are easily adjusted from ~10 to over 300,000. Not only does the SEM produce topographical information as optical microscopes do, it also provides the chemical composition information near the surface.

In a typical SEM, a source of electrons is focused into a beam, with a very fine spot size of ~5 nm and having energy ranging from a few hundred eV to 50 KeV, that is rastered over the surface of the specimen by deflection coils. As the electrons strike and penetrate the surface, a number of interactions occur that result in the emission of electrons and photons from the sample, and SEM images are produced by collecting the emitted electrons on a cathode ray tube (CRT). Various SEM techniques are differentiated on the basis of what is subsequently detected and imaged, and the principle images produced in the SEM are of three types: secondary electron images, backscattered electron images and elemental X-ray maps. When a high-energy primary electron interacts with an atom, it undergoes either inelastic scattering with atomic electrons or elastic scattering with the atomic nucleus. In an inelastic collision with an electron, the primary electron transfers part of its energy to the other electron. When the energy transferred is large enough, the other electron will emit from the sample. If the emitted electron has energy of less than 50 eV, it is referred to as a secondary electron. Backscattered electrons are the high-energy electrons that are elastically scattered and essentially possess the same energy as the incident or primary electrons. The probability of backscattering increases with the atomic number of the sample material. Although backscattering images cannot be used for elemental identification, useful contrast can develop between regions of the specimen that differ widely in atomic number, Z. An additional electron interaction in the

SEM is that the primary electron collides with and ejects a core electron from an atom in the sample. The excited atom will decay to its ground state by emitting either a characteristic X-ray photon or an Auger electron, both of which have been used for chemical characterization and will be discussed later in this chapter. Combining with chemical analytical capabilities, SEM not only provides the image of the morphology and microstructures of bulk and nanostructured materials and devices, but can also provide detailed information of chemical composition and distribution.

The theoretical limit to an instrument's resolving power is determined by the wavelengths of the electron beam used and the numerical aperture of the system. The resolving power, R, of an instrument is defined as:

$$R = \frac{\lambda}{2NA} \tag{8.7}$$

where λ is the wavelength of electrons used and NA is the numerical aperture, which is engraved on each objective and condenser lens system, and a measure of the electron gathering ability of the objective, or the electron providing ability of the condenser. Figure 8.5 shows SEM pictures (A and B), together with TEM image with electron diffraction

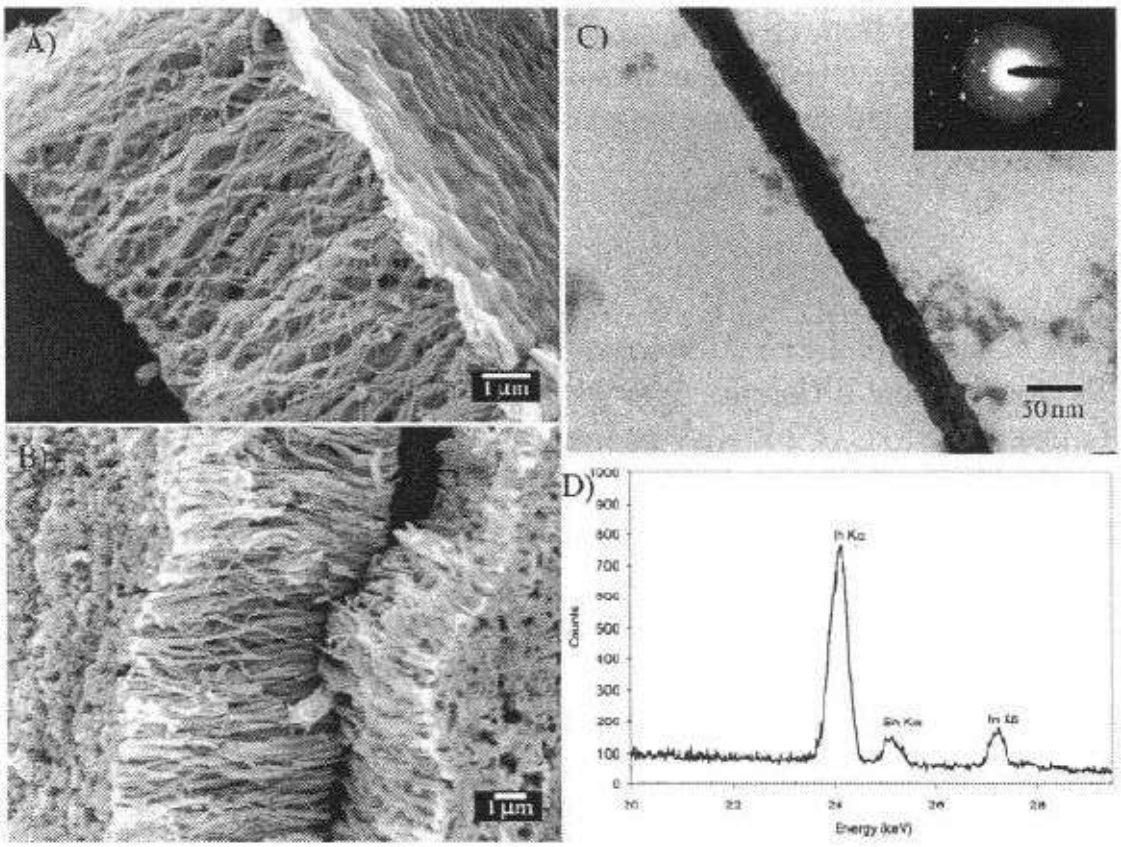

Fig. 8.5. (A) and (B) SEM images of nanorod arrays (C) TEM image with electron diffraction pattern, and (D) the EDS spectrum of indium doped tin oxide (ITO) grown by template-based sol-gel electrophoretic deposition. [S.J. Limmer, S. Vince Cruz, and G.Z. Cao, unpublished results (2003).] (only A and B)

pattern (C) and the spectrum of EDS (D) of nanorod arrays of indium doped tin oxide (ITO) grown by sol-gel electrophoretic deposition.[23]

8.2.4. *Transmission electron microscopy (TEM)*

In TEM, electrons are accelerated to 100 KeV or higher (up to 1 MeV), projected onto a thin specimen (less than 200 nm) by means of the condenser lens system, and penetrate the sample thickness either undeflected or deflected. The greatest advantages that TEM offers are the high magnification ranging from 50 to 10^6 and its ability to provide both image and diffraction information from a single sample.

The scattering processes experienced by electrons during their passage through the specimen determine the kind of information obtained. Elastic scattering involves no energy loss and gives rise to diffraction patterns. Inelastic interactions between primary electrons and sample electrons at heterogeneities such as grain boundaries, dislocations, second-phase particles, defects, density variations, etc., cause complex absorption and scattering effects, leading to a spatial variation in the intensity of the transmitted electrons. In TEM one can switch between imaging the sample and viewing its diffraction pattern by changing the strength of the intermediate lens.

The high magnification or resolution of all TEM is a result of the small effective electron wavelengths, λ, which is given by the de Broglie relationship:

$$\lambda = \frac{h}{\sqrt{2mqV}} \tag{8.8}$$

where m and q are the electron mass and charge, h is Planck's constant, and V is the potential difference through which electrons are accelerated. For example, electrons of 100 KeV energy have wavelengths of 0.37 nm and are capable of effectively transmitting through ~0.6 μm of silicon. The higher the operating voltage of a TEM instrument, the greater its lateral spatial resolution. The theoretical instrumental point-to-point resolution is proportional[24] to $\lambda^{3/4}$. High-voltage TEM instruments (with e.g. 400 KV) have point-to-point resolutions better than 0.2 nm. High-voltage TEM instruments have the additional advantage of greater electron penetration, because high-energy electrons interact less strongly with matter than lower-energy electrons. So it is possible to work with thicker samples on a high-voltage TEM. One shortcoming of TEM is its limited depth resolution. Electron scattering information in a TEM image originates from a three-dimensional sample, but is projected onto a two-dimensional detector.

Therefore, structure information along the electron beam direction is superimposed at the image plane. Although the most difficult aspect of the TEM technique is the preparation of samples, it is less so for nanomaterials.

Selected-area diffraction (SAD) offers a unique capability to determine the crystal structure of individual nanomaterials, such as nanocrystals and nanorods, and the crystal structures of different parts of a sample. In SAD, the condenser lens is defocused to produce parallel illumination at the specimen and a selected-area aperture is used to limit the diffracting volume. SAD patterns are often used to determine the Bravais lattices and lattice parameters of crystalline materials by the same procedure used in XRD.[1] Although TEM has no inherent ability to distinguish atomic species, electron scattering is exceedingly sensitive to the target element and various spectroscopy are developed for the chemical composition analysis. Examples include Energy-dispersive X-ray Spectroscopy (EDS) and Electron Energy Loss Spectroscopy (EELS).

In addition to the capability of structural characterization and chemical analyses, TEM has been also explored for other applications in nanotechnology. Examples include the determination of melting points of nanocrystals, in which, an electron beam is used to heat up the nanocrystals and the melting points are determined by the disappearance of electron diffraction.[25] Another example is the measurement of mechanical and electrical properties of individual nanowires and nanotubes.[26–28] The

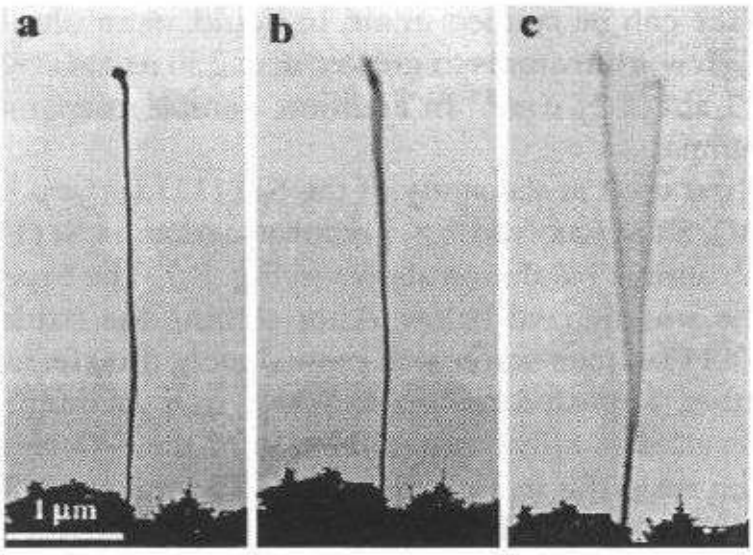

Fig. 8.6. A selected Si nanowires at (a) stationary, (b) the first harmonic resonance with the vibration plane parallel to the viewing direction, and (c) the resonance with the vibration plane perpendicular to the viewing direction. A slight difference in the resonance frequencies in (b) and (c) results from the anisotropic structure of the nanowire. [Z.L. Wang, *Adv. Mater.* **12**, 1295 (2000).]

technique allows a one-to-one correlation between the structure and properties of the nanowires. Figure 8.6 shows TEM micrographs of a silicon nanowire when stationary and vibrating at resonance frequencies,[26] from which the Young's modulus of this silicon nanowire is determined.

8.2.5. *Scanning probe microscopy (SPM)*

SPM is unique among imaging techniques in that it provides three-dimensional (3-D) real-space images and among other analysis techniques in that it allows spatially localized measurements of structure and properties. Under optimum conditions subatomic spatial resolution is achieved. SPM is a general term for a family of microscopes depending on the probing forces used. Two major members are STM and AFM. The principles of electron tunneling and atomic forces have been already discussed in Chapter 7. For more details, the readers are recommended to an excellent book[7] and references therein.

STM was first developed by Binnig and his coworkers in 1981,[29] and AFM was invented a few years later.[30] The limitation of STM, which is restricted to electrically conductive sample surface, is complemented by AFM, which does not require conductive sample surface. Therefore, almost any solid surface can be studied with SPM: insulators, semiconductors and conductors, magnetic, transparent and opaque materials. In addition, surface can be studied in air, in liquid, or in ultrahigh vacuum, with fields of view from atoms to greater than 250 $\mu m \times 250 \mu m$, and vertical ranges of about 15 μm.[31] In addition, sample preparation for SPM analysis is minimal.

STM was first used in the study of the Si (111) surface.[32] In ultrahigh vacuum (UHV), STM resolved 7×7 reconstruction on Si (111) surface in real space with atomic resolution shown in Fig. 8.7. The experimental procedures can be summarized below. After etching the oxide with an HF solution, the (111) silicon wafer was immediately transferred to the STM in UHV chamber. Repeated heating to 900°C in a vacuum not exceeding 3×10^{-8} Pa resulted in effective sublimation of the SiO layer grown during the transfer, resulting in a clean surface. The micrographs were taken at 2.9 V with tip positive. Only unidirectional scans were recorded to avoid nonlinear effects of the scanning piezoelectric drives.

As summarized by Lang *et al.*[33] in their excellent tutorial article, SPM has been developed to a wide spectrum of techniques using various probe and sample surface interactions, as shown in Fig. 8.8. The interaction force may be the interatomic forces between the atoms of the tip and those

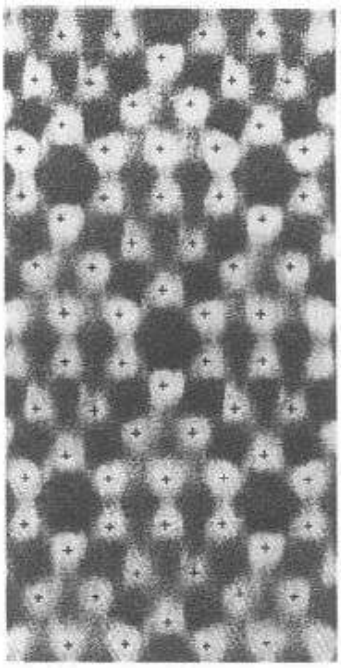

Fig. 8.7. (a) STM imagine of 7×7 reconstruction on Si (111) surface in real space with atomic resolution. (b) Modified adatom model. The underlying top-layer atom positions are shown by dots, and the remaining atoms with unsatisfied dangling bonds carry circles, whose thickness indicates the measured depth. The adatoms are represented by large dots with corresponding bonding arms. The empty potential adatom position is indicated by an empty circle in the triangle of adjacent rest atoms. The grid indicates the 7×7 unit cells. [G. Binnig, H. Rohrer, C. Gerber, and E. Weibel, *Phys. Rev. Lett.* **50**, 120 (1983).]

of a surface, short-range van der Waals forces, or long-range capillary forces, or stick-slip processes producing friction forces. Modifying the tip chemically allows various properties of the sample surface to be measured. Depending on the type of interactions between the tip and the sample surface used for the characterization, various types of SPM have been developed. Electrostatic force microscopy is based on local charges on the tip or surface, which lead to electrostatic forces between tip and sample, which allow a sample surface to be mapped, i.e. local differences in the distribution of electric charge on a surface to be visualized. In a similar way, magnetic forces can be imagined if the tip is coated with a magnetic material, e.g. iron, that has been magnetized along the tip axis, which is magnetic force microscopy.[34] The tip probes the stray field of the sample and allows the magnetic structure of the sample to be determined. When the tip is functionalized as a thermal couple, temperature distribution on the sample surface can be measured, which is scanning thermal microscopy.[35] The capacity change between tip and sample is evaluated in scanning capacitance microscopy,[36] whereas locally resolved measurement of the chemical potential is done by Kelvin probe microscopy.[37] The

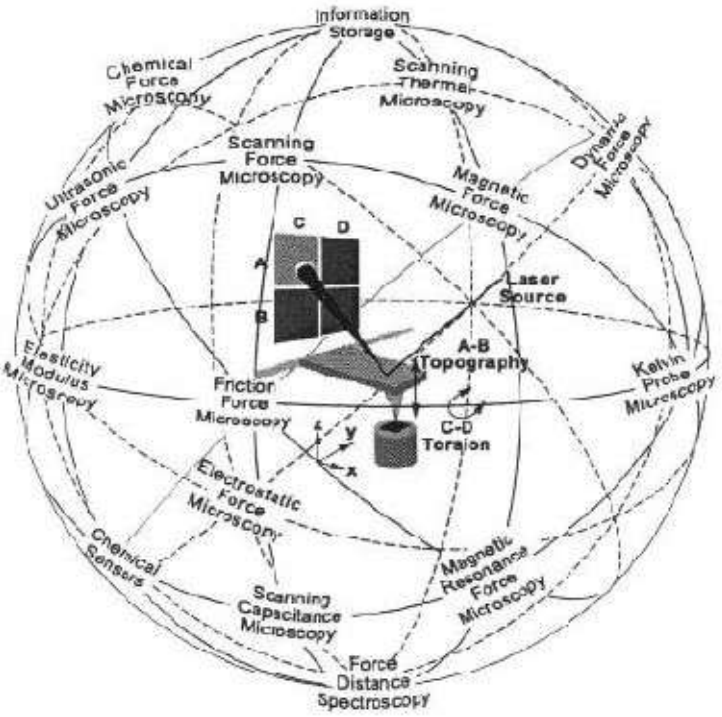

Fig. 8.8. SPM consists of a wide spectrum of techniques using various probe and sample surface interactions. [H.P. Lang, M. Hegner, E. Meyer, and Ch. Gerber, *Nanotechnology* **13**, R29 (2002).]

tip can be driven in an oscillating mode to probe the elastic properties of a surface, which is referred to as elastic modulus microscopy. At high oscillation frequencies (cantilevers with high resonance frequency), further information on inter-atomic forces between tip and sample can be obtained, which is referred to as dynamic force microscopy.

Near-Field Scanning Optical Microscopy (NSOM) can be considered as yet another member of SPM. The fundamentals of NSOM have been summarized in a previous chapter when the near-field optical lithography for the fabrication of nanostructures was discussed, and detailed information can be found in Refs. 38–41. NSOM breaks the diffraction limit ($\lambda/2$) to the resolution of ordinary microscopy by scanning an optical probe (source or detector) in close proximity to the sample. The resolution of a NSOM is dependent on the probe size and the probe and sample separation. When both dimensions are much smaller than the optical wavelength, the resolution in the NSOM experiment is also much smaller than the optical wavelength. In typical NSOM apparatus and experiments, the sample is irradiated through a sub-wavelength aperture in the probe, which is typically a tapered, metal-coated single mode optical fiber with an aperture of a few tens of nanometers at one end.[42] The probe-sample distance is regulated by scanning the lateral shear force interaction of the probe with the sample during the scanning process.[43] During the scanning

Unit - V Application of Nano Materials

Chapter 9

Applications of Nanomaterials

9.1. Introduction

Nanotechnology offers an extremely broad range of potential applications from electronics, optical communications and biological systems to new materials. Many possible applications have been explored and many devices and systems have been studied. More potential applications and new devices are being proposed in literature. It is obviously impossible to summarize all the devices and applications that have been studied and it is impossible to predict new applications and devices. This chapter will simply provide some examples to illustrate the possibilities of nanostructures and nanomaterials in device fabrication and applications. It is interesting to note that the applications of nanotechnology in different fields have distinctly different demands, and thus face very different challenges, which require different approaches. For example, for applications in medicine, or in nanomedicine, the major challenge is "miniaturization": new instruments to analyze tissues literally down to the molecular level, sensors smaller than a cell allowing to look at ongoing functions, and small machines that literally circulate within a human body pursuing pathogens and neutralizing chemical toxins.[1]

Applications of nanostructures and nanomaterials are based on (i) the peculiar physical properties of nanosized materials, e.g. gold

nanoparticles used as inorganic dye to introduce colors into glass and as low temperature catalyst, (ii) the huge surface area, such as mesoporous titania for photoelectrochemical cells, and nanoparticles for various sensors, and (iii) the small size that offers extra possibilities for manipulation and room for accommodating multiple functionalities. For many applications, new materials and new properties are introduced. For example, various organic molecules are incorporated into electronic devices, such as sensors.[2] This chapter intends to provide some examples that have been explored to illustrate the vast range of applications of nanostructures and nanomaterials.

9.2. Molecular Electronics and Nanoelectronics

Tremendous efforts and progress have been made in the molecular electronics and nanoelectronics.[3–12] In molecular electronics, single molecules are expected to be able to control electron transport, which offers the promise of exploring the vast variety of molecular functions for electronic devices, and molecules can now be crafted into a working circuit as shown schematically in Fig. 9.1.[3] When the molecules are biologically active, bioelectronic devices could be developed.[2,13] In molecular electronics, control over the electronic energy levels at the surface of conventional semiconductors and metals is achieved by assembling on the solid

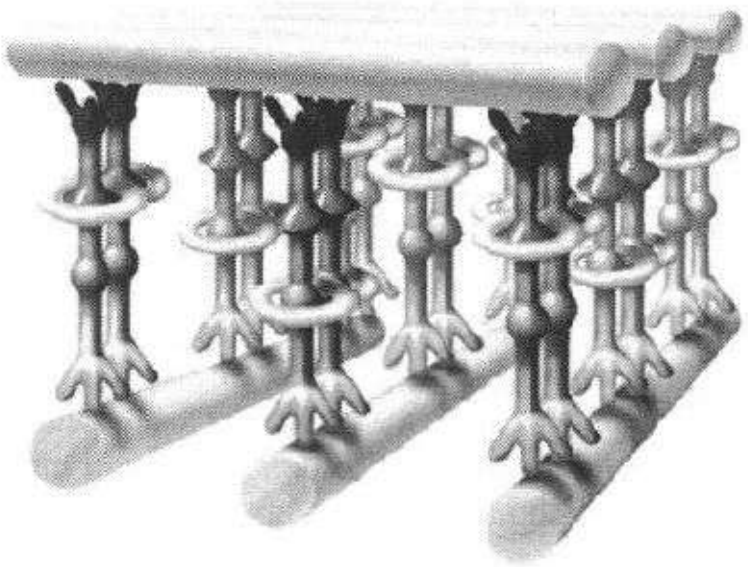

Fig. 9.1. Schematic showing that molecules can now be crafted into working circuit, though constructing real molecular chips remains a big challenge. [R. F. Service, *Science* **293**, 782 (2001).]

surfaces, poorly organized, partial monolayers of molecules instead of the more commonly used ideal ones. Once those surfaces become interfaces, these layers exert electrostatic rather than electrodynamic control over the resulting devices, based on both electrical monopole and dipole effects of the molecules. Thus electronic transport devices, incorporating organic molecules, can be constructed without current flow through the molecules. The simplest molecular electronics are sensors that translate unique molecular properties into electrical signals. Sensors using a field effect transistor (FET) configuration with its gate displaced into a liquid electrolyte, and an active layer of molecules for molecular recognition were reported in early 1970's.[14] A selective membrane is inserted on the insulator surface of the FET, and this permits the diffusion of specific analyte ions and construction of a surface dipole layer at the insulator surface. Such a surface dipole changes the electric potential at the insulator surface and, thus, permits the current going through the device. Such devices are also known as ion-selective FET (ISFET) or chemical FET (CHEMFET).[2,15,16] Thin films attached to metal nanoparticles have been shown to change their electrical conductivity rapidly and reproducibly in the presence of organic vapors, and this has been exploited for the development of novel gas sensors.[17,18] The monolayer on metal nanoparticles can reversibly adsorb and desorb the organic vapor, resulting in swelling and shrinking of the thickness of the monolayer, thus changing the distance between the metal cores. Since the electron hopping conductivity through the monolayers is sensitively dependent on the distance, the adsorption of organic vapor increases the distance and leads to a sharp decrease in electrical conductivity.

Many nanoscale electronic devices have been demonstrated: tunneling junctions,[19–21] devices with negative differential resistance,[22] electrically configurable switches,[23,24] carbon nanotube transistors,[25,26] and single molecular transistors.[27,28] Devices have also been connected together to form circuits capable of performing single functions such as basic memory[23,24,29] and logic functions.[30–33] Ultrahigh density nanowires lattices and circuits with metal and semiconductor nanowires have also been demonstrated.[34] Computer architecture based on nanoelectronics (also known as nanocomputers) has also been studied,[35,36] though very limited. Various processing techniques have been applied in the fabrication of nanoelectronics such as focused ion beam (FIB),[37–39] electron beam lithography,[34,40] and imprint lithography.[33] Major obstacles preventing the development of such devices include addressing nanometer-sized objects such as nanoparticles and molecules, molecular vibrations, robustness and the poor electrical conductivity.

Au nanoparticles have been widely used in nanoelectronics and molecular electronics using its surface chemistry and uniform size. For example, Au nanoparticles function as carrier vehicles to accommodate multiple functionalities through attaching various functional organic molecules or biocomponents.[41] Au nanoparticles can also function as mediators to connect different functionalities together in the construction of nanoscale electronics for the applications of sensors and detectors. Various electronic devices based on Au nanoparticles and Au_{55} clusters have been explored.[42–44] In particular, single electron transistor action has been demonstrated for systems that contain ideally only one nanoparticle in the gap between two electrodes separated by only a few nanometers. This central metal particle represents a Coulomb blockade and exhibits single electron charging effects due to its extremely small capacitance. It can also act as a gate if it is independently addressable by a third terminal. An electrochemically addressable nanoswitch, consisting of a single gold particle covered with a small number of dithiol molecules containing a redox-active viologen moiety has been demonstrated, and the electron transfer between the gold substrate and the gold nanoparticle depend strongly on the redox-state of the viologen.[45]

Single-walled carbon nanotubes have also been intensively studied for nanoelectronic devices, due to the semiconducting behavior of different allotropes.[46] Examples of single-walled carbon nanotube nanoelectronic devices include single-electron transistors,[47–49] FET,[30,50,51] sensors,[52,53] circuits,[54] and a molecular electronics toolbox.[55] Carbon nanotubes have been explored for many other applications, such as actuators,[56,57] sensors,[58,59] and thermometers made of multiple-walled carbon nanotubes filled with gallium.[60]

9.3. Nanobots

A very promising and fast growing field for the applications of nanotechnology is in the practice of medicine, which, in general, is often referred to as nanomedicine. One of the attractive applications in nanomedicine has been the creation of nanoscale devices for improved therapy and diagnostics. Such nanoscale devices are known as nanorobots or more simply as nanobots.[61] These nanobots have the potential to serve as vehicles for delivery of therapeutic agents, detectors or guardians against early disease and perhaps repair of metabolic or genetic defects. Similar to the conventional or macroscopic robots, nanobots would be programmed to perform specific functions and be remotely controlled, but possess a much smaller size, so that they can travel and perform desired functions inside

the human body. Such devices were first described by Drexler in his book, Engines of Creation in 1986.[62]

Haberzettl[61] described what nanobots would do in practice in medicine, which is briefly summarized below. Nanobots applied to medicine would be able to seek out a target within the body such as a cancer cell or an invading virus, and perform some function to fix the target. The fix delivered by the nanobots may be that of releasing a drug in a localized area, thus minimizing the potential side effects of generalized drug therapy, or it may bind to a target and prevent it from further activity thus, for example, preventing a virus from infecting a cell. Further in the future, gene replacement, tissue regeneration or nanosurgery are all possibilities as the technology becomes more mature and sophisticated.

Although such capable and sophisticated nanobots are not yet realized, many functions in much simplified nanobots are being investigated and tested in the lab. It is also being argued that the nanobots would not take the conventional approach of macroscopic robots. Examples include:

(1) Architecture or structure to carry the payload, known as carrier: Three groups of nanoscale materials have been studied extensively as a structure or vehicle to carry various payloads. The first group is carbon nanotubes or buckyballs, the second group various dendrimers, and the third various nanoparticles and nanocrystals.
(2) Targeting mechanisms to guide the nanobots to the desired site of action: The most likely mechanisms to be employed are based on antigen or antibody interactions or binding of target molecules to membrane-bound receptors. The navigation system for nanobots would be most likely to use the same method that the human body uses, going with the flow and "dropping anchor" when the nanobots reached its target.
(3) Communication and information processing: Single molecular electronics may offer simple switch function of on and off, optical labeling would be a more readily achievable reality.
(4) Retrieve of nanobots from human body: Retrieve of nanobots from human body would be another challenge in the development of nanobots. Most nanodevices could be eliminated from the body through natural mechanisms of metabolism and excretion. Nanodevices made of biodegradable or naturally occurring substances, such as calcium phosphate, would be another favorable approach. "Homing" nanobots would be ideal, which can be collected and removed after performing the desire function. The possible negative impacts of nanobots include the pollution and clog of systems in human body, and the nanobots may become "out of control" when some functions are lost or nanobots malfunction.

9.4. Biological Applications of Nanoparticles

Biological applications of colloidal nanocrystals have been summarized in an excellent review article, and the following text is mainly based on this article.[63] One important branch of nanotechnology is nanobiotechnology. Nanobiotechnology includes (i) the use of nanostructures as highly sophisticated scopes, machines or materials in biology and/or medicine, and (ii) the use of biological molecules to assemble nanoscale structures.[63] The following will briefly describe one of the important biological applications of colloidal nanocrystals: molecular recognition. But there are many more biological applications of nanotechnology.[64–66]

Molecular recognition is one of the most fascinating capabilities of many biological molecules.[67,68] Some biological molecules can recognize and bind to other molecules with extremely high selectivity and specificity. For molecular recognition applications, antibodies and oligonucleotides are widely used as receptors. Antibodies are protein molecules created by the immune systems of higher organisms that can recognize a virus as a hostile intruder or antigen, and bind to it in such a way that the virus can be destroyed by other parts of the immune system.[67] Oligonucleotides, known as single stranded deoxyribonucleic acid (DNA), are linear chains of nucleotides, each of which is composed of a sugar backbone and a base. There are four different bases: adenine (A), cytosine (C), guanine (G), and thymine (T).[67] The molecular recognition ability of oligonucleotides arises from two characteristics. One is that each oligonucleotide is characterized by the sequence of its bases, and another is that base A only binds to T and C only to G. That makes the binding of oligonucleotides highly selective and specific.

Antibodies and oligonucleotides are typically attached to the surface of nanocrystals via (i) thiol-gold bonds to gold nanoparticles,[69,70] (ii) covalent linkage to silanized nanocrystals with bifunctional crosslinker molecules,[71–73] and (iii) a biotin-avidin linkage, where avidin is adsorbed on the particle surface.[74,75] When a nanocrystal is attached or conjugated to a receptor molecules, it is "tagged". Nanocrystals conjugated with a receptor can now be "directed" to bind to positions where ligand molecules are present, which "fit" the molecular recognition of the receptor[76] as schematically shown in Fig. 9.2. This facilitates a set of applications including molecular labeling.[63,77–79] For example, when gold nanoparticles aggregate, a change of color from ruby-red to blue is observed, and this phenomenon has been exploited for the development of very sensitive colorimetric methods of DNA analysis.[80] Such devices are capable of detecting trace amounts of a particular oligonucleotide sequence and distinguishing between perfectly

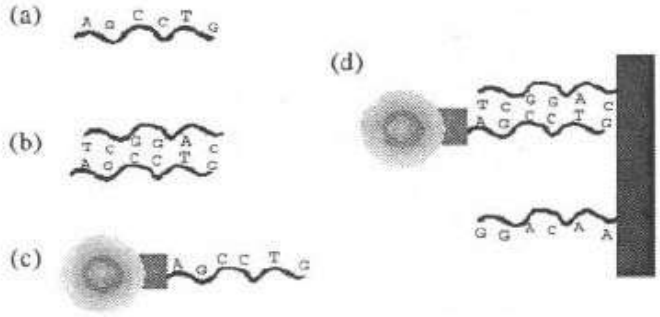

Fig. 9.2. DNA as a molecular template to arrange nanoscale objects. (a) One oligonucleotide composed of six bases (A,G,C,C,T,G). (b) One oligonucleotide (AGCCTG) bound to a complementary oligonucleotide. (c) Conjugate formed between a silanized CdSe/ZnS nanocrystal and an oligonucleotide with six bases. (d) The nanocrystal-oligonucleotide conjugate binds to an oligonucleotide with complementary sequence that is immobilized on a surface, but does not bind to oligonucleotides with different sequences. [W.J. Parak, D. Gerion, T. Pellegrino, D. Zanchet, C. Micheel, S.C. Williams, R. Boudreau, M.A. Le Gros, C.A. Larabell, and A.P. Alivisatos, *Nanotechnology* **14**, R15 (2003).]

complementary DNA sequences and those that exhibit different degrees of base pair mismatches.

9.5. Catalysis by Gold Nanoparticles

Bulk gold is chemically inert and thus considered to be not active or useful as a catalyst.[81,82] However, gold nanoparticles can have excellent catalytic properties as first demonstrated by Haruta.[83] For example, gold nanoparticles with clean surface have demonstrated to be extremely active in the oxidation of carbon monoxide if deposited on partly reactive oxides, such as Fe_2O_3, NiO and MnO_2. γ-alumina,[84] and titania[85,86] are also found to be reactive. Figure 9.3 shows a STM image of Au nanoparticles $TiO_2(110)$-(1×1) substrate as prepared before a $CO{:}O_2$ reaction.[85] The Au coverage is 0.25 ML, and the sample was annealed at 850 K for 2 min. The size of the images is 50 nm by 50 nm.[85] Au nanoparticles also exhibit extraordinary high activity for partial oxidation of hydrocarbons, hydrogenation of unsaturated hydrocarbons and reduction of nitrogen oxides.[83]

The excellent catalytic property of gold nanoparticles is a combination of size effect and the unusual properties of individual gold atom. The unusual properties of gold atom are attributable to the so-called relativistic effect that stabilizes the $6s^2$ electron pairs.[81,87] The relativistic effect is briefly described below. As the atomic number increases, so does the mass of nucleus. The speed of the innermost $1s^2$ electrons has to increase to maintain their position, and for gold, they attain a speed of 60% light

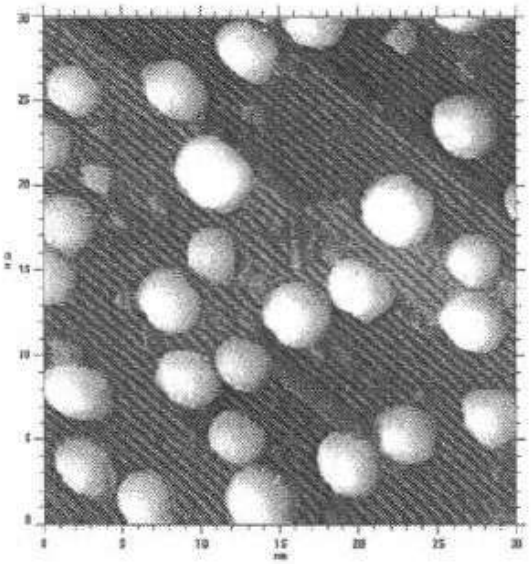

Fig. 9.3. A STM image of Au on TiO_2 (110)-(1 × 1) substrate as prepared before a $CO:O_2$ reaction. The Au coverage is 0.25 ML, and the sample was annealed at 850 K for 2 min. The size of the images is 30 nm by 30 nm. [Courtesy of Prof. D. Wayne Goodman at Texas A&M University, detailed information seen M. Valden, X. Lai, and D.W. Goodman, *Science* **281**, 1647 (1998).]

speed. A relativistic effect on their mass results in the 1*s* orbital contraction. Then all the outer *s* orbitals have to contract in sympathy, but *p* and *d* electrons are much less affected. In consequence, the 6 s^2 electron pair is contracted and stabilized, and the actual size of Au is ~15% smaller than it would be in the absence of the relativistic effect. Further, much of the chemistry of gold, including the catalytic properties, is therefore determined by the high energy and reactivity of the 5*d* electrons. This relativistic effect explains why gold differs so much from its neighbors. Essential requirements for high oxidation activity of gold particles include: small particle size (not larger than 4 nm),[88] use of "reactive" support, and a preparative method that achieves the desired size of particle in intimate contact with the support. As the size of gold nanoparticles is sufficiently small, (i) the fraction of surface atoms increases, (ii) the band structure is week, so surface atoms on such small particles behave more like individual atoms, and a greater fraction of atoms are in contact with the support, and the length of the periphery per unit mass of metals rises.

Thiol-stabilized gold nanoparticles have also been exploited for catalysis applications. Examples include asymmetric dihydroxylation reactions,[89] carboxylic ester cleavage,[90] electrocatalytic reductions by anthraquinone functionalized gold particles[91] and particle-bound ring opening metathesis polymerization.[92] It should be noted that the abovementioned catalytic applications are based on the carefully designed

chemical functionality of the ligand shell, instead of the potential catalytic activity of a nanostructured clean metal surface.

9.6. Band Gap Engineered Quantum Devices

Band gap engineering is a general term referring to the synthetic tailoring of band gaps[93,94] with the intent to create unusual electronic transport and optical effects, and novel devices. Obviously, most of the devices based on semiconductor nanostructures are band gap engineered quantum devices. However, the examples discussed in this section are focused mainly on the device design and fabrication of quantum well and quantum dot lasers by vapor deposition and lithography techniques.

9.6.1. *Quantum well devices*

Lasers fabricated using single or multiple quantum wells based on III–V semiconductors as the active region have been extensively studied over the last two decades. Quantum well lasers offer improved performance with lower threshold current and lower spectra width as compared to that of regular double heterostructure lasers. Quantum wells allow the possibility of independently varying barriers and cladding layer compositions and widths, and thus separate determination of optical confinement and

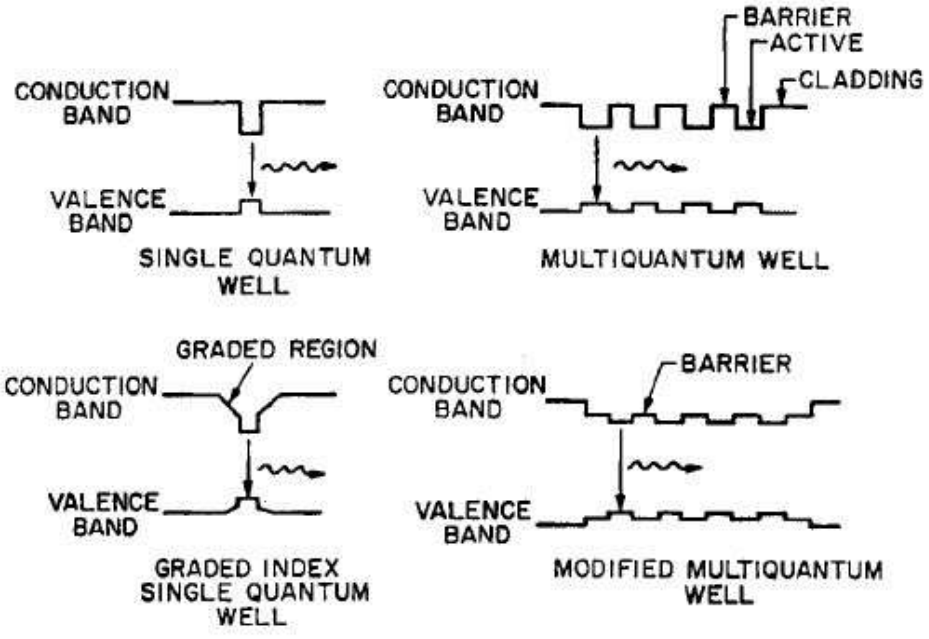

Fig. 9.4. Schematic energy band diagrams of different types of quantum well structures used to optimize the laser performance. [P.K. Bhattacharya and N.K. Dutta, *Ann. Rev. Mater. Sci.* **23**, 79 (1993).]

electrical injection. Quantum well lasers were first fabricated using the GaAs/AlGaAs material systems,[95,96] and Fig. 9.4 shows schematic energy band diagrams of different types of quantum well structures used to optimize the laser performance.[97] One of the main differences between the single quantum well and the multiple quantum well lasers is that the confinement factor of the optical mode is significantly smaller for the former. This results in higher threshold carrier and current densities for single quantum well lasers; however the confinement factor of single quantum well lasers can be significantly increased using a graded-index cladding structure.[98] InGaAsP/InP is another material system used in the fabrication of quantum well lasers.[99,100] InGaAsN/GaAs quantum wells are yet another example.[101] Strain has been explored and introduced into quantum well lasers, since strain can alter the band structure parameters significantly to produce many desirable features such as better high temperature performance resulting from reduced Auger recombination, small chirp, and high bandwidth.[97] Other quantum well optical devices have also been extensively studied and include quantum well electroabsorption and electro-optic modulators, quantum well infrared photodetectors, avalanche photodiodes and optical switching and logic devices.

Blue/green light-emitting diodes (LED) have been developed based on nanostructures of wide-band gap II–VI semiconductor materials.[102] Such devices take direct advantages of quantum well heterostructure configurations and direct energy band gap to achieve high internal radiative efficiency. Various LED at short visible wavelengths have been fabricated based on nanostructures or quantum well structures of ZnSe-based materials[103,104] and ZnTe-based materials.[105]

Blue/green lasers were first demonstrated[106,107] in a p–n injection diode that employed a configuration sketched in Fig. 9.5.[102] In this structure, the Zn(S,Se) ternary layers were introduced to serve as cladding layers for the optical waveguide region with the ZnSe layers and thus provide the electronic barriers for the (Zn,Cd)Se quantum wells. A lot of effects have been devoted to the improvement of materials and structure-design from the above structure.[108,109] The typical blue/green lasers operate continuously at room temperature and emit a significant amount of power with wavelengths ranging from 463 to 514 nm depending on the actual structure. The various laser structures are composed of (Zn,Mg)(Se,S) and Zn(Se,S) cladding layers with (Zn,Cd)Se quantum wells and possess a graded ohmic contact consisting of Au metal on a pseudo-alloy of Zn(Se,Te).

Heterojunction bipolar transistor (HBT) is an example of nanostructured devices based on GeSi/Si nanostructures.[110,111] For this structure, the GeSi layer is thick enough so that no quantum confinement occurs. In

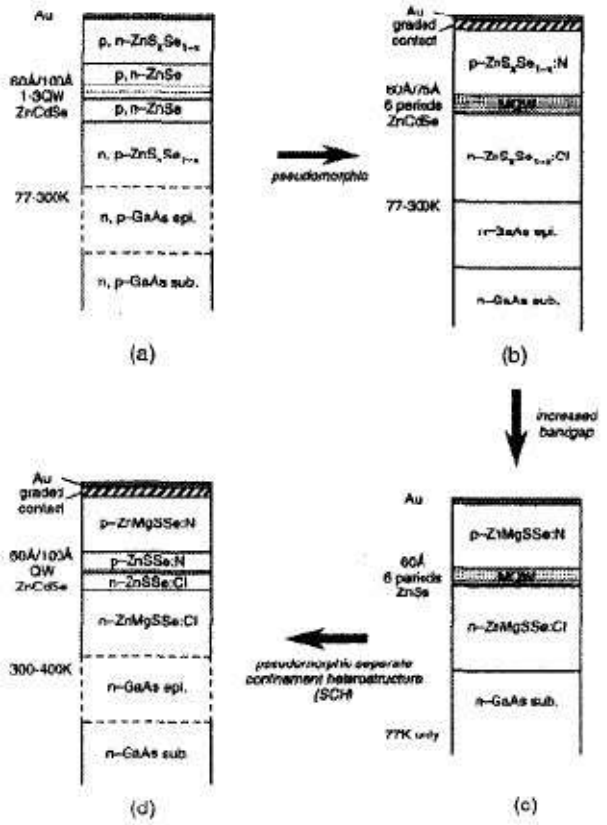

Fig. 9.5. Schematic diagrams of key blue/green laser diode configurations and their evolution from the initial laser design to the later laser design. [L.A. Kolodziejski, R.L. Gunshor, and A.V. Nurmikko, *Ann. Rev. Mater. Sci.* **25**, 711 (1995).]

the operation of a bipolar transistor, by applying a small current to the base, a large amount of current can flow from the emitter to the collector if the gain is high. Comparing to the conventional bipolar junction transistor, the HBT offers an advantage of reduction of hole injection into the emitter, due to the valence band discontinuity. The barrier to the hole injection is exponentially sensitive to the valence band offset, ΔE_v.

9.6.2. *Quantum dot devices*

The key parameter that controls the wavelength is the size of the dot. Large sized dots emit at longer wavelengths than small sized ones. Quantum dot heterostructures are commonly synthesized by molecular beam epitaxy at the initial stages of strained heteroepitaxial growth via the layer-island or Stranski–Krastanov growth mode.[112,113]

Quantum dots have been established their use in lasers and detectors. Quantum dot lasers with ultralow-threshhold current densities and low sensitivity to temperature variations have been demonstrated.[114,115] Intersublevel detectors made of quantum dot nanostructures were found

not sensitive to normal-incidence light.[116] For the lasers using the quantum dot media often suffer from insufficient gain for the device to operate at the ground state wavelength, due to the combined consequence of the low density of states and the low area density of dots that is normally used. Several techniques have been developed to overcome this barrier. For example, several layers of quantum dots are used to increase the modal gain. Other methods include coating the laser facets to increase their reflectivity and lengthen the laser cavity.

The efficiency of luminescence from quantum dot structures depends on a number of factors including the capture of the carriers within the dots, the minimization of nonradiative recombination channels within the dots and in the surrounding matrix, and the elimination of defects at the hetero-interfaces. Embedding quantum dots inside an appropriate quantum well structure (also referred to as active region) demonstrated dramatically enhanced emission efficiency and low threshold current, due to the improved structural and optical properties of the embedding layers, and the enhanced ability of capturing and confining carriers to the vicinity of the dots.[117,118] Further structural improvement can be achieved by sandwiching quantum dots in a compositionally graded quantum well.[119] When the quantum dots of InAs are inserted at the center of compositionally graded $In_xGa_{1-x}As$ layers, the relative emission efficiency has been increased by nearly an order of magnitude over the emission of dots inside a constant composition (In,Ga)As structure.

9.7. Nanomechanics

In the previous two chapters, we have discussed the applications of SPM in the field of imaging surface topography and measurement of local properties of sample surface (Chapter 8) and nano manipulation and nanolithography in fabrication and processing of nanodevices. In this chapter, we will briefly introduce another important application of SPM, i.e. nanodevices derived from SPM. Although many devices are being investigated and more are to be developed in the conceivable future, we will take two examples to illustrate the possibilities and general approaches, specifically, nanosensors and nanotwizers.

Lang *et al.*[120] made an excellent summary of the applications of AFM cantilever based sensors in their tutorial article. When the surface of a cantilever or a tip is functionalized in such a way that a chemically active and a chemically inactive surface is obtained, chemical or physical processes on the active cantilever surface can be observed using the temporal

evolvement of the cantilever's response. Cantilevers can be used as a nanomechanical sensor device for detecting chemical interactions between binding partners on the cantilever surface and in its environment. Such interactions might be produced by electrostatic or intermolecular forces. At the interface between an active cantilever surface and the surrounding medium, the formation of induced stress, the production of heat or a change in mass can be detected. In general, detection modes can be grouped into three strands: static mode, dynamic mode and heat mode as illustrated in Fig. 9.6.[120]

In the static mode, the static bending of the cantilever beam due to external influences and chemical/physical reactions on one of the cantilever's surfaces is investigated. The asymmetric coating with a reactive layer on one surface of the cantilever favors preferential adsorption of molecules on this surface. In most cases, the intermolecular forces in the adsorbed molecule layer produce a compressive stress, i.e. the cantilever bends. If the reactive coating is polymer and adsorbing molecules can diffuse, the reactive coating will swell and the cantilever beam will bend. Similarly, if the cantilever beam emerges into a chemical or biochemical solution, the asymmetric interaction between the cantilever beam and the surrounding environment results in bending of the cantilever beam. Many new concepts and devices have been explored.[121–124]

In dynamic mode, the cantilever is driven at its resonance frequency. If the mass of the oscillating cantilever changes owing to additional mass

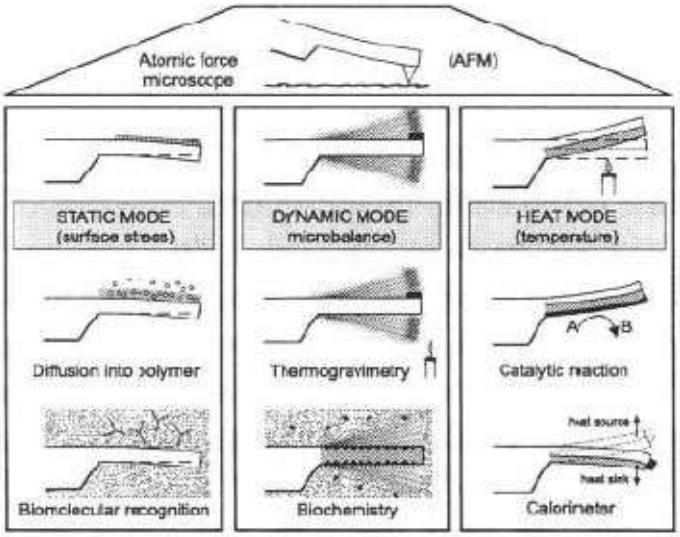

Fig. 9.6. AFM cantilever based sensors with detection modes being grouped into three strands: static mode, dynamic mode and heat mode. [H.P. Lang, M. Hegner, E. Meyer, and Ch. Gerber, *Nanotechnology* **13**, R29 (2002).]

deposited on the cantilever, or if mass is removed from the cantilever, its resonance frequency changes. Using electronics designed to track the resonance frequency of the oscillating cantilever, the mass changes on the cantilever are derived from shifts of resonance frequency. The cantilever can be regarded as a tiny microbalance, capable of measuring mass changes of less than 1 pg.[125] In dynamic mode, active coatings should apply on both surfaces of the cantilever to increase the active surface where the mass change takes places. Dynamic mode works better in gas than in liquid, which complicates the exact determination of the resonance frequency of the cantilever. More examples are available in Ref. 126.

In heat mode, the cantilever is coated asymmetrically, one surface with a layer having a different thermal expansion coefficient than that of the cantilever itself. When such a cantilever is subjected to a temperature change, it will bend. Deflections corresponding to temperature changes in the micro-Kelvin range can be easily measured. If the coating is catalytically active, e.g. a platinum layer facilitates the reaction of hydrogen and oxygen to form water. In such a case, heat is generated on the active surface and will result in bending of the cantilever. Such a method can also be used in the study of phase transition and measurement of thermal properties of a very small amount of materials.[127,128]

Although the above discussion has been limited on the single cantilever nanosensors, the same principle is readily applicable to multiple cantilever nanosensors. For example, a SPM cantilever array consisting of more than 1000 cantilevers have been fabricated.[129]

9.8. Carbon Nanotube Emitters

There have been numerous reports describing studies on carbon nanotubes as field emitters,[130–136] since the discovery of carbon nanotubes. Standard electron emitters are based either on thermionic emission of electrons from heated filaments with low work functions or field emission from sharp tips. The latter generates monochromatic electron beams; however, ultrahigh vacuum and high voltages are required. Further, the emission current is typically limited to several microamperes. Carbon fibers, typically 7 μm in diameter, have been used as electron emitters; however, they suffer from poor reproducibility and rapid deterioration of the tip.[137] Carbon nanotubes have high aspect ratios and small tip radius of curvature. In addition, their excellent chemical stability and mechanical strength are advantageous for application in field emitters. Rinzler *et al.*[132] demonstrated laser-irradiation-induced electron field emission from an individual multiwall

nanotube. Although the emission current of a single tube is constrained because of its very small dimensions, an array of nanotubes oriented perpendicular to an electrode would make an efficient field emitter.

De Heer and co-workers first demonstrated a high-intensity electron gun based on field emission from an array of oriented carbon nanotubes.[130] Field emission current densities of $\sim 0.1\ mA/cm^2$ were observed when a voltage of 200 V was applied, and a current density of $>100\ mA/cm^2$ was realized at 700 V. The gun was reported to be air stable and inexpensive to fabricate, and functions stably and reliably for long time. However, later research found a gradual degradation with time of the emission performances on both single-wall carbon nanotube and multiwall carbon nanotube emitters.[135] The degradation was explained by the destruction of nanotubes by ion bombardment with ions either from gas phase ionization or anode emission. It was also found that the degradation of single-wall carbon nanotube emitter is significantly faster (a factor ≥ 10), since they are more sensitive to electron or ion bombardment.

A flat panel display based on nanotube field emission was also demonstrated.[134] A 32×32 matrix-addressable diode nanotube display prototype was fabricated and a steady emission was produced in 10^{-6} torr vacuum. Pixels were well defined and switchable under a half-voltage "off-pixel" scheme. A fully sealed field emission display of 4.5 inch in size has been fabricated using single-wall carbon nanotube—organic binders.[138] The nanotubes were vertically aligned using paste squeeze and surface rubbing techniques, and fabricated displays were fully scalable at temperatures as low as 415°C. The turn-on field of 1 V/μm and brightness of $1800\ cd/m^2$ at 3.7 V/μm was observed on the entire 4.5 inch area from the green phosphor-indium-tin-oxide glass. Figure 9.7 shows a CRT lighting element equipped with aligned CNT emitters and the electron tube is 20 mm in diameter and 75 mm long.[139] A test of this cathode-ray tube lighting element suggested a lifetime of exceeding 10,000 h.[139]

Field emission properties of carbon nanotubes have been studied extensively. It was found that both aligned[130,134,140] and randomly[133,135,141,142] oriented nanotubes have impressive emission capabilities. Chen *et al.*[143] compared field emission data from aligned high-density carbon nanotubes with orientations parallel, 45°, and perpendicular to the substrate. The different orientations were obtained by changing the angle between the substrate and the bias electrical field direction. It was found that carbon nanotubes all demonstrated efficient field emission regardless of their orientations. The nanotube arrays oriented parallel to the substrate have a lower onset applied field, and a higher emission current density under the same electric field than those

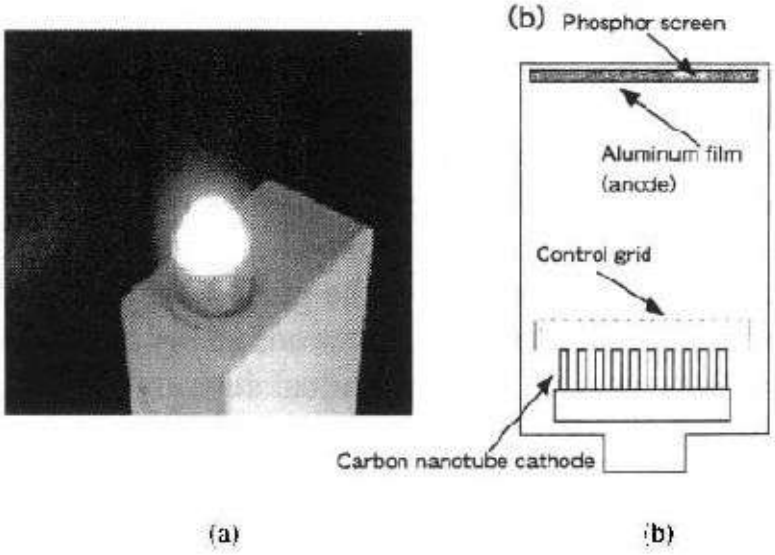

Fig. 9.7. A CRT lighting element equipped with aligned CNT emitters on SUS304 (a) operating device and (b) structure. The electron tube is 20 mm in diameter and 75 mm long. [H. Murakami, M. Hirakawa, C. Tanaka, and H. Yamakawa, Appl. *Phys. Lett.* **76**, 1776 (2000).]

oriented perpendicular to the substrate. The result indicates that electrons can emit from the body of nanotubes and carbon nanotubes can be used as linear emitter. The ability to emit electrons from the body of nanotubes was attributed to the small radius of the tubes and the presence of defects on the surface of carbon nanotubes. Saito and co-workers[144,145] have conducted field emission microscopy of single-wall nanotubes and open multiwall nanotubes. In addition to field emitters, carbon nanotubes have been explored for many other applications including sensors, scanning probe tips, hydrogen storage and Li batteries as summarized in an excellent review paper by Terrones.[146]

9.9. Photoelectrochemical Cells

The development of photoelectrochemical cells, also commonly known as photovoltaic cells or solar cells, emphasizes the need for a higher conversion efficiency of solar energy to electrical power. Photoelectrochemical devices consisting of silicon-based p–n junction materials[147,148] and other heterojunction materials,[148–150] most notably indium-gallium-phosphide/gallium-arsenide and cadmium-telluride/cadmium-sulfide, have been extensively studied for efficient light conversion, and have obtained the highest efficiency close to 20%,[147,148] as compared to cells based on other

materials. However, the high cost of production, expensive equipment, and necessary clean-room facilities associated with the development of these devices have directed exploration of solar energy conversion to cheaper materials and devices.

Sol-gel-derived titania films with a crystal structure of anatase and a mesoporous structure have been demonstrated as an excellent material for photoelectrochemical cells and have gained a lot of attention since its introduction by O'Regan and Grätzel.[151] Such devices are commonly referred to as dye-sensitized solar cells consisting of porous nanocrystalline titania (TiO_2) film in conjunction with an efficient light-absorbing dye, and have shown an impressive energy conversion efficiency of $>10\%$ at lower production costs.[152–155] Figure 9.8 shows the operation schematic of such a dye-sensitized mesoporous titania photovoltaic cell and a SEM micrograph of a mesoporous anatase titania film.[155] In such devices, TiO_2 functions as a suitable electron-capturing and electron-transporting material with a conduction band at 4.2 eV and an energy band gap of 3.2 eV, corresponding to an absorption wavelength of 387 nm.[156] In this process, the dye adsorbed to TiO_2 is exposed to a light source, absorbs photons upon exposure, and injects electrons into the conduction band of the TiO_2 electrode. Regeneration of the dye is initiated by subsequent hole-transfer to the electrolyte and electron capture after the completion of the I^-/I_3^- redox couple at the solid electrode–liquid electrolyte interface.

Nanostructures are advantageous for photoelectrochemical cell devices for high efficient conversion of light to electrical power due to its large

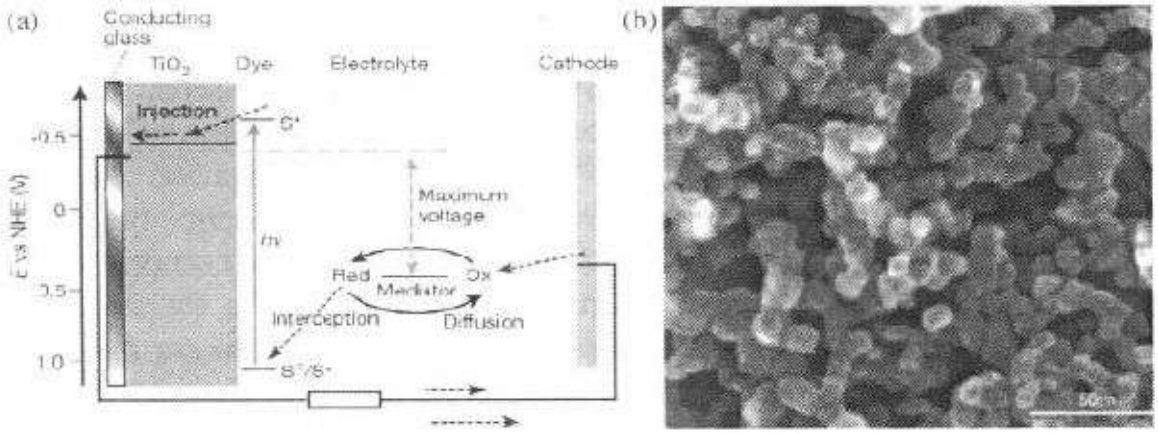

Fig. 9.8. (a) The operation schematic of such a dye-sensitized mesoporous titania photovoltaic cell and (b) a SEM micrograph of a mesoporous anatase titania film. [M. Grätzel, *Nature* **414**, 338 (2001).]

surface area at which photoelectrochemical processes take place. Many techniques have been investigated to synthesize TiO_2 electrodes to improve the structure for more efficient electron transport and good stability. Chemical vapor deposition of Ti_3O_5 has been utilized to deposit layered crystalline anatase TiO_2 thin films that are optically responsive and stable.[156] Gas-phase hydrothermal crystallization of $TiCl_4$ in aqueous mixed paste has been done to obtain crack-free porous nanocrystalline TiO_2 thick film through low-temperature processing.[157] Compression techniques of TiO_2 powder have also been used to form porous and stable films.[158] The most common and widely used technique for the preparation of crack-free TiO_2 thick film for use as suitable electron-transporting electrodes involves the preparation of TiO_2 paste by way of sol-gel processing of commercially-available TiO_2 colloidal precursors containing an amount of organic additives and followed with hydrothermal treatment. This conventional method requires the deposition of the prepared paste by either doctor-blading, or spin coating, or screen-printing on a transparent conducting substrate.[159–161] Moderate temperature sintering is utilized to remove the organic species and to connect the colloidal particles. Typical thickness of mesoporous TiO_2 film[153–155] using this method ranges from 2 μm to 20 μm, depending on the colloidal particle size and the processing conditions, and the maximum porosity obtained by this technique has reported to be ~50% with an average pore size around 15 nm and internal surface area of $>100\,m^2/g$.

Although various techniques have been utilized and explored to synthesize a more efficient structure of TiO_2 film to enhance the electrical and photovoltaic properties of solar cell devices, the capability of these devices to surpass the 10% light conversion efficiency has been hindered. Efforts to find other solar cell devices with various broad-band semiconducting oxide materials, including ZnO[162–164] and SnO_2[164,165] films, have been made for possible improvement of the current state of TiO_2-based dye-sensitized solar cell devices. Composite structures consisting of a combination of TiO_2 and SnO_2, ZnO or Nb_2O_5 materials,[164,166,167] or a combination of other oxides,[168–170] have also been examined in an attempt to enhance the overall light conversion efficiency. In addition, hybrid structures comprised of a blend of semiconducting oxide film and polymeric layers for solid-state solar cell devices have been explored in an effort to eliminate the liquid electrolyte completely for increased electron transfer and electron regeneration in hopes of increasing the overall efficiency.[171–173] So far, these devices have achieved an overall light conversion efficiency of up to 5% for ZnO devices,[162] up to 1% for SnO_2 devices,[165] up to 6% for composite devices,[165] and up to 2% for hybrid devices,[171] all of which are still less efficient than solar cell devices based on dye-sensitized TiO_2 mesoporous film.

9.10. Photonic Crystals and Plasmon Waveguides

9.10.1. *Photonic crystals*

Photonic crystals have a broad range of applications.[174,175] Examples readily for commercialization include waveguides and high-resolution spectral filters. Photonic crystals allow for guiding geometries such as 90° corners.[176] Potential applications are photonic crystal lasers, light emitting diodes and photonic crystal thin films to serve as anticounterfeit protection on credit cards. Ultimately, it is hoped that photonic crystal diodes and transistors will eventually enable the construction of an all-optical computer.

A photonic-band-gap (PBG) crystal, or simply referred to as photonic crystal, is a spatially periodic lattice consisting of alternating regions of dielectric materials with different refractive indices.[177] The concept of PBG crystals was first proposed by Yablonovitch[178] and John[179] in 1987, and the first experimental realization of 3D photonic crystal was reported in 1991.[180] Figure 9.9 shows a schematic of one-, two-, and three-dimensional photonic crystals. Because of its long-range order, a photonic crystal is capable of controlling the propagation of photons in much the same way as a semiconductor does for electrons: that is, there exists a forbidden gap in the photonic band structure that can exclude the existence of optical modes within a specific range of frequencies. A photonic band gap provides a powerful means to manipulate and control photons, and can find many applications in photonic structures or systems. For example, photonic crystals can be used to block the propagation of photons irrespective of their polarization direction, localize photons to a specific area at restricted frequencies, manipulate the dynamics of a spontaneous or stimulated emission process, and serve as a lossless waveguide to confine or

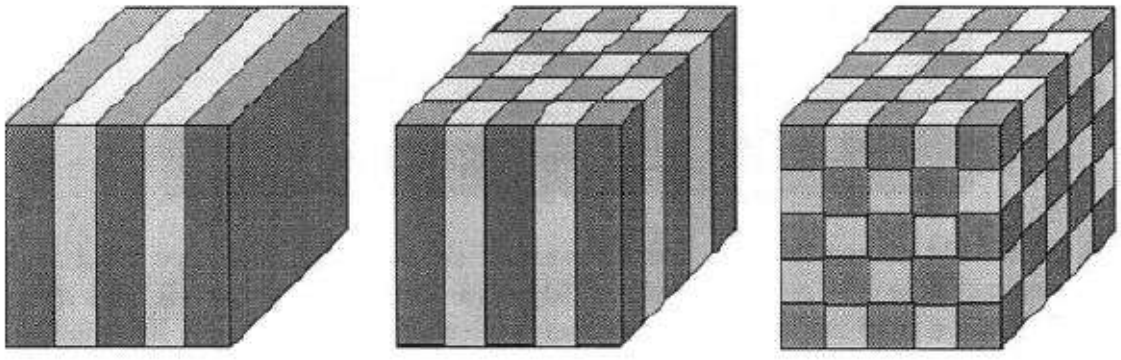

Fig. 9.9. Schematic representing one-, two-, and three-dimensional photonic crystals consisting of alternating regions of dielectric materials.

direct the propagation of light along a specific channel. It should also be noted that photonic crystals work at all wavelengths and, thus, find applications in the near-infrared telecommunication window or visible region if the size of the periodic structures (lattice constants) is appropriately chosen. A number of methods have been explored for the fabrication of photonic crystals.[181] Examples include layer-by-layer stacking techniques[182,183] electrochemical etching,[184] chemical vapor deposition,[185] holographic lithography,[186] and self-assembly of monodispersed spherical colloids.[187,188] Figure 9.10 shows SEM micrograph of a periodic array of silicon pillars fabricated using deep anisotropic etching. The silicon pillars are 205 nm in diameter and 5 μm tall. This structure possesses a band gap of ~1.5 μm for transverse magnetic polarization. By removing an array of pillars, a waveguide bend is fabricated. Input and output waveguides are integrated with the two-dimensional photonic crystal.[189]

A complete or full band gap is defined as the one that can extend over the entire Brillouin zone in the photonic band structure.[190] An incomplete band gap is often referred to as a pseudo gap, because it appears only in the transmission spectrum along a certain direction of propagation. A complete band gap can be considered as a set of pseudo gaps that overlap for a certain range of frequencies over all three dimensions of space.

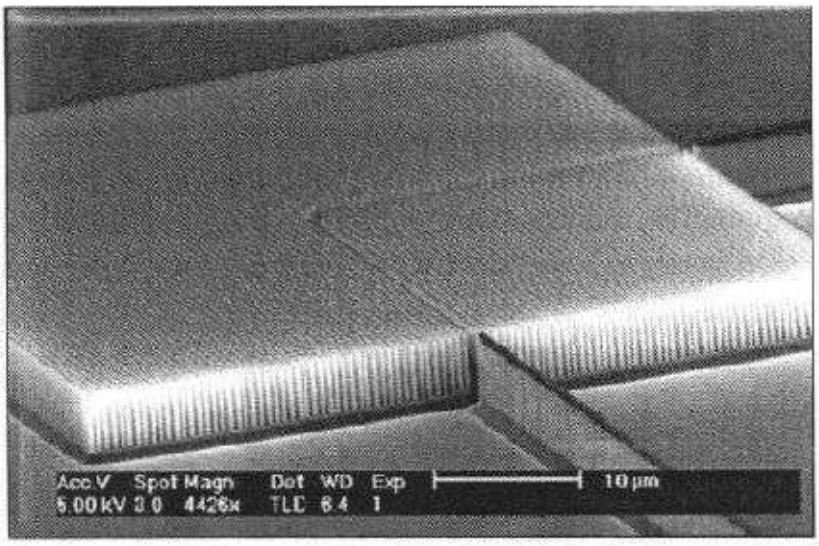

Fig. 9.10. SEM micrograph of a periodic array of silicon pillars fabricated using deep anisotropic etching. The silicon pillars are 205 nm in diameter and 5 μm tall. This structure possesses a band gap of ~1.5 μm for transverse magnetic polarization. By removing an array of pillars, a waveguide bend is fabricated. Input and output waveguides are integrated with the photonic crystal. [T. Zijlstra, E. van der Drift, M. J. A. de Dood, E. Snoeks, and A. Polman, *J. Vac. Sci. Technol.* **B17**, 2734 (1999).]

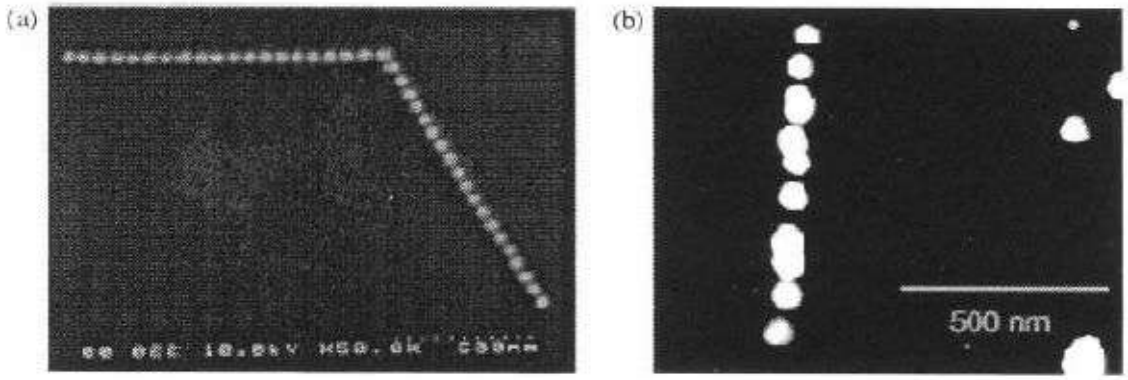

Fig. 9.11. (a) SEM image of a 60° corner in a plasmon waveguide, fabricated using electron beam lithography. The gold dots are ~50 nm in diameter and spaced by ~ 75 nm (center-to-center). (b) Straight plasmon waveguide made using 30 nm diameter colloidal gold nanoparticles. The particles were assembled on a straight line using an AFM in contact mode, and subsequently imaged in non-contact mode. [S.A. Maier, M.L. Brongersma, P.G. Kik, S. Meltzer, A.A.G. Requicha, and H.A. Atwater, *Adv. Mater.* **13**, 1501 (2001).]

9.10.2. *Plasmon waveguides*

Plasmon waveguides are optical devices based on surface plasmon resonance of noble metal nanoparticles. The surface plasmon resonance is due to the strong interaction between the electric field of light and free electrons in the metal particle, which has been discussed in the previous chapter. Arrays of closely spaced metal nanoparticles set up coupled plasmon modes that give rise to coherent propagation of electromagnetic energy along the array via near-field coupling between adjacent particles.[191–193] The dipole field resulting from a plasmon oscillation in a single metal nanoparticle can induce a plasmon oscillation in a closely spaced neighboring particle due to near field electrodynamic interactions.[193,194] It has been shown that electromagnetic wave can be guided on a scale below the diffraction limit and around 90° corners or bending radius $\ll$ wavelength of light as shown in Fig. 9.11.[191] Electron beam lithography and AFM nanomanipulation have been applied to fabricate plasmon waveguides with gold nanoparticles of 30 and 50 nm in diameter, and the center-to-center space was three times of the particle radius.[191]

9.11. Summary

This chapter provided some examples to illustrate some applications of nanostructures and nanomaterials. It is apparent that many more